Kinetic and Mechanistic Investigation of Asymmetric Organocatalytic Reactions

A thesis submitted to Imperial College London for the degree of Doctor of Philosophy and the Diploma of Membership of Imperial College

By

Natalia Zotova

Department of Chemical Engineering and Chemical Technology
Imperial College London
United Kingdom

June 2008

Abstract

The utilisation of the reaction progress kinetic methodology to advance the mechanistic understanding of the asymmetric proline catalysed aldol and α-aminoxylation reactions is demonstrated in this work. Mechanistically meaningful reaction rate laws that describe the catalytic cycles of these reactions are derived experimentally, using initially the power law driving force analysis. With the aid of the employed kinetic methodology it is shown that the processes occurring on the catalytic cycle can be deconvoluted from the influence of the reactions occurring off the cycle, and each may be studied separately. It is also shown that the synergetic efforts of experimental kinetic and spectroscopic studies are capable of suggesting and ultimately disclosing the role of additives in these reactions and understanding of catalyst deactivation pathways.

In order to obtain more support towards the kinetically derived mechanistic implications, kinetic isotope studies of the aldol reaction were performed. Experimental kinetic data fit to the derived rate model helped to assess and refine the proposed mechanism of the aldol reaction in a quantitative manner and consider other factors that potentially may affect the reaction. The rationalisation of the difference in kinetic behaviour of the aldol and α-aminoxylation reactions is discussed. The proposed elucidation is also supported by reaction simulations performed using COPASI simulation software.

Acknowledgments

The completion of this work would not have been possible without the support and contribution of the individuals to whom I would like to dedicate this section. I was very fortunate to make good friends within and outside of our research group, who made my life in London even more pleasant and fulfilling. Firstly, I would like to thank my supervisor Prof. Donna Blackmond for her guidance and encouragement throughout my PhD, her skill in cultivating my interest in conducting the research and also the ability to listen to my concerns and motivate me when things were not going to plan. I am also thankful to Prof. Alan Armstrong for his assistance and advice concerning many of the chemistry aspects of my work.

Many thanks go to all personnel involved in spectroscopic analysis in the department of Chemistry for their excellent support, in particular Peter Haycock and Dick Sheppard. I also would like to acknowledge Darren Ryde in the department of Chemical Engineering and Michel Boekkerink[1] and Ken Stares[1] from Mettler Toledo for their enthusiasm in helping to eliminate installation issues with the FTIR tools.

I want to thank all my current fellow research group members and also those with whom I began my PhD, in particular Martin Klussmann "Klusi", Suju Mathew, Axel Franzke and Antonio Ferretti, for everyday help in the lab, laughter during and after work and, of course, "Friday Pints" in the union pub. A special thank you goes to Emma Emanuelsson-Patterson for her time spent during my initial involvement in this research and, more recently for her advice with structuring this thesis. Also many thanks go to my friends Egidijus Auksorius, Sharon Inman, Marina Kuimova and Naiem Hussain for being brilliant friends.

Finally, I would like to thank my mum, my sister and Martin for your constant encouragement and love you have given me. This thesis I would like to dedicate to YOU!

[1] Currently employed somewhere else

Contents

List of Schemes

List of Figures

List of Tables

Abbreviations and Nomenclature

ATR – attenuated total reflectance;

o-CBA – o-chlorobenzaldehyde;

DFT – density functional theory;

DMF – dimethylformamide;

DMFu – 2,5-dimethylfuran;

DMSO – dimethylsulfoxide;

FTIR – Fourier transform infrared spectroscopy;

IC – initial conditions;

IS – internal standard;

KIE – kinetic isotope effect;

MS – Mass spectroscopy;

NMR – Nuclear magnetic resonance;

SKIE – secondary kinetic isotope effect.

α – molar absorptivity coefficient (in $M^{-1}cm^{-1}$)

$[\mathbf{C}]_{total}$ – total catalyst concentration (in M);

[**e**] – Excess (in M);

ee – enantiomeric excess;

E^+ - electrophile;

ϕ^*_{TS} – fractionation factor;

ΔH_{rxn} – thermodynamic heat of reaction (in $J \cdot mol^{-1}$);

K – equilibrium constant;

k_1, k_{-1}, k_2, k_3 – rate constants (units vary);

K_{mm} – Michaelis-Menten constant (in M);

$\boldsymbol{l}$ – light passage through the sample, (in cm);

Nu^- – nucleophile;

q – heat flow, (in W);

rate – reaction rate (in $M \cdot s^{-1}$);

$rate_{max}$ – maximum rate (in s^{-1});

[**S1**] – Substrate concentration (in M);

t – time (in s).

Chapter 1

Introduction

The utilisation of catalysts enables the successful rate enhancement of chemical reactions that otherwise, despite being thermodynamically favoured, would be too slow to proceed within a reasonable time. Catalysis has allowed the advancement of many technological processes in various industries including petrochemical, pharmaceutical, agrochemical and fine chemical industries.[1, 2]

Generally there are three types of catalysis that can be distinguished: homogeneous, heterogeneous and bio catalysis. While heterogeneous catalysis is widely used in the chemical and petrochemical industries, homogeneous and bio-catalysis are generally much more selective and are often employed during the production of complex pharmaceuticals.[1] Bio-catalysis usually employs enzymes or their synthetic prototypes, catalytic antibodies.[3] Although this catalysis induces very high selectivity, the narrow scope towards the substrates is its main drawback.[4] Therefore homogeneous catalysis is often used in addition to achieve a high selectivity but complement the scope of bio-catalysis. Many such catalytic reactions employ catalysts that possess a careful choice of ligands in order to direct the reacting molecules to the desired product with desired efficiency. As a

consequence of some such reactions highly functionalised molecules may be formed which possess chirality, a feature of objects that are non-superimposable but are mirror images of one another, as are left and right hands.

1.1 Chiral Molecule

Two non-superimposable molecules that are mirror images of one another are called enantiomers and considered to be chiral. Despite the fact that enantiomers have the same chemical and physical properties, their structural difference is responsible for different biological and pharmacological effects. Therefore chiral compounds are vital to any living system and play an important role in science and technology.[5] A variety of metabolic reactions and other biological processes occur where the specific enzymes, receptors, and other natural compounds only recognise substrates with a specific chirality, in the way that hands fit into gloves. These effects are exhibited when chiral molecules interact with other chiral molecules. Enantiomers can smell and taste differently due to the presence of chiral molecules in the human's receptors sensing smell or taste. For example, the *R*-enantiomer of limonene has a distinctive fresh citrus scent while its mirror image, *S*-limonene, smells of turpentine with a lemon note. (*R*/*S* labelling is based on the rule of priority of the four substituents on the chiral carbon: *R*-form identifies clockwise decrease in priority or atomic weight of substituents; while *S*-form – the anticlockwise.) Some other compelling examples of a dramatic enantiomeric influence are when one enantiomer of a compound has beneficial therapeutic effects while the other is detrimental. Naproxen, a compound well-known as an anti-inflammatory drug, must be used in its enantiomerically pure *S*-form. Its mirror image, *R*-naproxen can cause liver poisoning, due to analgesic inefficiency.[6] However the awareness of this phenomenon intensified when the teratogenic effects (interference with embryonic development) of thalidomide, developed as an antinausea drug, emerged in the 1960s. Thalidomide was produced as a racemic mixture: equal quantities of both enantiomers.[7] However only the

R enantiomer of thalidomide is effective against nausea, while its *S* enantiomer causes birth defects.[1]

In order to prevent similar undesirable side effects that a racemic mixture can cause, and encourage the production of enantiomerically pure drugs the US Food & Drug Administration ("FDA") issued a policy on chiral drugs in 1992.[7] Such regulations in conjunction with recent advances in the synthesis of enantiomerically pure compounds resulted in the significant increase in the proportion of single-enantiomer drugs. In 2006, 94% of all chiral drugs approved by the FDA contained a single enantiomer.[7] Chemists in pharmaceutical, agrochemical and fine chemical industries are increasingly called upon to mimic what nature does so easily and so well. This challenge can be met through a variety of technologies, such as separation, resolution, or asymmetric synthesis involving chiral auxiliaries and catalysts.[8]

1.1.1 Selective Production of a Chiral Molecule

Although nature normally produces chiral molecules as a single enantiomer, the formation of a single enantiomer in the lab is not so straightforward and often a single enantiomer has to be isolated from a formed racemic pool of two enantiomers.

Resolution is one of the oldest methods used to separate two enantiomers by changing their physical properties through the insertion of a chiral molecule with which both enantiomers can react.[6] The resulting molecules may then be separated physically based on their different properties. Kinetic resolution, which is also commonly used, is a similar method although based on a difference in the reactivity of enantiomers in a reaction with an added chiral molecule.[9] The main drawback of both resolution methods is that they are highly wasteful if the undesired enantiomer cannot be used. Therefore alternative ways of obtaining a single enantiomer were required.[6, 8]

[1] There are indications that thalidomide racemises in the body, so even as a chirally pure drug it would have teratogenic effects.

More economic methods involving chiral starting materials or auxiliaries have been known for a long time and are also employed in industry.[6] As an example, Pfizer's initial route to the heart disease drug *Lipitor* was realised through a chiral auxiliary, which presents a synthetic equivalent of the chiral acetate enolate.[10] This chiral compound introduces a temporary chiral centre that forces asymmetric formation of the additional chiral centre by means of steric hindrance. Finally, the chiral auxiliary can be removed, which is often performed by hydrolysis.[10, 11] Although the use of chiral auxiliaries and the natural chiral pool can be a versatile method, the necessity to use stoichiometric amounts and additional steps of introducing and removing the auxiliaries makes it occasionally even less efficient than resolution.[6, 8] Further, it is not always easy to find a well suited natural starting material of a desired chirality.[6] Thus the use of a catalyst that can be continually regenerated to complete many turnovers is an alternative method which provides the best atom economy for the production of enantiomerically pure compounds.[12]

1.1.2 Asymmetric catalysis

Catalysis that relies on chiral catalysts that are capable of creating a handed environment is called asymmetric catalysis. This environment directs the outcome in such a way, that one enantiomer is favoured over the other. Although asymmetric catalysis is not yet as widely employed on an industrial scale, it generates a tremendous academic and industrial interest.[13] The importance of advancing asymmetric catalysis was demonstrated by the Nobel Prize for Chemistry awardees (2001) Knowles and Noyori "for their work on chirally catalysed hydrogenation reaction", and Sharpless "for his work on chirally catalysed oxidation reaction".[1] A growing number of direct catalytic methods to acquire a chiral molecule have been developed in recent years.[8]

One of the earliest methods employs the transition metal complexes as a catalyst with appropriate chiral ligands to direct the reaction. The development of these catalysts was in particular driven by the progress in

[1] http://nobelprize.org/nobel_prizes/chemistry/laureates/2001/index.html

the techniques available for their characterisation and hence understanding of the implication of their structure for function.[14] However often metal catalysts are bulky, expensive and sensitive to air, therefore small organic molecules, in which interest has been recently rekindled, as catalysts of asymmetric reactions may be a useful alternative or be complementary.[15, 16] The discovery of the amino acid, L-proline, as a catalyst of the intermolecular aldol reaction caused intensive activity in the development of new catalysts and the discovery of transformations where these catalysts can be employed. In addition the synthetic scope was shown to be broad, allowing introduction of nitrogen and oxygen atoms adjacent to a carbonyl group: formation of α-animation and α-aminoxylations products.[17, 18]

1.1.3 The Potential of Asymmetric Organocatalysis

It is important to mention that many organocatalysts, in particular L-proline, are of relatively low cost and are commercially available. They are unaffected by moisture and oxygen providing ease of handling. Therefore this may add an additional advantage over the metal based catalysts. Furthermore, the ever stringent regulatory restrictions on the levels of metal residues in pharmaceutical products and waste streams,[19] make organocatalysis a very appealing method for the production of chiral products free of traces of metals. Therefore in view of existing advantages, this recently rediscovered[1] catalytic method is of both academic and commercial interest.[20]

1.2 Understanding of Catalytic Reactions and Kinetic Analysis

Although catalytic technology offers many advantages, such as atom and process economy, abatement of waste and pollution, catalytic reactions add mechanistic complexity to the technological process.[1] The participation of a catalyst in a chemical reaction changes and complicates a reaction pathway by evolving with reaction substrates to form various catalytic

[1] The first reaction catalysed by L-proline was discovered as early as 1970's however it is not until 2000 the broad scope of this catalysis has been shown.

intermediates, however, at the end of a reaction the catalyst emerges in its original form.[1, 21] Since a catalyst makes it possible to obtain a final product by a different more energetically favourable pathway, it can also affect the yield and selectivity of a reaction. Therefore the understanding of how this pathway occurs may be useful for process development and process economics. Typically this study is performed through detailed mechanistic investigation on the molecular level of the breakage of bonds in reactants and formation of bonds in products and requires advanced experimental techniques.[1] Traditional mechanistic investigation, which is often undertaken by chemists,[22] primarily involves attempts at observation of the various catalytic species on and off the reaction cycle. This is often achieved with the help of spectroscopic scrutiny using mass spectroscopy (MS), nuclear magnetic resonance (NMR), Fourier transform infrared (FTIR) spectroscopy etc. Furthermore, some other mechanistic probes are also employed, such as computational chemistry, isotopic exchange and solvent effect studies. Halpern in 1981 identified a major limitation with this approach: the failure to relate all findings determined from the prevalent structural and spectroscopic studies to the catalytic cycle through the essential kinetic measurements.[23]

Kinetic analysis of catalytic reactions dates back to 1913 when Michaelis and Menten formulated the correlation between enzymatic reaction rate and substrate concentration.[24] This knowledge allows the mathematical definition of rate laws that describe sequences of the elementary steps of the reaction and, hence, directly relate rate to a reaction mechanism that illustrates how molecules react via intermediates to form, ultimately, the product. Unfortunately kinetic analysis in terms of mathematics is often considered complicated where more than one substrate concentration changes simultaneously. To overcome this problem and simplify the mathematics, kinetics is traditionally evaluated by employing pseudo-zero order conditions in one substrate concentration at a time. In this case for each substrate a separate set of experiment is performed, where concentration of one substrate is artificially fixed at a high concentration, while determining the kinetic order in the concentration of another.[21] This

conventional kinetic approach involves experimental data obtained by carrying out the reactions under conditions far removed from those of practical operation, which may add complications and even change the mechanism of a catalytic reaction. Further, methodologies based on the initial rate data, where a series of experiments is carried out at different initial concentrations and the initial rate is determined for each run, can increase the number of required experiments even more and can lead to ambiguous results in case where a catalyst precursor requires activation.[21, 24] This type of approach cannot provide information about critical issues such as catalyst deactivation/activation although occasionally the presence of a significant reverse reaction or formation of by-products can be avoided.

The reaction progress kinetic analysis methodology recently developed by our group offers a way to overcome the above setbacks of the conventional kinetic approach and obtain experimental data under synthetically relevant conditions.[25] It allows a reduction in the number of experiments while increasing the wealth of obtained kinetic information extracted per experiment. This is because this methodology in contrast to traditional kinetic methods relies on a careful mathematical design of experiments, reaction stoichiometry and on *in situ* experimental tools, which provide accurate and continuous kinetic data sets.

1.3 Thesis Objectives

The introduction has highlighted the value of a kinetic analysis, using the reaction progress kinetic analysis methodology, to extract the maximum amount of information from the minimum number of experiments of high density data. The importance of chiral molecules and weight that asymmetric catalysis has with regard to other methods in the formation of chiral compounds has also been discussed. Organocatalysis amongst the available asymmetric catalyses appears to be academically attractive; however, many transformations have been reported while few experimental kinetic and mechanistic studies have been carried out. These systems show potential for industrial application and moreover catalysts are less expensive and also easy to handle.

The overall aim of this work is to demonstrate the advantageous application of the methodology of reaction progress kinetic analysis in elucidation of the catalytic reaction pathways and therefore to reassess the importance of kinetic analysis in complex organic reactions. The aim of the work is achieved by revealing a broader mechanistic understanding of asymmetric L-proline catalysed reactions, centred upon a comprehensive kinetic study. Two asymmetric reactions considered are: (*i*) aldol and (*ii*) α-aminoxylation, which are both efficient in producing chiral building blocks for the synthesis of the natural products and many non-natural drug molecules.[26, 27] To test the scope of obtained mechanistic knowledge, in addition to proline, its derivative L-proline-tetrazole was also employed.

The primary goal of any kinetic study of a catalytic reaction is to develop a mechanistically meaningful reaction rate law that describes the catalytic cycle. However this can only be achieved when processes occurring on the catalytic cycle can be deconvoluted from those occurring off the cycle. This research demonstrates that with the help of the reaction progress kinetic analysis methodology such knowledge can be acquired and then a driving forces analysis of the reactions can be performed. This analysis can in turn be related to the steady-state rate law based on a proposed set of elementary reaction steps that comprise the catalytic cycle.

A final aim was to compare and discuss the obtained kinetics for both aldol and α-aminoxylation, reactions again highlighting how reaction progress kinetic analysis leads to quantitative mechanistic information.

1.4 Thesis Outline

This thesis is organised as follows. In Chapter 2 the approach to traditional kinetic analysis is compared with reaction progress kinetic analysis, which is a foundation of the current work. The theory behind the derivation of the steady-state rate equation and its usage with reaction progress kinetic analysis are described in detail.

In Chapter 3, an overview of the employed chemistry is provided. The acquired knowledge on mechanisms of proline catalysed reactions is reviewed in details. Also the scope of proline catalysed aldol reactions is shown.

In Chapter 4, an initial kinetic analysis of aldol reaction is carried out. The model aldol reaction and the general experimental set up are discussed.

In Chapter 5, the study of the processes occurring on the cycle and off cycle of the aldol reaction using kinetic and spectroscopic investigations is carried out. The catalysts deactivation pathway is proposed. The effect of water on the rate of aldol reaction in the absence of catalyst deactivation is discussed here. The aldol reaction catalysed by L-proline is also compared to the catalysis by L-proline-tetrazole.

In Chapter 6, detailed kinetic modelling of the aldol reaction is performed. Initially, the global kinetics of the aldol reaction are discussed in terms of a driving force analysis. The observed concentration dependencies are then related to the elementary steps of the proposed mechanism, where the rate limiting step is identified. This is also supported by kinetic isotope effect. Finally, the experimental data are fitted to the rate model.

In Chapter 7, kinetic observations in aldol and α-aminoxylation reactions are compared. This prompted investigations of the interaction of additive species on the catalytic cycle of these reactions. Finally, the results of simulations using the COPASI software of the behaviour of these reactions with additives are presented.

In Chapter 8, a summary of the work and the possible future work directions are presented.

Chapter 2

Methodology of Reaction Progress Kinetic Analysis

One ultimate goal of any kinetic analysis is to find the most suitable mathematical equation to fit obtained experimental data. This allows predicting the rates of a reaction at any given set of the initial conditions. At the same time a mathematical equation must describe the pathway of molecules around the catalytic cycle. Therefore it is essential to consider a number of issues. First, the choice of the mathematical equation must provide a bridge between the elementary steps of a complex catalytic reaction on the molecular level and the globally observed kinetics. Second, the quality of the experimental data must be sufficient for a confident fit of a mathematical expression. Further, oversimplified approximations can similarly prevent a useful outcome.

Therefore these concerns will be discussed here. It will be shown how the methodology of reaction progress kinetic analysis helps to avoid the pseudo-zero order simplification which is often used in a two-substrate reaction. Furthermore, additional benefits this methodology possesses will also be exposed. Thereafter the main *in situ* tools employed in the current work will be introduced here.

2.1 Advantages of Reaction Progress Kinetic Analysis

A frequent approach of obtaining a mathematical expression that describes the rate of a particular catalytic reaction is through the rates of elementary steps that may take place during this reaction. The elementary steps describe the formation of active intermediates as a consequence of the involvement of a catalyst during a reaction. Often the concentration of active intermediate is not readily measurable, therefore an approximation is assumed to express the rate through concentration variables that can be measured. The commonly applied steady-state approximation implies no build up of the active species and therefore makes the net rate of the change of these species negligible or equal zero.[21] As example, Michaelis-Menten equation 2.1 [K_{mm} = Michaelis-Menten constant (in M); [**S1**] = concentration of substrate 1, (in M); rate_{max} = maximum rate that reaction can obtain before the saturation kinetics in [**S1**] is achieved, (in s^{-1})], which was the first mathematical expression correlating rate and concentration, may be developed using the steady-state law.

$$\text{rate} = \frac{\text{rate}_{max}[\mathbf{S1}]}{K_{mm} + [\mathbf{S1}]} \qquad (2.1)$$

Although this mathematical expression was developed for one-substrate enzymatic reactions (Scheme 2.1a) it is now widely used for any catalytic reaction and even for those involving more than one substrate, for example as one shown in Scheme 2.1b for a two-substrate catalytic reaction.[21, 24, 28, 29] In fact, the Michaelis-Menten equation 2.1 can be easily represented via the two-substrate steady-state rate equation 2.2 (the derivation of which can be found in the Appendix 4) by combining elementary steps rate constants k_1, k_{-1} and k_2 and a total catalyst concentration $[\mathbf{C}]_{total}$ as it is shown in equation 2.3.

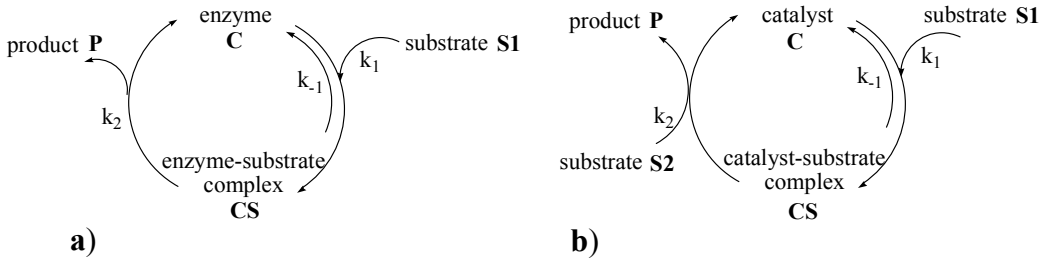

Scheme 2.1 Catalytic reaction network for a) one-substrate reaction; b) two-substrate reaction.

$$\text{rate} = \frac{k_1 k_2 [\mathbf{S1}][\mathbf{S2}][\mathbf{C}]_{total}}{k_{-1} + k_1[\mathbf{S1}] + k_2[\mathbf{S2}]} \qquad (2.2)$$

$$\text{rate} = \frac{k_2 [\mathbf{S1}][\mathbf{S2}][\mathbf{C}]_{total}}{\frac{k_{-1} + k_2[\mathbf{S2}]}{k_1} + [\mathbf{S1}]} \qquad (2.3)$$

Where,

$$\frac{k_{-1} + k_2[\mathbf{S2}]}{k_1} = K_{mm}\,; \quad k_2[\mathbf{S2}][\mathbf{C}]_{total} = \text{rate}_{max}$$

Equation 2.3 highlights an additional complexity that arises with the two substrates reaction: the kinetic parameters describing the mechanism by equation 2.1 are not any more constant but vary with the concentration of the second substrate.

Reaction progress kinetic analysis deals with simultaneously changing concentrations in this mathematical expression by relating the variables among one another via their stoichiometric coefficients. In the catalytic cycle of scheme 2.1b, *X* number of molecules of substrate **S1** reacts with *Y* number of molecules of substrate **S2** in order to obtain *Z* number of molecules of product **P**. Hence each time when a molecule of one substrate is consumed, the molecule of the second substrate is also used up. However the initial difference between two substrate concentrations, which is called *excess* [equation 2.4: [**e**] = *excess* (in M)], should stay constant throughout the course of a reaction at constant reaction densities or volume.[25] In such a case, knowledge of the initial *excess* enables

establishment of the relationship between the concentrations of all reactants at any point of a reaction. Kinetic analysis under synthetically reasonable conditions, with both substrates changing concentration, can be performed when the relationship between them is known.

$$[\mathbf{e}] = \frac{[\mathbf{S1}]_0}{X} - \frac{[\mathbf{S2}]_0}{Y} \qquad (2.4)$$

The advantage of using *excess* can be expressed mathematically: when the concentration of the second substrate **S2** in the steady-state rate equation 2.2 is substituted via the *excess*. The rearranged equation 2.5 shows that $[\mathbf{S1}]$ is only variable at a given set of conditions: constant catalyst concentration, and constant elementary rate constants.

$$\text{rate} = \frac{a'[\mathbf{S1}][\mathbf{e}] + [\mathbf{S1}]^2}{1 + b'[\mathbf{S1}]}[\mathbf{C}]_{total} \qquad (2.5)$$

Where,

$$a' = \frac{k_1 k_2}{k_{-1} + k_2[\mathbf{e}]}; b' = \frac{k_1 + k_2}{k_{-1} + k_2[\mathbf{e}]}$$

The value of *excess* can be large, small; it may be positive, negative or equal zero. Nevertheless, in order to avoid synthetically unreasonable conditions where pseudo-zero order dependency in one substrate is approximated, the value should be chosen such that the concentration of both substrates are within the range to be used in practical application.

Hence a major significance of the methodology comes from its ability to relate two substrate concentrations. As long as the value of *excess* is known, it is sufficient for kinetic analysis of a two-substrate reaction to follow the change in concentration of only one substrate **S1**. The concentration of **S1** can always be related back to the concentration of **S2** via *excess*.

2.1.1 Detecting Catalyst Instability

An additional complexity in catalytic reactions evolves in the cases where the catalyst deactivates over the course of the reaction or the concentration of active catalyst sites changes due to the inhibition/ activation by a substrate or a product. The simple cyclic mechanism presented in Scheme 2.1b for a two-substrate reaction implicitly assumes that the overall concentration of catalytic species within the cycle is constant over time and consecutive turnovers. Hence the study of such competing processes maybe important and useful for two major reasons: (*i*) the industrial viability of catalytic reactions may be dependent upon quantifying catalyst deactivation – it is usually necessary to minimize catalyst deactivation and (*ii*) a true mechanistic understanding of complex multi-step reactions can be only gained if catalyst deactivation is separated from the intrinsic reaction kinetics.[30] If the assumption of constant catalyst is not valid, reaction orders derived from kinetic analysis based on this assumption might be false: that is, if the competing processes are not taken into account, the reaction orders determined will not represent the intrinsic kinetic orders.[31]

When two experiments are carried out with the same *excess* and under identical conditions albeit different initial concentrations of substrates $[\mathbf{S1}]$ and $[\mathbf{S2}]$, the catalytic stability of a reaction can be probed. Equation 2.5 indicates that in such case these two reactions are essentially the same, but initiated from two different starting points. Hence, the kinetic data from these two experiments, when plotted in a manner of the graphical rate equation, that is rate versus substrate concentration, must fall on top of each other. In other words the rates at the same substrate concentration should be equal for both reactions, as it is shown in Figure 2.1a.

If reaction rates are different at the same substrate concentrations, as in Figure 2.1b, this indicates that reactions are subjected to influences other than those described in the rate law of equation 2.5. The lack of overlay in two sets of experiments in Figure 2.1b carried out with the same *excess* value may suggest that catalyst deactivation or product inhibition occurs,

since the reaction that has completed more turnovers (reaction that initially had higher substrate concentrations) exhibits a slower rate under otherwise identical conditions. Once such behaviour has been observed, then future experiments are necessary so that the absence of overlay in the kinetic data may be attributed to one of the possible causes.

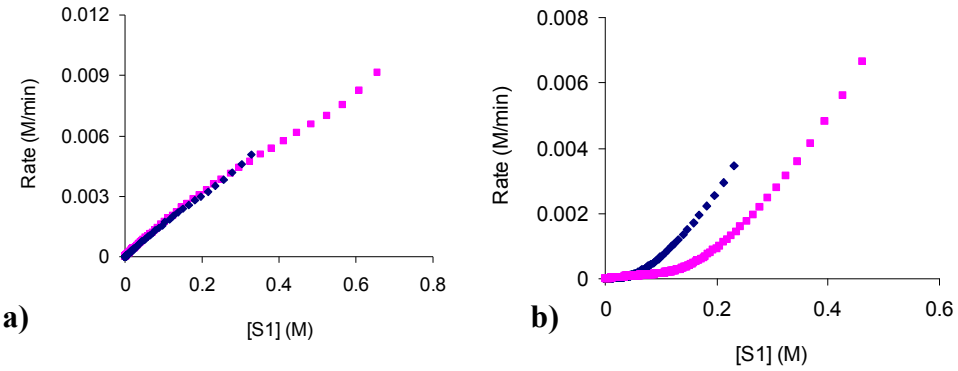

Figure 2.1 Experiments with the same value of *excess*: a) two reactions are not influenced by any other effects rather than described in the rate law b) two reactions are influenced by additional effects.

2.1.2 Obtaining Concentration Dependencies

The mathematical rate equation, several common approximations and detection of the catalytic instability have all been discussed. One goal of a mechanistic approach to kinetic analysis is to probe how rate is affected by various substrate concentrations in order to test the validity of a proposed rate expression. Under synthetically reasonable conditions this can be done by performing several experiments with different values of *excess*.[25]

The rate equation 2.5 contains only two adjustable parameters a′ and b′, while the reaction mechanism described by equation 2.2 has three rate constants: k_1, k_{-1} and k_2. This is analogous to a system of simultaneous equations with more unknowns than independent equations. In order to find a unique solution of such equation system, an additional equation is required. Therefore at least two experiments carried out at different *excess* can supply an extra equation and in principle allow a unique solution for all three rate constants.

The value of carrying out experiments at different values of excess is clear for the case of the rate expression developed in Equation 2.5 for the mechanism proposed in Scheme 2.1b. However, the scope of this kinetic analysis may be broadened to consider cases where the mechanism is not known a priori, where proposing a steady-state rate expression may not be possible. Then by approximating the kinetic dependency to a power law rate expression, the concentration dependencies **m** and **n** can be found using two different excess experiments as shown in Equation 2.6. As discussed in detail for experimental results (see Chapter 6), this methodology allows a general "driving force analysis" of concentration dependencies, which may then be used along chemical information to propose a mechanistic rate expression that describes the elementary steps of a catalytic cycle.

$$\text{rate} = k \cdot [\mathbf{S1}]^{\mathbf{m}} \cdot [\mathbf{S2}]^{\mathbf{n}} = k \cdot [\mathbf{S1}]^{\mathbf{m}} \cdot \left(Y \cdot \left(\frac{[\mathbf{S1}]}{X} - [\mathbf{e}] \right) \right)^{\mathbf{n}} \qquad (2.6)$$

Furthermore, this approach of understanding the reaction concentration dependencies under synthetically reasonable conditions allows streamlining process development and process scale up in cases where development timeline do not allow a full mechanistic analysis of the elementary steps in a catalytic cycle.

2.2 Acquisition of Experimental Data

As has been suggested, the lack of high quality of experimental data can compromise the mathematical model: for example, several different models may be fit to the same data. Therefore the accuracy of conclusions that can be drawn using kinetic analysis is highly dependent on the quality and quantity of data that can be acquired.[32]

Constant volume batch reactors, which are employed in the current work, are one of the standard settings for kinetic data collection that traditionally involve concentration or conversion measurements via sampling experiments. The discrete sampling method carries some significant limitations for further detailed kinetic analysis. First of all only a limited

number of samples can be obtained per a reaction. Even though it may not be a drawback for a simple system, with an increasing complexity in a catalytic system the frequency of data collection can be of a crucial matter. For example, in palladium catalysed hydrogenation reactions the critical point of changing kinetics could be missed if only concentration analysis by discrete sampling experiments would be carried out.[33] Another disadvantage worth mentioning is accuracy loss during sample withdrawal from reaction mixture for off-line analysis due to the alteration of chemical composition. Both shortcomings can affect the accuracy of estimated kinetic parameters regardless the analysis method employed: either using the graphical approach or nonlinear regression analysis.

With significant advances in experimental and computational techniques there are more sophisticated tools developed capable of monitoring the entire progress of a reaction – *in situ* tools. These instruments provide voluminous data sets (rate, concentration, time), which are of high quality and accuracy. Hence the mentioned disadvantages can be overcome and more viable information can be obtained. Now there are accessible *in situ* NMR, UV-Vis, and FTIR spectrometers and, additionally, reaction calorimeters, which, in contrast to the former tools, measure directly the concentration differential or, in other words, the rate of a reaction.

2.2.1 Reaction Calorimetry

Calorimetry, which the main purpose is the measurement of energy, is one of the older scientific instruments with the records of its utilization dating back to the 18th century.[34] The basic concept of a calorimeter attributes to the phenomenon that nearly every process liberates or consumes the infinite amount of energy in the form of heat. Differential scanning and bomb calorimeters are among the most common instruments used in industrial settings for the process safety, quality control, and measurement of various thermodynamic properties of a sample.[35]

Further, however, reaction calorimeters expanded the application of calorimetry in process development and quality and safety control.[34]

Reaction calorimeters, in contrast to other type of calorimetry, are based on the measurement of heat flow evolved or consumed during the reaction as a function of time while maintaining precise control of the reaction mixture temperature. Measuring the temporal heat flow allows employment of the reaction calorimeter in monitoring of reaction kinetics in addition to thermodynamic properties of a chemical process.

Hence the main principle of the reaction calorimetry is based on the measurement of heat flow over the course of a reaction, which is directly proportional to the global rate of a catalytic network under isothermal conditions. However, the measured heat flow reflects the reaction rate only in the absence of substantial thermal effects caused by other processes. Equation 2.6 demonstrates the relationship between overall reaction rate and the heat flow $\boldsymbol{q}$ measured by the reaction calorimeter under isothermal conditions. The rate is proportional to heat flow through the thermodynamic heat of a reaction $\Delta \boldsymbol{H}_{\text{rxn}}$, which is the total heat produced per mole of substrate consumed. This thermodynamic parameter is proportional to the integral of the temporal heat flow profile. The fractional conversion of a limiting substrate is identical to the fractional heat evolution at any time during the course of a reaction, written in Equation 2.7. Substrate and product concentration profiles can be calculated via the fractional conversion and the initial substrate concentration (see Appendix 1).

$$\text{rate} = \frac{q}{\Delta H_{rxn} \cdot reaction\ volume} \qquad (2.6)$$

$$\frac{\text{conversion}}{\text{conversion}_{end}} = \frac{\int_{t=0}^{t=t} q(t)dt}{\int_{t=0}^{t=t_{end}} q(t)dt} \qquad (2.7)$$

It must be noted that the equations 2.6 and 2.7 are only true when volume of the reaction is considered constant. This is possible when the density of the

reaction solution stays approximately unchanged during the transformation of the reactants to the product.

2.2.1.1 Caveats in the Reaction Calorimetry

It has already been suggested that multiple reactions may complicate the use of reaction calorimetry to monitor reaction rate. Two cases can be considered: *i*) consecutive and *ii*) parallel reactions.

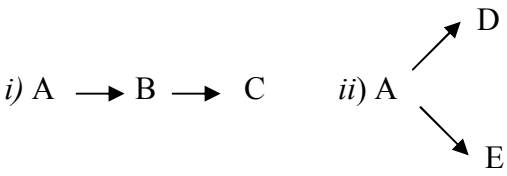

In case of the consecutive reactions (*i*), measured heat (q_{total}) equal to a summation of heats produced by the initial conversion of the substrate A to intermediate B (q_A) and consecutive conversion of this intermediate B to product C (q_B) as shown in equation 2.8:

$$q_{total} = q_A + q_B = (\text{rate}_A \Delta H_A + \text{rate}_B \Delta H_A) \cdot \textit{reaction volume} \quad \text{(eq. 2.8)}$$

Hence the caveat of this case is that the conversion of the initial (limiting) substrate cannot be obtained directly from the measured heat data before the heats of consecutive reactions are deconvoluted. Therefore additional analysis methods must be employed to enable determination of the heats of the separate consecutive reactions.[33]

In case of the parallel reactions (ii), measured heat (q_{total}) equal to a summation of heats produced by the formation of product D and product E from substrate A as shown in equation 2.9.

$$q_{total} = q_A^D + q_A^E = (\text{rate}_D \Delta H_D + \text{rate}_E \Delta H_E) \cdot \textit{reaction volume} \quad \text{(eq. 2.9)}$$

Hence in the similar manner the conversion of the initial substrate cannot be related to the formation of one particular product. However, if the selectivity between two products D and E is constant over the course of a reaction, then the heats produced by each reaction can be related via the mole fraction of these products.

The other point concerns the length of the reactions. When the reactions are slow (>ca 8 h), then the signal-to-noise ratio becomes low, which make impossible to use the data further for analysis. In the case of the very fast reactions (< ca 10 min) the measurement of the heat can be unreliable due to the lag time of the heat flow signal (see Section 4.2.2 for more detailed discussion on the lag time and the method used during this work to correct it).

Reaction calorimeters have already been exploited extensively for the kinetic studies of a few complex catalytic systems. During the study of palladium and platinum catalysed hydrogenation reactions, reaction calorimetry combined with other chemical analysis method allowed deconvoluting two consecutive hydrogenation reactions and determining the heat of formation of unstable in air intermediate, which otherwise could be difficult.[33] It also has proven to be a powerful tool in the investigations of rhodium catalysed Michael addition [36] and palladium catalysed amination reactions.[37, 38]

2.2.2 FTIR spectroscopy

Many spectroscopic methods, which are based on the interaction of radiation and a sample, have been around for several decades and mainly used for the structural identification of a component. However with significant technological progress, after discovery of attenuated total reflectance technology,[39] Fourier transform infrared (FTIR) spectroscopy may achieve a particular place in the in-depth study of catalytic reactions and, further, for kinetic analysis of complex systems.

Attenuated total reflectance (ATR) FTIR technology allows faster and more reproducible spectra acquisition and it is independent of the thickness of a sample.[1] The basic concept of this technology relies on the measurement of the change that occurs in an internally reflected infrared radiation when it contacts a sample and excites certain bonds to vibrate. An infrared light beam, directed onto the crystal with high refractive index, such as diamond

[1] Mettler Toledo ATR-FTIR manual

or ZnSe (zinc selenide), capable to protrude only a few microns (0.5μ-5μ) beyond the crystal surface and into a sample. Most importantly, the improved spectral acquisition and reproducibility together with the robustness of the ATR-FTIR spectrometers provide an excellent foundation for the time resolved spectroscopy to obtain a high quality temporal data.

The time resolved or *in situ* ATR-FTIR spectroscopy relies on the same Beer and Lambert principle which relates the concentration of a sample with the absorbance of infrared light radiation.[40] The change in infrared radiation intensity arises due to the absorption of this electromagnetic radiation by the vibration of the specific sets of bonds from within a molecule. As a consequence, the FTIR spectrometer collects the interferogram of a sample signal and after Fourier transform mathematical application outputs the specific spectrum of a sample. For example, C=O stretch of carbonyl bond appear at around 1700 cm^{-1} in a variety of molecules. The intensity of each peak can be related to the concentration of this molecule in a sample. Equation 2.10 [α = molar absorptivity coefficient, (in $M^{-1}cm^{-1}$); $\boldsymbol{l}$ = light passage through the sample, (in cm)] represents Beer & Lambert law which highlights that the absorbance $\boldsymbol{A}$ of a substrate is directly proportional to its concentration [**S1**] through the specific absorptivity α and light pathway $\boldsymbol{l}$.

$$\boldsymbol{A} = \alpha \boldsymbol{l} \cdot [\mathbf{S1}] \quad (2.10)$$

Hence the FTIR measurement directly provides the concentration or fractional conversion profiles of any component in the reaction. The more detailed process of obtaining kinetic experimental data is described in Appendix 1.

The rate of a reaction can be obtained as a derivative of the temporal concentration profile as shown in Equation 2.11.

$$\text{Rate} = -\frac{d[\mathbf{S1}]}{dt} \qquad (2.11)$$

An accurate determination of rate from this type of *in situ* tool requires high frequency of sampling.

2.2.3 The Validation of the *in situ* Tools

Whatever the technique is used to follow the progress of a reaction, it is important to confirm that the measurement correlates with actual conversion of substrate molecules to product. This can be done by occasionally sampling reaction mixture over the time and analysing the concentrations with a known analytical method (for example, HPLC, GC). Alternatively, a separate validated *in situ* technique that relies on a different property of a reaction can be employed and the substrate conversion verified.

2.3 Concluding Remarks

The advantages of reaction progress kinetic analysis methodology over the conventional kinetic approach have been discussed here. The overall goal of any kinetic analysis was also explained. However in order to perform kinetic analysis under synthetically relevant conditions the vital components was shown are: (1) the knowledge of the reaction stoichiometry; (2) the in situ acquired experimental data; and (3) careful mathematical design of experimental conditions.

Chapter 3

Organocatalytic Reactions: Background

The kinetic approach undertaken during the current study of the proline catalysed reactions has been discussed in the preceding chapter. Here it will be shown where the proline catalysis comes in the general classification of organocatalysts. Background knowledge of proline catalysis will also be provided, which is necessary for the further mechanistic study of the reactions with which we are concerned. Finally, the importance of the aldol and α-aminoxylation reactions will be demonstrated.

3.1 General Classification of Organocatalysts

One particular feature of many organocatalysts is a possession of two functionalities of opposite character – basic and acidic, which allows activation of both the unmodified donor and the electrophile, in a way mimicking processes in nature.[41] Although organocatalysts are not the only catalysts having such qualities (some metal complexes have the same feature),[42] this makes them an important area of research in recent years. Often organocatalysts are classified with regard to their ability to initiate catalysis into four general groups: *Bronsted base* and *Bronsted acid* catalysts; *Lewis base* and *Lewis acid* catalysts.[16, 43]

Although hydrogen bonding plays an important role in most of organocatalysis,[44] in *Bronsted base* and *Bronsted acid* catalysis hydrogen bonding takes an immediate role, i.e. initiation of a catalytic cycle occurs via deprotonation and protonation of a substrate, respectively. Such catalysis schematically is depicted in Scheme 3.1. The typical example of the *Bronsted base* catalysis is hydrocyanation reactions of aldehydes[45] or imines.[46] In such a case, a lone pair of nitrogen in a catalyst (Cat_B:), as commonly occurs as cyclopeptides. This species interacts with hydrogen cyanide (schematically called HS in Scheme 3.1a) by means of hydrogen bonding, consequently forming a carbanion ($Cat_BH^+S^-$), or cyanide ion. The cyanide ion coordinates aldehydes or imines in such a way that to form various chiral nitriles. *Bronsted acid* catalysis[47] often involves reactions of imines (S: in Scheme 3.1b) catalysed by catalysts containing urea or thiourea motifs (Cat_AH).[48] Hydrogen bonding between urea hydrogen and the nitrogen of an imine substrate is formed as a consequence of the proton transfer producing substrate carbcation ($Cat_AS^-H^+$). The latter is attacked by an activated nucleophile to form amine products.

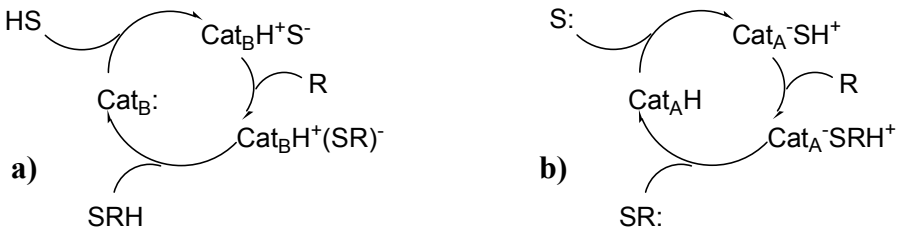

Scheme 3.1 a) Bronsted base catalysis b) Bronsted acid catalysis.

Lewis base and *acid* catalysts act as a base or acid, donating or accepting an electron pair, as depicted in Scheme 3.2. *Lewis acid* catalysts are often involved in the catalysis of phase transfer reactions, where two substrates are located in different phases: the organic solvent phase and the aqueous phase.[49] The catalysts facilitate the migration of the nucleophile (S: in Scheme 3.2b), such as cyanide salts,[50] from one phase to the another, where reaction can proceed. Cinchona alkaloids and their derivatives are often the catalysts in alkylation of glycine derivatives[51] and epoxidation of enones[52] proceeding via *Lewis acid* catalysis.

Scheme 3.2 a) Lewis base catalysis b) Lewis acid catalysis.

Lewis base catalysts occur as a dominative group in organocatalysis operating through the diverse mechanism.[16] Substrates can be converted either to activated nucleophile or electrophile. In all cases the catalytic cycle is initiated by donating the lone electron pair of a catalyst (Cat_B:) to a substrate consequently forming active species such as nucleophilic ammonium enolate,[53] electrophilic iminium ion,[54] nucleophilic enamine[55] and etc as depicted in Scheme 3.2a.

Enamine along with iminium catalysis became a powerful strategy that has delivered the highly useful and enantioselective reactions.[56] It is believed that these two types of catalysis are interrelated and occur with catalysts that possess secondary amine functionality, such as L-proline shown in Figure 3.1 (L- and D- labelling of two enantiomers is typically used with natural amino acids and sugar compounds and identifies the ability of two enantiomers to rotate the plane of polarised light passed through a solution of the compound: L-enantiomer rotates to the left, while D- to the right). The lone pair of nitrogen of L-proline and its derivatives allows it to react as a nucleophile with carbonyl compounds, while at the same time, the acid functionality may help to facilitate the subsequent interactions.[27] Such an asset ensured the name for proline of a "micro-aldolase"[27] or a "simplest enzyme".[41]

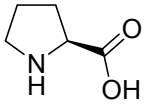

Figure 3.1 Structure of natural amino acid L-proline.

The reversible reaction between an amine catalyst and a carbonyl substrate, first forms a tetrahedral hemiaminal species (Scheme 3.3). Upon loss of water, an iminium ion is found. The iminium ion is capable of reacting with various nucleophiles, such as dienes in the Diels-Alder reactions.[57] Rather than reacting with other substrates, the iminium ion may deprotonate to form a nucleophilic enamine intermediate mimicking the catalysis by class I aldolases. The electron density at the C=C double bond enables the enamine to react as a nucleophile with various electrophiles, such as aldehydes,[27] imines[58] or undergoes pericyclic transformations.[59, 60] Therefore introduction of a nucleophilic or electrophilic substrate may induce respectively iminium ion or enamine catalysis due to these intermediates being in equilibrium.

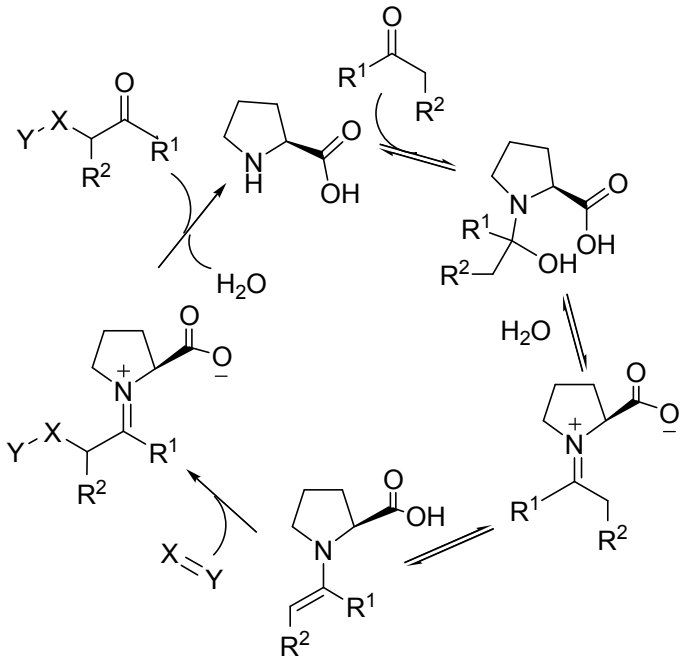

Scheme 3.3 Catalytic cycle via enamine intermediate proposed in analogy to class I aldolases enzymes.

3.2 The Mechanistic Milestones in Enamine Catalysis

The implication of the enamine intermediate in proline catalysed reactions has been considered as early as 1970's when the proline was first discovered to catalyse the intramolecular aldol reaction by Hajos, Parrish and Eder, Sauer and Wiechert.[59, 60] A new bond is made during the nucleophilic attack by enamine and is accompanied by the assistance from the carboxylic

acid group of the enamine toward the oxygen of the attacked electrophile. Finally in order to release the product and the catalyst back into the cycle, one molecule of water, released during formation of the enamine, hydrolyses the product iminium ion (Scheme 3.3).[56]

3.2.1 Evidence Against Enamine Catalysis

Despite observation of enamine intermediates in biochemical catalysis[61] the enamine intermediate formed from proline has not been isolated and its detection remains elusive.[62, 63] Swaminathan and co-workers were the first who have attempted to carry out the investigation of the enamine formation by NMR and FTIR techniques, neither of which was able to detect this intermediate.[63]

3.2.2 Evidence Supporting Enamine Catalysis

The support towards enamine catalysis comes predominantly from computational studies.[64] Theoretical investigations by Houk and co-workers evaluated several mechanistic possibilities.[65] Their results showed that the transition state occurring via an enamine intermediate with the participation of a carboxylic proton is the most energetically favourable in both inter and intramolecular aldol reactions. The intermolecular hydrogen bond stabilises the developing ionic charges in the transition state and therefore reduces energy barrier. The influence of polar solvents on hydrogen bonds in aldol reactions can be seen through even lower energy barriers.[66, 67]

These theoretical calculations were also able to rationalise the experimentally observed asymmetric selectivity in the proline catalysed reactions.[68, 69] It was suggested that the most energetically favourable enamine structure, which is responsible for the formation of a major enantiomer, has its double bond pointing away from carboxylic acid moiety. The ultimate conformation of the product is also dependent on the position of incoming electrophile. Generally, a large substituent of electrophile assumes the pseudo-equatorial arrangement (Scheme 3.4a), while the

pseudo-axial position of the substituent (Scheme 3.4b) will instigate the opposite stereoselectivity.[68]

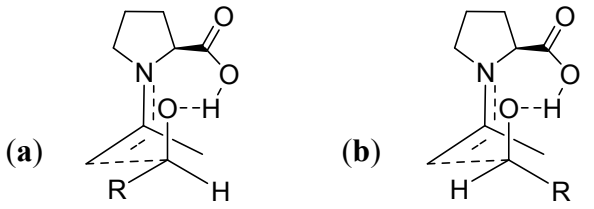

Scheme 3.4 Arrangement of a large substituent of electrophile during the C-C bond formation instigating the opposite product stereoselectivity: (a) equatorial; (b) axial.

Marquez et al recently published intriguing results obtained by ESI-MS spectroscopy, which revealed the possible presence of an enamine intermediate in the aldol reaction.[70] However the same group has been unable to observe the oxazolidinone of proline and acetone, which is readily detectable by NMR,[71] while the oxazolidinones between proline and an aldehyde were observed. The discussed experimental procedures allow the differentiating the enamine from the oxazolidinone via their fragmentation patterns; however, since these two isomers are likely to be in a rapid equilibrium (Scheme 3.5), it is uncertain if this produces an unambiguous result. Spectroscopic studies by Gryko and co-workers of the condensation of acetone with proline derivatives, where the ESI-MS technique was also employed, observed the corresponding imidazolidinethionone but was unable to distinguish the enamine explicitly.[72]

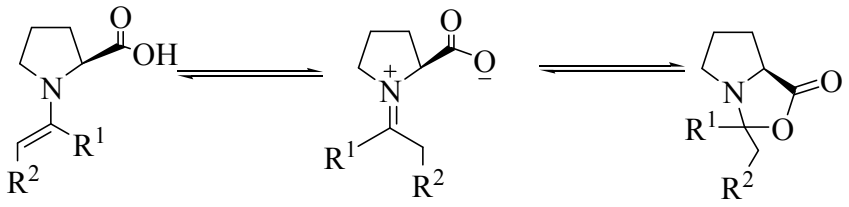

Scheme 3.5 Rapid equilibrium between enamine and oxazolidinone.

Spectroscopic observation of oxazolidinones between amine catalysts and carbonyl substrates has also suggested that it could be an active reaction intermediate. However due to the lack of its nucleophilicity, the existence of oxazolidinones were considered to be more likely "parasitic" in the

proline catalysed reactions.[71] Nevertheless, this assumption has recently been challenged by proposing a role of oxazolidinones from proline and ketone in the stereochemical outcome of the proline-catalysed reactions.[73]

Additional experimental evidence supporting the existence of enamine intermediate in the proline catalysis comes from the experiments carried out by List el al in the presence of isotopically labelled ^{18}O-water.[71] The incorporation of up to 90% of the ^{18}O in the aldol product signifies the formation of a water molecule which takes part in the final hydrolysis step. This indirectly supports the initial formation of iminium ion/enamine species.

There are only limited results published concerning kinetic investigations of proline catalysed reaction. Most findings regarding the aldol reactions provide one point analyses where rate/conversion is not investigated over the time of the reaction.[74, 75] Also, knowing that various "parasitic" reactions with the proline may prevail, deconvolution of processes on and off the cycle should be critical for valid mechanistic conclusions to be reached. This has not been a case, as will be discussed in the context of the role of water (Chapter 5).[75] Assuming enamine catalysis in the aldol reaction, a conclusion about rate acceleration by water is counterintuitive unless product hydrolysis is the rate limiting step.[76] Aldol reactions catalysed by nornicotine, which is also thought to occur via an enamine mechanism, show slower rates when carried out in water.[77] There is still no definitive knowledge on the rate limiting step in that case, which in fact was proposed on the basis of the computational studies and with respect to similar mechanisms in enzymatic chemistry.[29, 67] Although, the rate limiting step can be simply assessed by a kinetic study, none was performed in the previous works.

3.3 Solvent Effect

Solvent effects in proline catalysis are not straightforward and could affect rate/conversion and enantiomeric excess of the reactions. Moreover rate is also limited by the proline's low solubility in most organic solvents and

therefore the solvent effect is often misleading. Despite this, the choice of a solvent is often based on the nature of reacting components. For example, the predominant solvent media for the aldol reactions are the polar dimethylsulfoxide (DMSO) or dimethylformamide (DMF). As it has been highlighted earlier, such solvents may be important in stabilising the ionic charge of the transition state, and, hence, lowering the energy barrier. When aldol reactions are performed in the less polar solvents, such as chloroform, or polar protic, such as methanol, the significant decrease in the reaction rate is observed, which also accompanied by the fall in the enantiomeric excess.

Nevertheless, the solvents in the general enamine catalysis are not limited to highly polar ones. A number of reactions are successfully performed in chloroform,[78, 79] dichloromethane[80] and acetonitrile.[60, 81] As example, the α-aminoxylation reaction showed outstanding performance in both chloroform and dimethylsulfoxide, reaching 99% in enantiomeric excess and conversion, while α-amination in dichloromethane.[26, 79]

3.4 The L-Proline catalysed Aldol Reactions

The general mechanistic knowledge concerning proline catalysis has been discussed. Next the scope of aldol reactions catalysed by proline will be examined. This discussion should provide an understanding of possible reaction outcomes and suggest the best set of reactions for further mechanistic investigation.

The aldol reaction is one of the most fundamental and effective processes for forming carbon-carbon (C-C) bonds in organic chemistry and biochemistry. Typical components of an aldol reaction include a carbonyl pro-nucleophile such as an aldehyde, ketone or carboxylic acid derivative, and a carbonyl electrophile, usually an aldehyde. These reactions are not straightforward in working out the outcome as many aldehydes and ketones can form their homo-aldolisation products. In order to avoid or significantly reduce the unwanted products, appropriate conditions must be chosen. In addition, there is a general rule for aldol reactions that helps in controlling

the outcome. It implies that (*i*) only one carbonyl must be capable of enolization, while (*ii*) the other carbonyl must be more electrophilic than the enolizable carbonyl.[6] Possession of α-H in the structure of carbonyls makes enolization possible and, commonly, reduces carbonyl electrophilicity. Electrophilicity or reactivity towards nucleophilic attack by enolate, generally, improves with decrease in number of α-H. When rule is not followed, the yield and selectivity of a cross-aldol product is expected to decline. Therefore aldol reactions catalysed by proline can be divided into two main categories: reactions between ketones and (*i*) non-enolizable aldehydes and (*ii*) enolizable aldehydes. Many of these reactions catalysed by proline provided efficient routes towards a number of natural products.[82-90]

3.4.1 Reactions between Ketones and Non-enolizable Aldehydes

As it could be predicted, the proline catalysed aldol reactions, such as in Scheme 3.6 between ketones as aldol donors and non-enolizable aldehydes, such as aromatic, α-branched and some α-cyclic aldehydes, as aldol acceptors, should show the best performance, which was also demonstrated by several researchers.[27, 91] Since aldehydes generally are more electrophilic than ketones, the enamine (which, in a way, is a form of enolate) of the ketone attacks more reactive aldehydes, rather than itself, consequently forming the crossed aldol product.

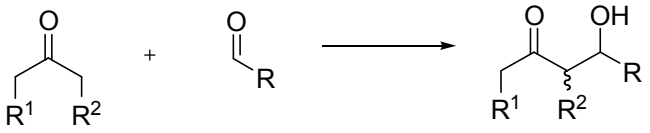

Scheme 3.6 Aldol reactions between ketone and non-enolizable aldehydes.

This proline catalysed aldol reaction with acetone as an aldol donor has received the most attention. In such reactions the cross-aldol product was formed with 96-99 % enantiomeric excess (*ee*) and in yields varying between 81-97% for the aliphatic α-branched aldehydes and with 60-84%

enantiomeric excess and in 62-94% yields for cyclic and aromatic.[27, 91, 92] As aldol donors, several other ketones were tested, such as cyclic ones,[93, 94] where aldol product was achieved in slightly lower yields of 41-85%, however with comparable enantiomeric excess of 76-97%. Utilization of hydroxyacetone as an aldol donor allowed obtaining a range of vicinal diols in 51-95% yields and with 67-99% enantiomeric excess.[95]

3.4.2 Reactions between Ketones and Enolizable Aldehydes

Reactions between ketones and α-unbranched aldehydes as aldol acceptors, shown in Scheme 3.7 present a challenging endeavour. Both α-unbranched aldehydes and ketones are capable of undergoing enolization and attack a more electrophilic carbonyl of a mixture, which in this case is the aldehyde. As expected, along with the cross-aldol product, these reactions lead to the undesirable homo-aldolization products, which reduce the yield of the cross-aldol product.[93]

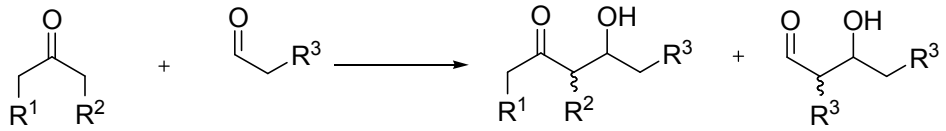

Scheme 3.7 Aldol reactions between ketone and α-unbranched aldehydes.

Therefore yields obtained for such proline catalysed cross-aldol reactions varied between 22-38% and with enantiomeric excess of 36-97%.[91, 93, 95] However the enolization of α-unbranched aldehydes was successfully utilized in the aldol reactions with non-enolizable ketones, like ketomalonate, which is shown in Scheme 3.8. The important attribute of such ketones must be high reactivity; otherwise an enolizable aldehyde would rather react with itself. Jorgensen showed that aldol product of such proline catalysed reactions can be obtained in high yield of 88-94% and with reasonable enantiomeric excess of 84-90%.[96]

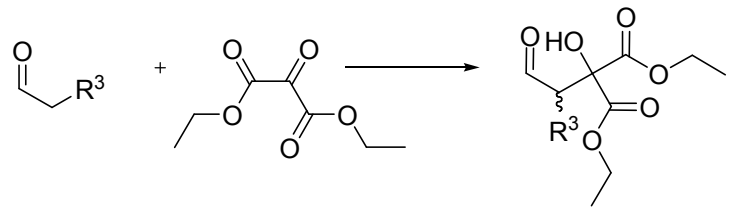

Scheme 3.8 Aldol reactions between α-unbranched aldehydes and ketomalonate.

The other significant milestone in proline catalysis was achieved by MacMillan and co-workers who developed a method of carrying out cross-aldolisation with high selectivity.[97] Slow injection of the enolizable α-unbranched aldehydes into the reactive mixture with various aldehydes allowed the aldol product to be obtained in reasonable yields of 80-87% and with 99% of enantiomeric excess.

The practical application of the proline catalysed aldol reaction was extended with several other aldol donors and acceptors. It worth mentioning 4-thianone, as an aldol donor, which is utilized in the formation of polypropionate-derived pheromones[75, 83] and tetrapropionate synthons[82] and dioxanone[84-86] with α-oxyaldehydes[87, 88] in the synthesis of various carbohydrates, such hexose,[87] azasugars,[85] polyols and aminols.[86] As aldol acceptors α-ketoesters,[89] α-keto phosphonate[90] were employed to produce tertiary alcohols that are extremely important for the synthesis of enantiomerically pure natural products and pharmaceuticals.

3.5 Concluding Remarks

To conclude this chapter, it must be said, that the understanding of proline catalysed reactions has been greatly assisted by advanced analytical technologies, and also by theoretical/computational chemistry, which support the likelihood of an enamine intermediate in proline catalysis despite the fact that this species has not been isolated or observed spectroscopically. Nevertheless, it was shown that kinetic and mechanistic investigations in organocatalysis have been much slower to follow.

The broad scope of proline catalysed aldol reactions has also been demonstrated, which can be utilised in the production of several natural

products and maybe in future pharmaceuticals. Therefore to continue the investigation of these reactions, broadening our mechanistic understanding may be a key factor in increasing the awareness and prospects of this catalysis for industrial application.

Chapter 4

Experimental Set up and Initial Kinetic Investigation of the Aldol Reaction

The preceding chapters highlighted several mechanistic aspects of proline catalysis showing a likelihood that this catalysis may occur via enamine intermediate. Therefore kinetic information may provide an additional support for this mechanism. Hence this chapter will be concerned with the initial kinetic investigation, which was carried out for the model L-proline catalysed aldol reaction chosen for our studies. Here the same excess protocol will be employed, which as described in preceding sections can assess the catalytic robustness. Primarily, such an investigation is concerned with understanding and deconvoluting the role of processes on and off the catalytic cycle, which, as it has been noted, is critical before moving on to detailed kinetic analysis of the cycle itself. Also this chapter discusses the general experimental set up and procedures employed in the current research during the kinetic investigation. The set up is common for both aldol and α-aminoxylation reactions and, if otherwise, the procedure is indicated in the text.

4.1 The Model Reaction – The Aldol Reaction Selected for the Kinetic Investigation

For the purpose of reducing the complexity of the current investigation, the standard aldol system employs the aldehyde that does not possess an α-H, such as aromatic aldehydes. In such a case, the formation of a major side-product – aldehyde homo-aldol product – will not be possible. Acetone is often used as an aldol donor, in addition is inexpensive ketone, and therefore was chosen as the enolizable carbonyl in the reaction shown in Scheme 4.1.

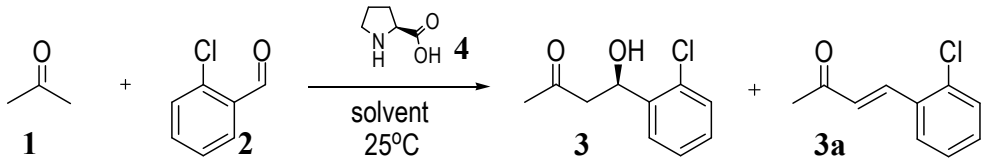

Scheme 4.1 Standard aldol reaction between acetone and *o*-CBA.

DMSO and DMF were shown to be the most desirable solvents for use with the aldol reactions (see sections 3.3-3.4) and were therefore chosen in the current study. Hence the aldol reaction of Scheme 4.1 used as a model during current mechanistic study is a reaction between acetone **1** and aromatic aldehyde – *o*-chlorobenzaldehyde (*o*-CBA) **2** carried out in DMSO (DMF) at room temperature. The product of this reaction is *β*-hydroxy ketone **3**. The major side product that was observed during this reaction is α,β-unsaturated ketone, or aldol condensation product **3a**.[27]

4.2 The Experimental Set up during Kinetic Investigation

Reactions were carried out in Omnical Insight CPR220 reaction calorimeter with internal magnetic stirring, which allows continuous monitoring of the instantaneous enthalpy balance around the vessel. The sample vessel is a 16 mL septum-cap vial equipped with a stirring bar. This reaction calorimeter operates by a differential heat conduction principle in which the heat released or consumed by a reactive system is conducted away from the sample to the thermoelectric Peltier device. For external temperature

control, the calorimeter also incorporates a PC-controlled circulating bath, which additionally ensures the isothermal conditions of a reaction and reduces the signal noise. The heat flow data, measured at intervals of 2-6 seconds, is proportional to the reaction rate as was discussed in the paragraph 2.2.1. Prior to the start of an experiment, the calorimeter and external bath reaches a thermal equilibrium at the set reaction temperature.

For the typical experiment weighed amount of L-proline **4** (Lancaster) was directly added to the reaction vessel. Typically the amount of used solvent was as much as required to make the total reaction volume to 5 ml. After an addition of known amount of acetone (Aldrich) in case of aldol reaction, the tightly closed vessel was carefully placed in the calorimeter and stirred at 300 rpm until thermal equilibrium (ca. 40-60 minutes) was reached and the baseline was stable (±0.01mW/min). In order to avoid the contribution from sensible heat ($c_p\Delta T$ terms unrelated to reaction heat), which can arise due to the injection of solution of different temperature, a syringe containing known amount of the second substrate (aldehyde) was placed in the sample injection port of the calorimeter and was also allowed to reach thermal equilibrium with the rest of a reaction mixture. Once thermal equilibrium was reached, reaction was initiated by rigorously injecting this substrate into the reaction mixture. The syringe was weighed before and after injection in order to establish exact amount of the injected substrate. At the end of the reaction, when the heat flow signal returned to the baseline, the reaction sample was taken for the work up and further investigation by the appropriate analytical method, such as HPLC. The work up procedure is presented in the Appendix 2. Conversion was ascertained by determining the concentration of a limiting substrate remaining at the end of the reaction.

4.2.1 Correction of Heat of Mixing

Usually at the outset of a reaction, a very sharp heat flow signal was observed for both aldol and α-aminoxylation reactions. This signal is associated with the heat of mixing occurring when the injected aldehyde is mixed with the rest of the reaction components (see Appendix 1). This heat was quantified in the separate control experiments, performed under the

same conditions as an original reaction, albeit in the absence of the catalyst. Hence such experiments allowed separating the heat that arises due to the mixing from the heat produced by a reaction.

4.2.2 Correction of Heat Flow Signal: Lag Time

While calorimeter calibration to establish Joule effect constant (an increase in heat resulting from the passage of a current through a conductor) is performed by the manufacturer, the heat flow data obtained was corrected for the time which it takes for the heat from the reaction to reach the sensor: lag time. The calibration of the data can change the maximum heat observed, the shape of the heat flow curve and also shift the reaction time. This calibration is usually performed after the reaction has been completed.

Before initiating the calibration, it is ensured that a stable baseline has been achieved after each experiment. Then the calibration heater is switched on. The heater supplies constant heat (ca 16 mW) to the sample and the heat flow curve increases to this constant value. Ideally the heat flow increase to constant value should be instantaneous, however in practice, a lag time occurs (Scheme 4.2a: blue curve). Once a steady heat flow value is reached the calibration heater is turned off. The heat then falls to the baseline value achieved prior calibration, which again occurs with a delay (Scheme 4.2a: blue curve). This non-ideal behaviour is corrected by applying a mathematical correction to the data based on an algorithm that estimates the time lag (Tau parameter). This is estimated in such a way that the calibration curve is approximated to a square wave (Scheme 4.2a: pink curve). Once the Tau-correction value has been established it is applied to the entire measured heat flow data of an experiment (Scheme 4.2b). Typically the Tau-correction value is between 2-2.30 minutes and it is dependent on the reaction vessels and the port of the calorimeter used, and solvent system.

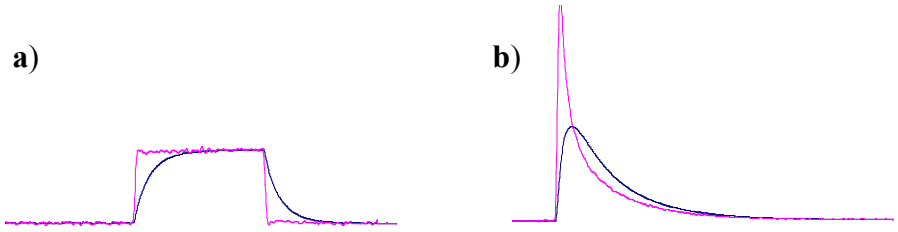

Scheme 4.2 Mathematical correction of heat flow data: a) square wave; b) experimental data. Blue line: uncorrected data; pink: corrected data.

4.3 Validation of Experimental Data

The importance of validating the obtained heat flow data was discussed earlier in Section 2.2.3. In the current work the fractional conversion obtained from the reaction calorimetry was always compared to the conversion obtained by FTIR and/or HPLC methods (Figure 4.1). Experimental procedure for reaction carried out in the *in situ* FTIR spectrometer (ReactIR 1000) is similar to the procedures used with reactions carried out in the reaction calorimeter discussed in preceding paragraphs, with the only difference that the total volume is 15 ml.

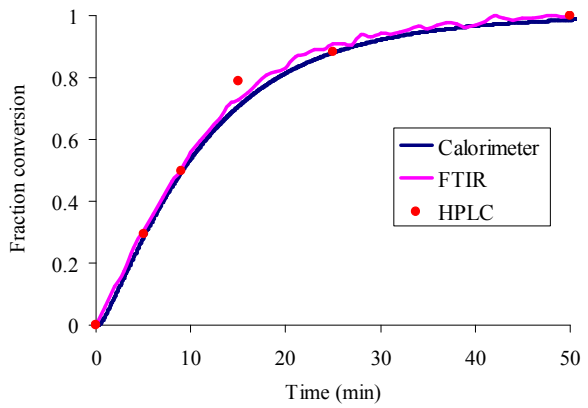

Figure 4.1 Fraction conversion vs. reaction time as measured by in situ reaction calorimetry and FTIR, and sample analysis by HPLC for the aldol reaction of Scheme 4.1 carried out in DMSO. Reaction conditions are: $[\mathbf{1}]_0 = 2.75$M, $[\mathbf{2}]_0 = 0.5$M, $[\mathbf{4}] = 0.05$M. Product enantiomeric excess = 68%. The furthest point is within 10% error bar.

In the case of the aldol reaction, as a rule, peaks belonging to *o*-CBA and aldol product at three wave numbers were followed: at 1594 cm^{-1} and 1270 cm^{-1} for *o*-CBA and at 1034 cm^{-1} for aldol product. In accordance with "Interpretation of infrared spectra practical approach" it was assumed

that 1594 cm^{-1} and 1270 cm^{-1} correspond to the aromatic ring stretch and skeletal C-C vibration of the *o*-CBA, respectively, while 1034 cm^{-1} – to the secondary alcohol C-O stretch of the product (Table 4.1).[98]

HPLC analysis was always used to determine the final reaction conversion or to determine the temporal conversion over the course of a reaction. The samples withdrawn from the reaction mixture over the course of the reactions were of such a size, that to keep the total reaction volume insignificantly affected. The procedure of sample work up for HPLC analysis is provided in the Appendix 2. Sampling was usually performed while monitoring the progress of a reaction by one of the *in situ* methods.

Table 4.1 Infrared spectrum: Various Group frequencies.

Origin	Group wavenumber (cm^{-1})	Assignment
C=C-C	1615-1580	Aromatic ring stretch
C-C	1350-1000	Skeletal vibration
C-O	~1100	Secondary alcohol

4.4 Initial Kinetic Runs of the Aldol Reaction

This paragraph presents the initial kinetic experiments of the aldol reaction of Scheme 4.1. The initial conditions for these experiments are presented in the Table 4.2. Figure 4.2a pictures the earlier statement suggesting that heat flow evolved during the reaction is directly proportional to the rate of this reaction (see paragraph 2.2.1), which is presented in Figure 4.2b. From these two plots it is possible to perceive that the aldol reaction exhibits overall positive order kinetics: the rate decreases over time when carried out in both dimethylsulfoxide (DMSO) and dimethylformamide (DMF), solvents. However the reaction rate is almost three times slower in DMF than in DMSO. This may be explained by the lower active catalyst concentration when the reaction is carried out in DMF; due to lower proline solubility in this solvent.

Table 4.2 Comparison of initial conditions (IC) of two reactions carried out at the same excess and concentrations of reaction components after 50% conversion ($C_{50\%}$).

Experiment	Solvent	[**1**]	[**2**]	[**e**]	[**4**]	[**3**]
E4.1: IC	DMSO/ DMF	2.75 M	0.50 M	2.25 M		0 M
4.2: IC		2.25 M	0.25 M	2.25 M	0.05 M	0 M
4.1: $C_{50\,\%}$		2.25 M	0.25 M	2.25 M		0.25 M

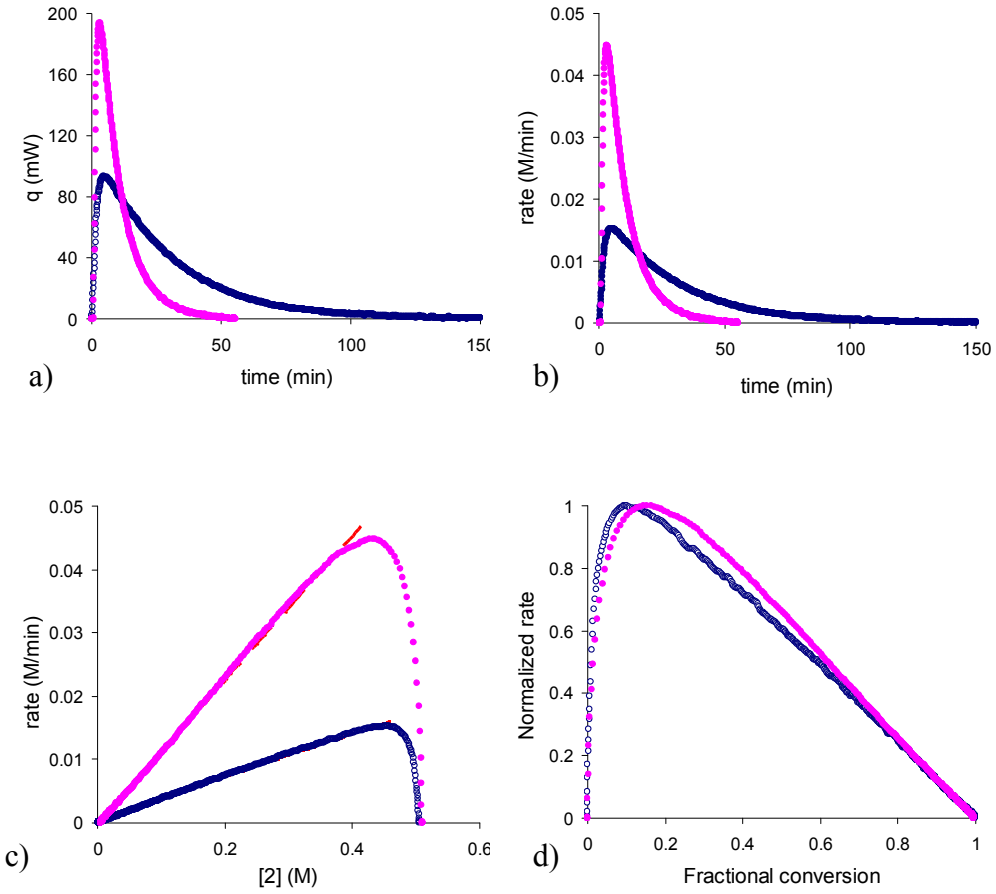

Figure 4.2 Initial kinetic analysis of the aldol reaction of Scheme 4.1. a) Temporal heat flow profile; b) temporal rate profile; c) graphical rate equation; d) normalised rate versus conversion. Full circles: reaction in DMSO; open circles: reaction in DMF.

The conclusion about positive order kinetics is even easier to reach when the experimental data is plotted as a graphical rate equation: rate versus limited substrate concentration as in Figure 4.2c. This graphical rate equation implies that the closer data are to the linear trend, the closer

reaction is to the overall first order kinetics. Figure 4.2d shows that normalised rates (each rate point is divided by maximum rate in the set) in both solvents fall on top of each other indicating that there is little if any solvent effect. Hence the mechanism of the aldol reaction was not affected by altering solvent properties.

4.4.1 Probing the Steady State Characteristic of the Aldol Reaction

The considerations of examining catalyst robustness over the course of a reaction have been discussed earlier (see paragraph 2.1.1). Here the steady state characteristics of the aldol reaction of Scheme 4.1 were challenged using the initial conditions displayed in Table 4.2. This table shows that two sets of conditions (E4.1 and E4.2) with different initial concentrations but the same *excess* were employed. A mass balance, for the aldol reaction of Scheme 4.1, tells that for each molecule of ketone **1** consumed, one molecule of aldehyde **2** is also consumed. Hence, in this case, *excess* is directly expressed through the difference of their initial concentrations as shown in Equation 4.1 [*excess* = [**e**] in equation 4.1).

$$[\mathbf{e}] = [\mathbf{1}]_0 - [\mathbf{2}]_0 \quad \text{(eq 4.1)}$$

The experimental kinetic data obtained from these experiments (E4.1 and E4.2) is presented in Figure 4.3 as a graphical rate equation. As can be seen, the graphical rate equations of these two experiments do not fall on top of each other: experiment E4.1 has lower rate at the same substrate concentration in both employed solvents. The lack of the overlay suggests that the aldol reaction may be influenced by the following effects: product inhibition or catalyst deactivation. Experiment 4.1 after 50% conversion (E4.1: C50%) has already some reaction product formed while the second experiment (E4.2) at the same substrate concentration has no reaction product as presented in the Table 4.2. Also due to the higher initial substrate concentrations in the E4.1, the catalyst had to perform more turnovers to reach the initial substrate concentrations of E4.2. Deactivation may be implied when additional turnovers result in lower rate, as in

experiment E4.1. These two effects should be examined to understand the course of lack of overlay.

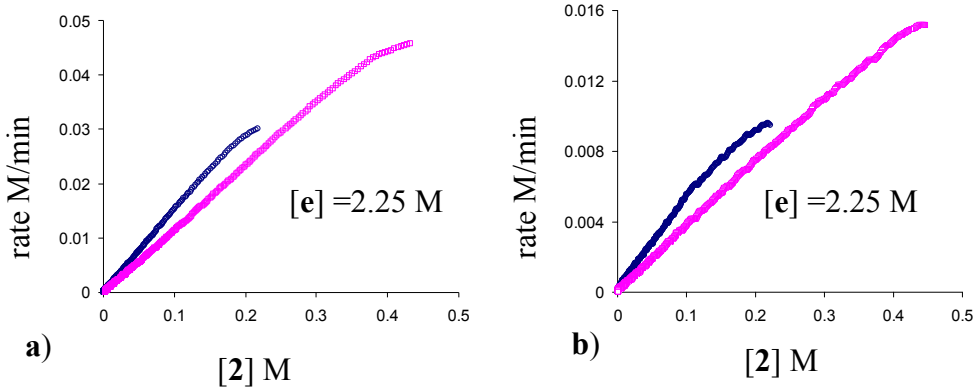

Figure 4.3 Comparison of rate versus [**2**] for two aldol reactions of Scheme 4.1 carried with the same *excess*. Initial conditions are given in table 4.2: pink squares denote E4.1; blue circles – E4.2. a) DMSO; b) DMF.

The possibility of a product inhibition can be discounted by performing the aldol reaction with addition of the aldol product **3** (0.25M). No change in the reaction rate was observed, indicating that the product has no influence on the reaction performance (see Chapter 7). Hence the lack of the overlay may be attributed to catalyst instability due to the effective siphoning of the active catalyst to the formation of some spectator species outside of the cycle.[71]

4.5 Concluding Remarks

The initial investigation of the L-proline catalysed aldol reaction showed that the aldol reaction behaves very similarly in both tested solvents (DMSO and DMF) however due to lower solubility of L-proline in DMF the rate is slower. Also in both solvents catalyst deactivation was observed when the experiments were carried out with the same value of *excess*. Therefore in order to obtain truthful concentration dependencies the cause of catalyst deactivation should be understood and prevented.

Chapter 5

Behaviour of Catalytic Spectators and Role of Water in L-Proline catalysed Aldol Reactions

In the previous chapter kinetic investigations using the same excess protocol showed catalyst deactivation occurring within the catalytic cycle during the aldol reaction. This chapter will investigate whether this catalyst deactivation can be implicated with the formation of oxazolidinone species that were observed by Pihko and co-workers between proline and aliphatic aldehydes.[74, 75] Their careful work showed that with addition of water higher yields can be achieved in the proline catalysed aldol reactions, allowing lower excesses of donor (and even stoichiometric amounts) to be employed. Such finding has a great potential to widen the scope of proline catalysis and enhance its practical efficiency. The observation of higher yields in presence of water was associated with suppression of oxazolidinones derived from proline and aliphatic aldehyde.[74, 75] Thus it was suggested that the role of water is primarily to prevent catalyst deactivation, concluding that the intrinsic effect of water is to accelerate the rate of the aldol reaction. As pointed out by Janda and co-workers, however, rate acceleration by water in an enamine-based mechanism is counter-intuitive; enamine concentration, and therefore potentially the reaction rate should be suppressed by increasing water concentration.[76] Hence, the current study will convey the first detailed clarification of the intriguing question concerning the role of water in proline catalysed aldol

reactions, separating the processes occurring within the catalytic cycle and off cycle.[76, 99] Along with the kinetic investigations, proline deactivation in the aldol reaction will be studied by employing alternative mechanistic tools. The performance of L-proline will also be compared to its derivative, L-proline-tetrazole.

5.1 Clarification of the Role of Water in the Proline Catalysed Aldol Reaction

5.1.1 Kinetic Investigations

Primarily in this study it was decided to test the effect that the presence of water has on the catalyst concentration over the course of the aldol reaction. As before, the two experiments employing the same *excess* protocol were performed. The initial conditions were the same as used in Table 4.2 (see Section 4.4) for the aldol reactions of Scheme 4.1 however additionally 0.2 M water was injected. The purpose of these two experiments was to test the proposals by Pihko and co-workers suggesting that water can eliminate catalyst deactivation. Reactions were carried in the reaction calorimeter as discussed in paragraph 4.2.

The graphical rate equations, displayed in Figure 5.1, constructed from these two experiments shows overlay. This implies that rates are the same at the same substrate concentration for both experiments with the same excess, signifying that the presence of at least 0.2M of water in the aldol reaction suppresses catalyst deactivation in both types of solvent. Proline concentration is stable under these conditions throughout the course of the reaction.

Pihko and co-workers demonstrated that water allows the aldol reactions to achieve the acceptable yields even under stoichiometric conditions.[75] Therefore the aldol reaction of Scheme 4.1 was also performed under stoichiometric conditions presented in Table 5.1 in order to test the catalytic stability over the course of such reactions.

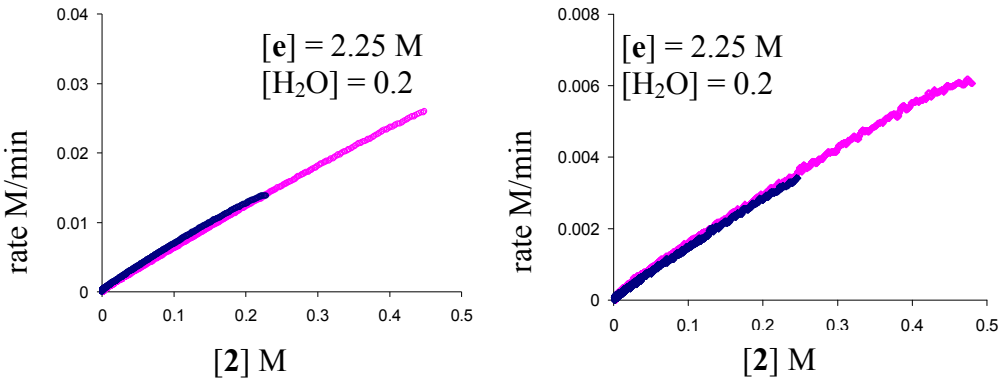

Figure 5.1 Comparison of rate versus aldehyde concentration [**2**] for the aldol reactions of Scheme 4.1 carried with the same *excess* with addition of water. Initial conditions are as displayed in Table 4.2. a) DMSO; b) DMF.

Table 5.1 Initial conditions (IC) employed in two sets of the reactions carried out with and without addition of water.

Experiment	Solvent	$[\mathbf{1}]_0$	$[\mathbf{2}]_0$	[**4**]	$[H_2O]$
E5.1: IC		1.00 M	1.00 M	0.1 M	0 M
5.2: IC	DMSO	0.51 M	0.51 M	0.1 M	0 M
5.3: IC		1.00 M	1.00 M	0.1 M	0.6 M
5.4: IC		0.51 M	0.51 M	0.1 M	0.6 M

In the absence of water the reaction with higher initial concentrations halts at less than 75% conversion as can be seen from Figure 5.2a (E5.1, pink curve). When reaction was initiated with the lower initial concentrations the higher yields and rates were achieved [Figure 5.2a (E5.2, blue curve)]. Knowing that two reactions were carried out under different initial concentrations but identical otherwise conditions (same *excess* and catalyst concentration), the observed plot suggests that catalyst lost its reactivity or its concentration decreased so, that the reaction E5.1 cannot be catalysed as effectively as the reaction E5.2. If first order kinetics is assumed in the catalyst concentration then it is possible to imply from the plot in Figure 5.2 that ca. 64% of catalyst was made inactive in experiment E5.1 at 0.4M of [**2**].

However, addition of water boosts the reaction conversion so that the overlay between two experiments (E5.3-5.4) with the same *excess* value was obtained as can be seen from Figure 5.2b. These results suggest that under these conditions proline is stable within the course of the reaction and is not being siphoned off to form inactive species outside the catalytic cycle. These results confirm Pihko's observation[74, 75] suggesting that with addition of water the reaction is capable of proceeding in quantitative yields both stoichiometric and acetone excess conditions.

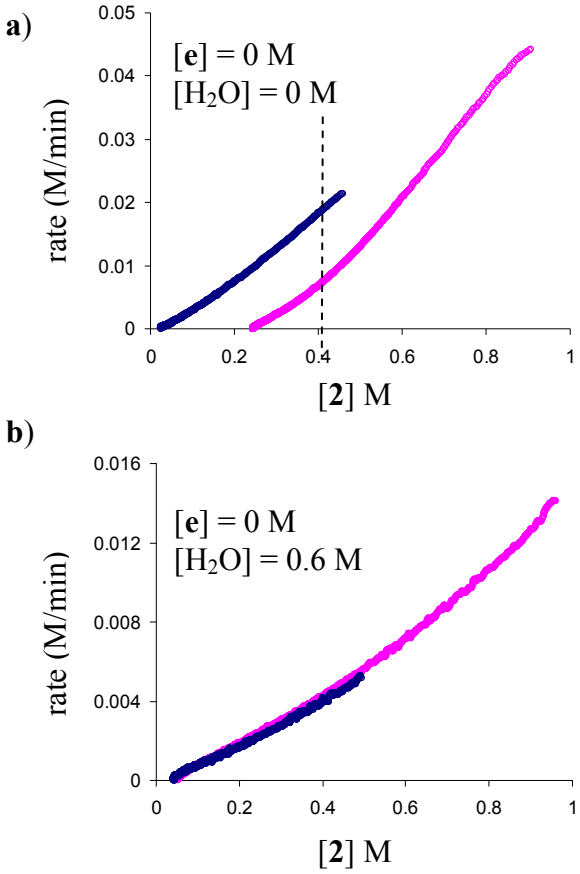

Figure 5.2 Aldol reaction of Scheme 4.1 carried out under stoichiometric conditions in DMSO with initial conditions displayed in Table 5.1: a) 0 M H_2O; b) 0.6 M H_2O. Dashed line emphasizes the difference in the rates of the two reaction carried out at identical substrate concentration conditions.

While these reactions run to nearly completion in the presence of water, it can be observed from Figures 4.7, 5.1 and 5.2 that water suppressed the rate. For example, for the reactions under stoichiometric conditions (Figure 5.2), the initial rate of the reaction in the experiment E5.1 compared to the initial rate in the experiment E5.3 is higher by approximately three-folds. This

result calls into question the proposal of the Pihko group concerning the rate acceleration by water.[75] While their experiments allowed them to observe changes in yield, their measurements did not allow them to address the question of reaction rate.

A more detailed study concerning the role of water in the proline catalysed aldol reaction in DMSO was pursued over a broad range of conditions by varying the donor **1** concentration from the stoichiometric amount to almost five-fold excess. The amount of water at constant initial substrate concentrations was varied from 0.2 M to 1.8 M (Table 5.2). The kinetic data obtained from these experiments are shown in Figure 5.3. In all experiments the stability of catalyst concentration within the catalytic cycle over the course of the reaction has been confirmed with the same excess experiment (see Appendix 7).

Table 5.2 Initial conditions (IC) for the experiments with the varying amount of water between 0.2M and 1.8M.

Experiment	$[\mathbf{1}]_0$	$[\mathbf{2}]_0$	$[\mathbf{4}]$	$[H_2O]$
E5.5: IC	1.00 M	1.00 M	0.1 M	0.2; 0.4; 0.6; 1.0; 1.3 M
5.6: IC	1.75 M	0.50 M	0.03 M	0.2; 0.4; 0.6; 1.0; 1.4; 1.8M

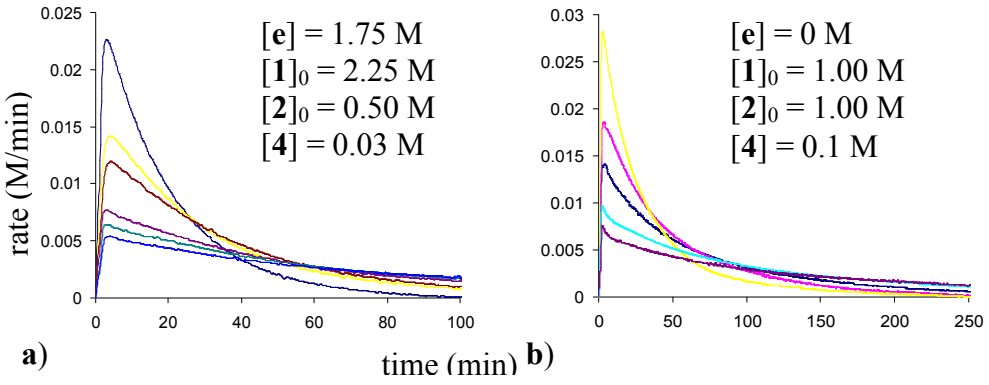

Figure 5.3 Reaction progress curves for the aldol reaction of Scheme 4.1 with initial conditions as listed on the graphs and added water from top to bottom (a) 0.2, 0.4, 0.6, 1.0, 1.4, 1.8 M; (b) 0.2, 0.4, 0.6, 1.0, 1.3 M.

The reaction progress curves in Figure 5.3 were fit to an exponential decay to provide pseudo first order rate constants, with correlation parameters between 0.92-0.99 showing a reasonable fit. The obtained rate constants for both sets of experiments were plotted as a function of concentration of added water in Figure 5.4.

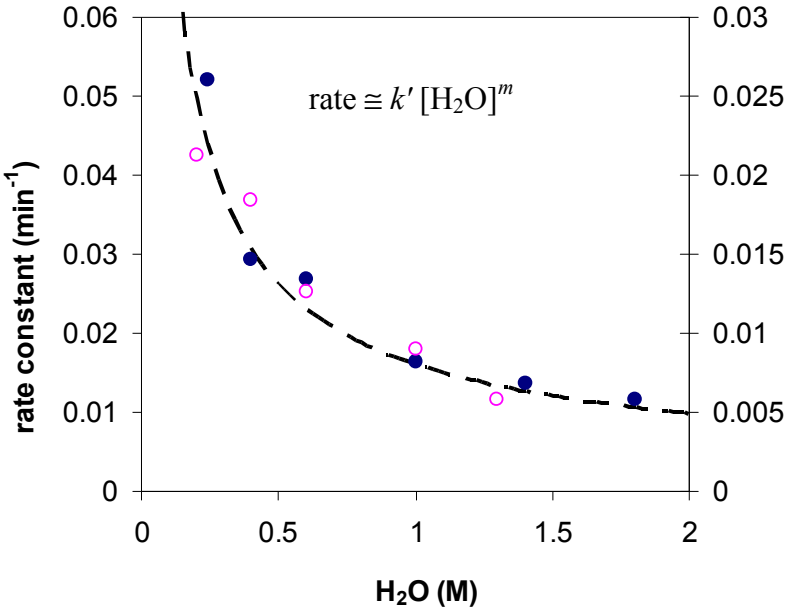

Figure 5.4 Pseudo first order rate constant for the aldol reaction of Scheme 4.1 as a function of added water. Open circles: stoichiometric conditions E5.5 (right axis); Full circles: 1.75M excess of **1** E5.6 (left axis). Dotted line represents the power law relationship as in equation 5.1: m = -0.70±0.04 obtained from Solver fitting.

Tables 5.3-5.4 summarize the rate constant values, conversions and enantiomeric excess (*ee*) values for each reaction. Figure 5.4 confirms our preliminary results from Figure 5.2 that the intrinsic role of water within the catalytic cycle is to suppress, rather than accelerate, reaction rate. This result is consistent with the generally accepted enamine mechanism for a case where the rate limiting step precedes product hydrolysis step (Scheme 3.3). The power law may be used to obtain the relationship between the rate of the aldol reaction and water concentration within the employed conditions. The magnitude of the power m=-0.70 can be estimated from fitting the power rate law at the constant substrate concentrations (for example using experiment E5.6) and changing water concentration ($0<[H_2O]<2$) to the data obtained from Michaelis-Menten type rate law as written in equation 5.1 [c_1 and c_2 are Michaelis-Menten type constants which include

initial substrate concentrations of experiment E5.6 and the rate constants obtained from the model 1 (see Equation 6.5 and Appendix 5.1 for rate constant values)][1] using Solver curve-fitting program and the SolvStat.xls macro for statistical calculations [100]. The detailed kinetic study investigating the global rate law of the aldol reaction will shed further light on the viability of this mechanism.

$$rate = \frac{c_1}{c_2 + [H_2O]} = k'[H_2O]^m \quad \text{(eq. 5.1)}$$

Table 5.3 Pseudo first order constants from the reaction progress data of Figure 5.3 a.

Entry	$[H_2O]$ (M)	Rate constant (min^{-1})	R^2	Conversion %	*ee* %
1	1.8	0.0116	0.99	87.8	69.0
2	1.4	0.0137	0.98	93.4	68.7
3	1.0	0.0164	0.92	98.1	68.5
4	0.6	0.0269	0.99	96.7	68.2
5	0.4	0.0293	0.99	98.3	69.0
6	0.24	0.0520	0.99	99.7	68.2

From tables 5.3 and 5.4 can be seen that the product enantiomeric excess (*ee*) has not been affected by addition of water in the experiments carried out under the same conditions. This suggests that water does not play a role in enantiodifferentiation. However, when reactions were carried out with the stoichiometric amounts of acetone (Table 5.4), slight decrease in the product enantiomeric excess can be noted. It is possible that the background uncatalysed reaction may contribute more in the stoichiometric reactions, which are much slower to completion than those run under excess of acetone.

[1] Both parameters of equation 5.1, *m* and *k'*, were estimated employing Solver.

Table 5.4 Pseudo first order constants from the reaction progress data of Figure 5.3 b.

Entry	$[H_2O]$ (M)	Rate constant (min^{-1})	R^2	Conversion %	*ee* %
1	1.3	0.0058	0.99	88.4	64.4
2	1.0	0.0090	0.98	91.4	64.4
3	0.6	0.0126	0.99	94.6	65.8
4	0.4	0.0184	0.97	94.8	64.7
5	0.2	0.0213	0.96	93.0	64.7

5.1.2 Spectroscopic study

The former investigation revealed conditions under which catalyst concentration can be kept stable over the course of the aldol reaction. Spectroscopic investigations were undertaken to probe the suggestion that water effect is associated with the formation of oxazolidinone. This study could provide the more in-depth spectroscopic information about species that participate actively in the catalytic cycle and species that are spectators sitting outside the cycle and possessing a "parasitic" role.[71] In addition the understanding of the role of water in the proline catalysis may also be enhanced.

Table 5.5 Initial conditions (IC) for the NMR experiment.

Experiment	Solvent	$[\mathbf{1}]_0$	$[\mathbf{2}]_0$	$[\mathbf{4}]$	$[H_2O]$
E5.7: IC	DMSO	2.75 M	0.50 M	0.1 M	0

Primarily this investigation was carried out using NMR spectroscopy and all NMR spectra were recorded using Bruker DRX-400 or AV-400 spectrometers. The study was initiated by ^{1}H-NMR spectroscopic monitoring of the proline catalysed aldol reaction of Scheme 4.1 in the absence of water (Figure 5.5). The reaction was carried out directly in the

NMR tube on the 1 ml scale and the employed conditions are presented in Table 5.5.

L-Proline was directly weighed into a 5mm NMR tube, thereafter the tubing was charged with appropriate amount of solvent as to make a total reaction volume of 0.8-1ml and shook. Thereafter the appropriate amount of acetone (**1**) was added. Several ^{1}H-NMR spectra were taken over time to see the interaction between proline and acetone. The reaction was initiated by addition of *o*-CBA (**2**) into reaction mixture and the subsequent reaction was monitored until completion.

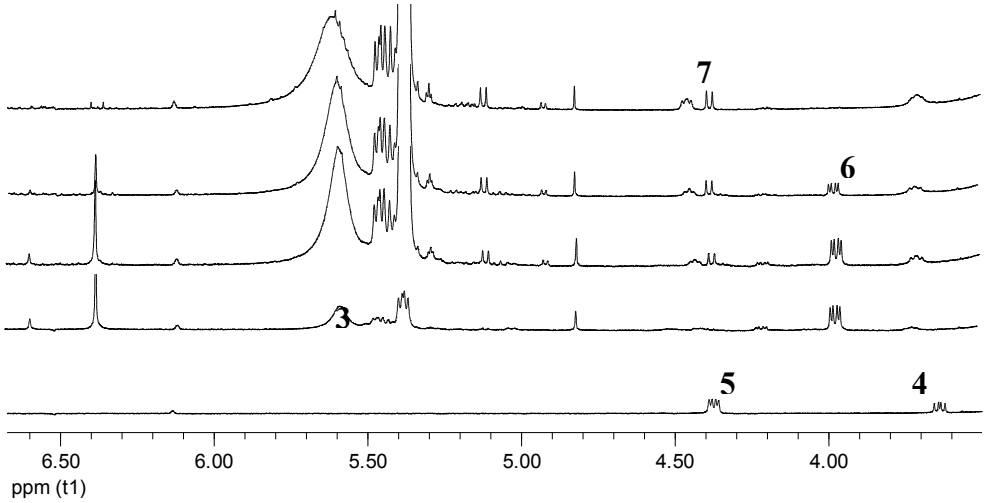

Figure 5.5 ^{1}H-NMR (400 MHz) spectra of the aldol reaction of scheme 4.1 carried out with *excess* = 2.25 M in d^{6}-DMSO at 25 ^{0}C. Bottom top: interaction between **1** and **4**, 2 minutes of the reaction (after addition of **2**), 10, 20, 60 minutes.

The interaction between proline and acetone revealed formation of acetone oxazolidinone species **5** that was described by List and co-workers.[71] The α-proton of **5** gave a strong resonance at 4.35 ppm (Figure 5.5, bottom spectra), which is in a good correlation with previously detected oxazolidinone formed between proline and acetone at 4.40 ppm.[71] It was also observed that proline promotes the formation of acetone self condensation product (diacetone alcohol) followed by further dehydration to mesityl oxide as it would be expected under acidic conditions.[6] Two methyl groups and hydroxy proton of diacetone alcohol and a vinyl-proton of mesityl oxide were identified by comparison with the reference samples obtained from Aldrich. However these products are formed in insignificant

amounts during the course of the aldol reaction and therefore they were not considered as the major side products.

It must be said that enamine formation itself was not detected. From investigation by Hiroi et al., who pre-made enamine from proline and substituted cyclohexanone, the possible resonance for the proton at the enamine bond was expected at around 5.40-5.92 ppm.[101] Due to the presence of such unsaturated bond the nuclei of a proton is less shielded from the applied magnetic field and therefore often shifts downfield from 4.5 to 6.5 ppm.

When *o*-CBA was injected into a mixture of L-proline and acetone in DMSO in order to initiate the aldol reaction, in addition to oxazolidinone (**5**), species **6** has formed within first few minutes of the reaction (Figure 5.5). The species **6** has disappeared over time while the second species **7** has prevailed. Consequently the investigation of the interaction of each reactant separately, acetone (**1**) and *o*-CBA (**2**), with proline was pursued.

These interactions were explored using an internal standard (**IS**, 2,5-dimethylfuran, DMFu) and conditions that enabled more quantitative analysis. L-Proline was carefully weighed into the glass vessel (used with the reaction calorimeter) and appropriate amount of solvent and DMFu was added into the vial as to make a total volume of 3ml. Then mixture was stirred at the constant temperature (25 °C) in the reaction calorimeter for 1 h in order to equilibrate the proline concentration and reach its solubility limit. Deuterium labelled d^6-acetone or *o*-CBA were added individually into suspension of L-proline in the solvent and mixed for 5-30 min. Thereafter a 1ml sample was prepared by filtering the mixture through 0.45μm filter in order to remove the excess of proline directly into 5mm NMR tube for an immediate ^{1}H-NMR spectrum record.

5.1.2.1 Interaction between L-Proline and Acetone

Although it was already confirmed with the same *excess* experiments that with addition of water active proline concentration does not change over the course of the reaction, careful investigation of the interaction between

proline and acetone allows measurement of the absolute solution proline concentration and how this is affected by the different fixed amounts of water. The change in the concentration of L-proline (**4**) was investigated by following the change in the integral of its α-proton at 3.62 ppm (also cross checking with the proton at 3.00 ppm that belongs to the pyrrolidine ring of L-proline) different fixed water concentrations (Figure 5.6). The experiments were carried out in a way described above in deuterium labelled d^6-DMSO, where L-proline (**4**) and deuterium labelled d^6-acetone were mixed together for 30 minutes. Deuterium labelled water (D_2O) was added at the time of charging the NMR tube with the solvent.

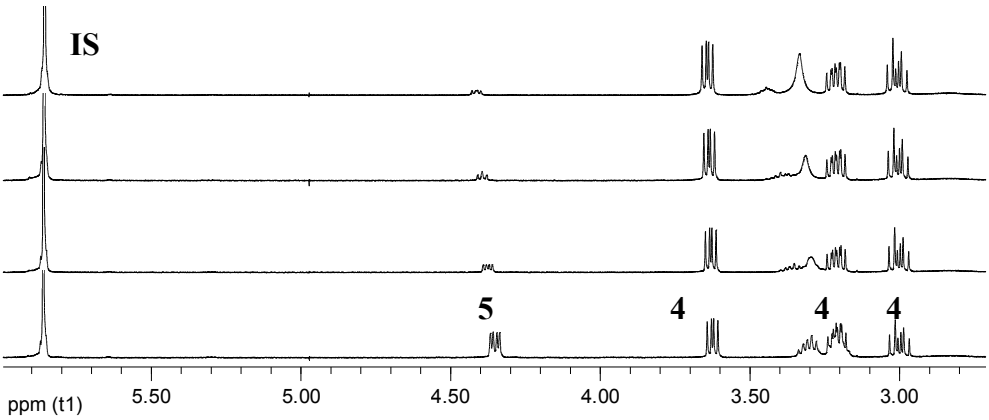

Figure 5.6 ^{1}H-NMR spectrum of the interaction between L-proline **4** and 2.75M d^6-acetone in d^6-DMSO in presence of D_2O. Bottom top: 0M D_2O, 0.23M D_2O, 0.45M D_2O, 0.66M D_2O.

The results obtained from ^{1}H-NMR study, shown in Figures 5.6 and 5.7, revealed that the concentration of solution phase proline increases slightly over the range of employed water concentrations, albeit not significantly, remains around 0.01M, while the amount of oxazolidinone (**5**) formed between L-proline (**4**) and d^6-acetone decreases so that the total amount of **4** and **5** mirrors the trend of **5**. Water suppresses more significantly the formation of **5** than it enhances the increase in concentration of solution **4**.

Although NMR results revealed only the formation of oxazolidinone (**5**), which formation is expected to occur via iminium ion intermediate **8** as shown in Scheme 5.1,[102] formation of nucleophilic enamine **9** between proline and acetone could be implied, as it should exist in the equilibrium with species **5** and **8**.

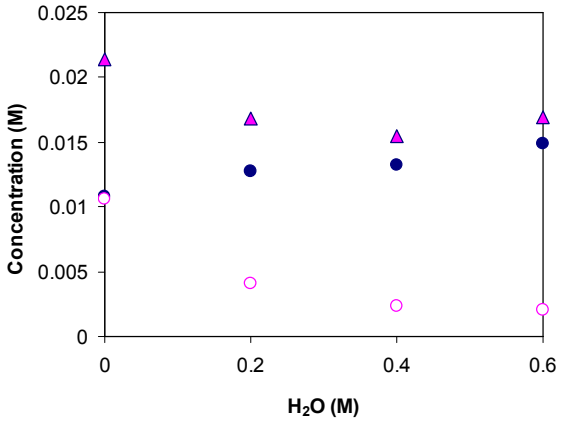

Figure 5.7 Concentration of **4** and **5** as a function of added water at 25 ^{0}C: [**4**]: full circles; [**5**]: open circles; [**4**]+[**5**]: full triangles.

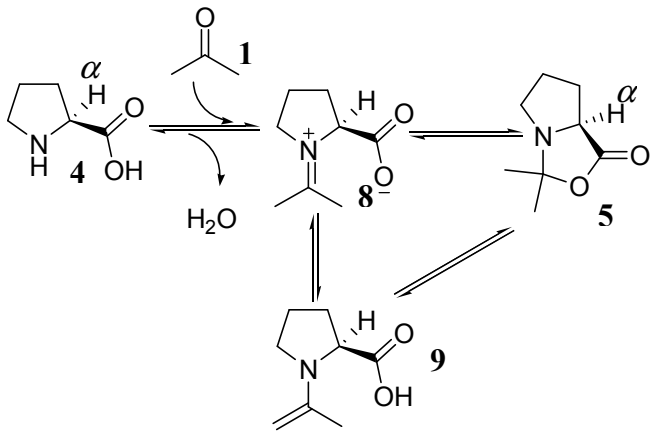

Scheme 5.1 Formation of oxazolidinone **5** and enamine **9** between proline (**4**) and acetone (**1**).

5.1.2.2 Interaction between L-Proline and *o*-CBA

The ^{1}H-NMR spectroscopic investigations of L-proline (**4**) and *o*-CBA (**2**) in d^{6}-DMSO revealed that species **6** and **7**, which were observed during the monitoring of the entire reaction, may be attributed to the interaction between **2** and **4** (Figure 5.8). The ^{1}H-NMR shifts for species **6**, representing a doublet of doublets, are in good agreement with Seebach's characterization of the oxazolidinone derived from proline and pivaldehyde.[103] Species **6** has therefore been tentatively assigned as the two diastereomers of the oxazolidinone derived from the interaction between the proline and **2**, which were observed in ratio **6a**:**6b** = 6:1. Although it was not possible to isolate species **6**, the diastereomeric species **7** were isolated. These species has been identified by spectroscopic analysis

(^{1}H-NMR, ^{13}C-NMR, COSY, NOESY, HMQC and HMBC) as the two diastereomers present in 2.5:1 ratio of **7a**:7**b** (all NMR data used to identify species is presented in the Appendix 3). The assignment of the absolute configurations has been based on obtained data and in analogy with similar species obtained by Orsini et al.[104]

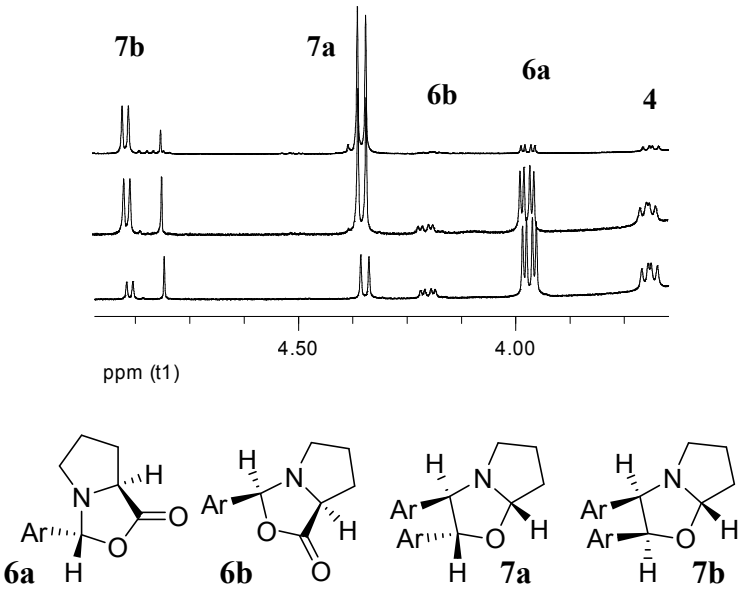

Figure 5.8 ^{1}H-NMR spectra of a temporal change in species **6** and **7** in the interaction between **2** and **4** at 25^{0}C in d^{6}-DMSO. Bottom top: 10, 30, 120 minutes.

The temporal change in the concentrations of **6, 7** and **4** in the absence of added water has been followed by ^{1}H-NMR spectroscopy. From this study it was observed that the concentration of **6** was roughly equal to that of solution proline (**4**) after 10 minutes of the experiment. At the consequence of the experiment, the concentration of **6** decreased to one-third of the initial value concomitant with the increasing concentration of **7** that ultimately equalled that of the initial solution proline concentration (Figure 5.9). Finally in about four-five hours from the start of the experiment, the species **6** and **4** have entirely disappeared and only species **7** was observed.

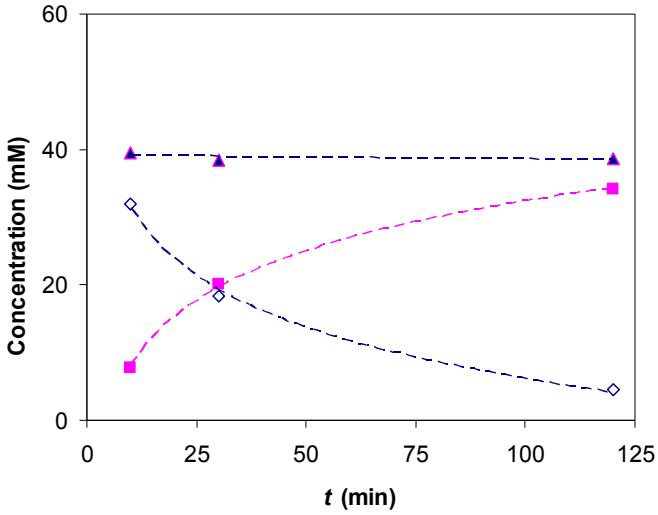

Figure 5.9 Temporal change in species **6** and **7** in the interaction between **2** and **4** at 25^0C in d^6-DMSO: [**6**]: open diamonds; [**7**]: full squares; [**6**] + [**7**]: full triangles.

The effect of water on the concentration of all species was also examined during this investigation. When mixing of **2** and **4** was carried out in the presence of 0.6 M water, the solution concentration of proline remained relatively unaffected while formation of both species **6** and **7** has been suppressed by more than 75%.

The species similar to **7** have been reported elsewhere, observed in the reactions between proline (**4**) and other aromatic aldehydes, such as benzaldehyde and *p*-nitrobenzaldehyde, and ketone, such as ethyl purivate.[104, 105] Therefore, on the basis of the current research in addition to analogy with previous studies,[104] it was proposed that irreversible deactivation of proline (**4**) in the presence of aromatic aldehydes and in the absence of added water occurs as shown in Scheme 5.2. Oxazolidinone type species **6** are reversibly formed as has previously been shown for electron rich aldehydes.[103] In the case of electron deficient aromatic aldehydes, such as **2**, the iminium ion species **10**, which is responsible for the formation of oxazolidinone **6**, may undergo decarboxylation to form the azomethine ylide **11**. Formed ylide may then react with a further aldehyde molecule, such as **2,** to form the stable 1-oxapyrrolizidine **7**. The suggestion that such species may be implicated in deactivation was a conjecture even in

the first report of intermolecular aldol reactions mediated by proline although experimental observations were not reported in that work.[27]

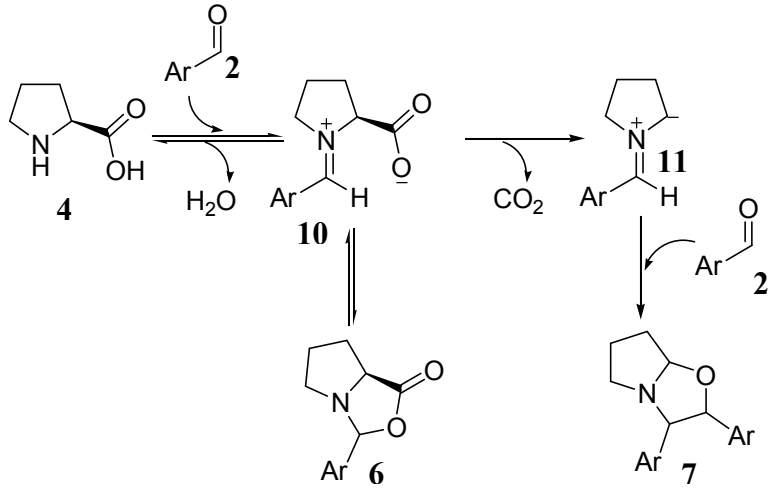

Scheme 5.2 Reaction between aromatic aldehydes such as **2** and proline (**4**).

This irreversible deactivation pathway has implications for the catalytic cycle in both the presence and the absence of water. The addition of water suppresses formation of the iminium ion **8** and the enamine/oxazolidinone (**9**/**5**) formed from **1** and **4** on the catalytic cycle shown in Scheme 5.1, as well as the iminium ion **10** from **2** and **4** off the cycle as shown in Scheme 5.2, due to Le Chatelier's principle. Suppression of **10** leads to the averting of **6**, **11** and **7**, driving more catalyst into the cycle. Thus two conflicting roles for water can be outlined, which signifies that increasing the water concentration:

(i) *Increases* the total catalyst **4** concentration available within the cycle due to the suppression of spectators such as **6** or **7**, and

(*ii*) *Decreases* the relative amount of the acetone enamine **9**, a key intermediate in the proline catalysis.

The net effect on the rate of the aldol reaction will depend on the balance of these two phenomena. The same is true for the aliphatic aldehydes which at ambient temperature form oxazolidinone species of type **6**.[103] The mechanistic point revealed by the current kinetic and spectroscopic study is

that for the aldol substrates under study, the intrinsic rate per active catalyst species within the cycle is suppressed by added water.

In the absence of water, irreversible deactivation of the catalyst due to the formation of **7** from one molecule of **4** and two molecules of **2** causes the reaction rate to be lower than that expected for the given initial concentration of **4** and **2** (Figures 4.7 and 5.2a). These arguments are based on the assumption, that the concentration of both **2** and **4** are driving forces of the reaction. Therefore it is important to consider the global kinetics of the proline catalysed aldol reaction in order to distinguish the rate-limiting step (see Chapter 6). Maximum achievable yield may also be limited due to loss of aldehyde **2** in the irreversible formation of **7**. However, the reversibly formed oxazolidinone **6** can be converted to the product at later stages in the reaction when low concentration of aldehyde shifts the equilibrium position away from **6**.

The formation of species **6** and **7** has been also observed in other aprotic polar solvents of various polarities such as DMF, N-methylpyrrolidone (NMP), acetonitrile (MeCN), tetahydrofuran (THF) and neat acetone. In addition the reaction in $CHCl_3$ produces a significant amount of **7**.[1]

5.2 Catalysis by Proline Derivative – Proline Tetrazole

Proline tetrazole (**12**), shown in Figure 5.10 was discovered as a more soluble alternative for the proline where carboxylic acid group was replaced by tetrazole functionality.[106] Tetrazoles themselves are known to have acidity similar to the carboxylic acids but typically higher solubilities and are used in medicinal chemistry as their substitutes. Proline tetrazole's increased reactivity was firstly explained by a greater charge stabilization of the transition state by the tetrazolic acid of the catalyst.[106, 107] The further reactivity study by Arvidsson group suggested that the main reason for the increased reactivity can be attributed to an inability of proline tetrazole to form parasitic spectator species such as oxazolidinones.[108] Hence the original aim of this study was to investigate the aldol reaction catalysed by

[1] Dr A. Franzke's unpublished results

proline tetrazole by applying the methodology of reaction progress kinetic analysis; and evaluate and compare the performance of two catalysts, proline tetrazole and proline. Although the study was not accomplished entirely due to the failure to understand the cause of observed deactivation, and therefore develop protocols to overcome it, some interesting findings about proline tetrazole catalysed aldol reactions were identified here.

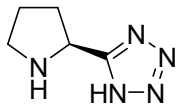

Figure 5.10 Structure of L-proline-tetrazole.

5.2.1 Initial Investigation of the Aldol Reaction Catalysed by L-Proline-Tetrazole

Proline tetrazole was synthesized by following the procedures described in several publications and its purity evaluated by NMR and MS analysis (see Appendix 3).[109] The aldol reactions of Scheme 4.1 catalysed by L-proline-tetrazole were carried out in the reaction calorimeter employing the experimental set up described in section 4.2. To verify the validity of the kinetic data, reactions were also monitored under the identical conditions by FTIR spectroscopy using the procedures described in section 4.3. Along these spectroscopic runs the samples for HPLC analysis were also collected, which were analysed using the same work up method provided in Appendix 2. The initial experimental conditions used during this study are summarised in Table 5.6. Figure 5.11 shows that the fractional conversion obtained by the reaction calorimetry is in a good agreement with the data obtained by FTIR and HPLC, suggesting that the measurement of the fractional conversion correlates with the actual conversion of *o*-CBA.

Table 5.6 Initial conditions (IC) employed in two sets of the reactions carried out with and without addition of water.

Experiments	Solvent	$[\mathbf{1}]_0$	$[\mathbf{2}]_0$	[**12**]	$[H_2O]$	[**e**]
E5.8: IC	DMSO	2.73	0.52	0.050	0.000	2.21
5.9: IC		2.49	0.29	0.050	0.000	2.20

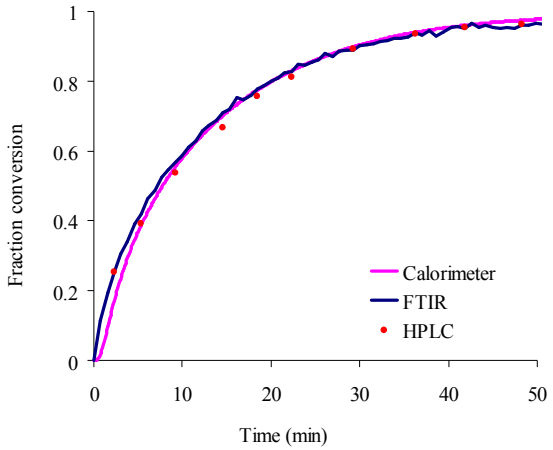

Figure 5.11 Fraction conversions vs. reaction time as measured by *in situ* reaction calorimetry and FTIR, and sample analysis by HPLC for the proline tetrazole catalysed aldol reaction of Scheme 4.1 carried out in DMSO. Reaction conditions are: $[\mathbf{1}]_0 = 2.73$M, $[\mathbf{2}]_0 = 0.5$M, [**12**] = 0.05M. Product enantiomeric excess = 70%.

As a standard procedure the same *excess* protocol was employed, as can be seen from Table 5.6, in order to verify whether the reaction is subjected to any influences other than substrate concentrations over the duration of the reaction. Figure 5.12 displays the obtained results from these experiments.

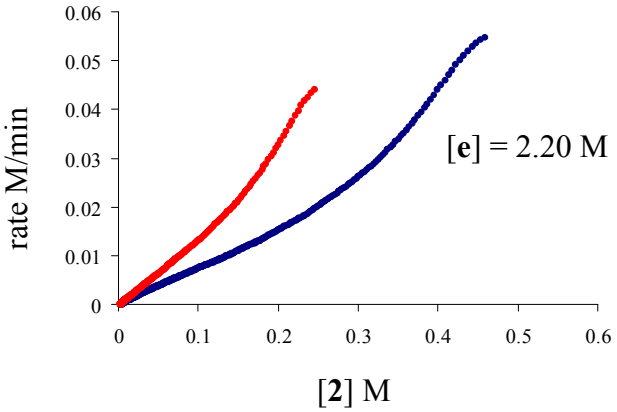

Figure 5.12 Comparison of rate versus [**2**] for aldol reactions of Scheme 4.1 catalysed by L-proline-tetrazole and carried out in DMSO under initial conditions as given in Table 5.6.

The curves in Figure 5.12, which are plotted as graphical rate equation of rate vs. [**2**], do not fall on top of each other, implying the possible presence of catalyst deactivation or product inhibition. Although from the shape of these curves, the second order kinetics may be implied in these reactions, it cannot be stated with certainty before the cause of the lack of the overlay was understood. Additional observations suggest that the L-proline-tetrazole (**12**) produces higher amounts of aldol condensation product **3a** than the proline (**4**) under similar reaction conditions (see Table 5.7).

Table 5.7 Comparison between performance of aldol reactions catalysed by L-proline and L-proline-tetrazole: reaction conditions are as displayed in table 4.1 and 5.6 respectively.

Experiments	Solvent	conversion %[1]	ee_S %	condensation %[2]
E4.1	DMSO	99.6	67.6	1.7
4.2		100.0	67.5	1.8
5.8		99.1	70.2	4.7
5.9		98.8	71.5	7.3

It is known that the aldol reaction must be carried out under non-acidic conditions to avoid the formation of the aldol dehydration product.[6] Therefore the higher formation of the condensation product during the reaction catalysed by proline-tetrazole may be associated with its pK_a value, which may be lower than of proline in DMSO, in a similar manner as it was noticed for tetrazoles (pK_a = 8.2 in DMSO) compared to acetic acid (pK_a = 12.3 in DMSO).[107]

5.2.2 Interaction between L-Proline-tetrazole and the Reaction Substrates

The lack of overlay between two experiments with the same *excess* value indicates possible catalyst deactivation or product/substrate inhibition. To dismiss possible product inhibition, reaction product was added into the

[1] *o*-CBA fraction conversion in %
[2] Aldol condensation product was calculated as amount of condensation per total amount of all products in %

aldol reaction catalysed by proline tetrazole at the start of the reaction (see Appendix 7). This experiment proved that the rate is not affected by the reaction product. Therefore next interaction between catalyst and reaction substrates was investigated.

Catalyst interaction was examined by ^{1}H-NMR spectroscopy using experimental set up described in paragraph 5.1.2. During the investigation of the interaction between acetone (**1**) and proline-tetrazole (**12**) three new peaks at 5.82 ppm, 4.15 ppm and 3.98 ppm were observed (Figure 5.13). From the relative integrated areas it was suggested that these three peaks belong to the same species. The peak at 5.82 ppm correlated well with a vinyl-proton at C=C double bond of possible enamine that was described by Hiroi and co-workers.[101]

By changing acetone (**1**) concentration in two consecutive experiments (0.6M, and 1.5M) while keeping the same amount of proline-tetrazole (**12**), it was confirmed that this new species exists in equilibrium with **1** and **2** (Figure 5.13). The relative amount of new species enhanced with an increase in the concentration of acetone: the ratio of 1:7 was observed between peak at 5.82 and α-proton of **12** at 4.8 ppm in the bottom spectrum; at higher amount of acetone (the top spectrum) the ratio between the same peaks changed to 1:2.4.

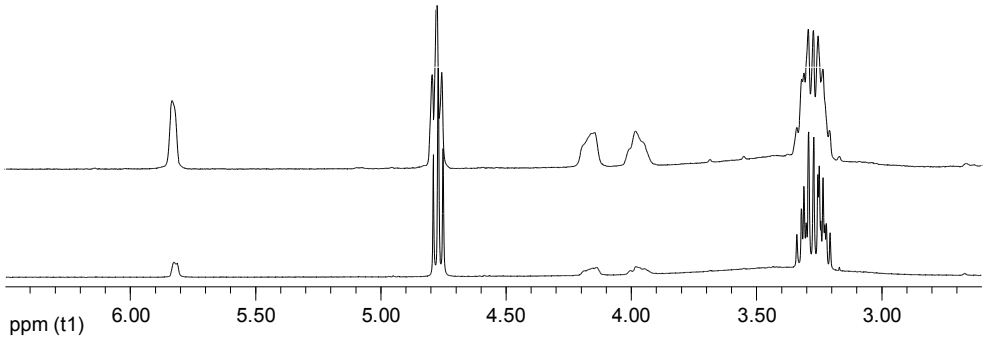

Figure 5.13 ^{1}H-NMR of the species formed from the interaction between **1** and 0.1M of [**12**] at 25 °C in DMSO. From bottom to top: 0.6M [**1**]; 1.5M [**1**].

In order to test the structure of the new species, the experiment with deuterium labelled d^{6}-acetone was carried out. If the new species are of enamine structure where peak at 5.82 ppm is a vinyl-proton at C=C double

bond of enamine, then this peak would not be visible when d^6-acetone is employed. Surprisingly, the signal of this proton at 5.82 ppm did not disappear as can be seen in Figure 5.14. This finding indicates that this proton belongs to the pyrrolidine ring fragment which left intact in the new species. Most likely, that an additional hetero-cycle is formed in the observed species, in a way resembling oxazolidinone **5** formed between proline and acetone. However in the case of proline-tetrazole this cycle is possibly imidazolidine ring, which is formed in addition to pyrrolidine and tetrazole rings. Hence in analogy to ^{1}H-NMR spectrum of proline-tetrazole, the signal at 5.82 ppm was assigned to α-H at C8 of imidazolidine **13** (Figure 5.14) formed between acetone and proline-tetrazole; signals at 4.15 and 3.98 ppm assigned to the well resolved two protons at the C5 next to N in pyrrolidine ring. The equilibrium constant for the formation of this species between **1** and **12** was estimated equalled to 0.017, which is surprisingly much smaller than it was estimated for the proline (0.12),[71] suggesting that more proline-tetrazole sits as a free catalyst species.

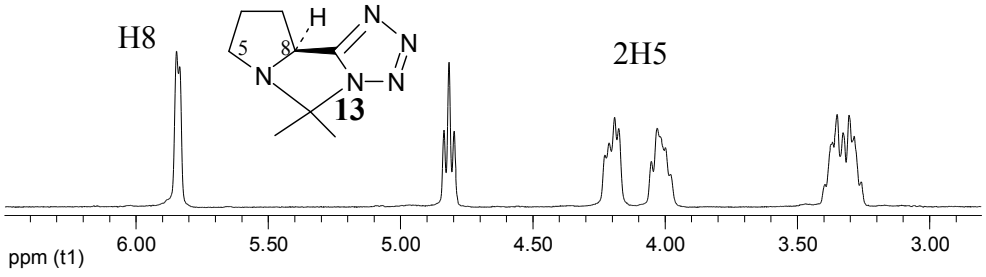

Figure 5.14 ^{1}H-NMR of the species formed from the interaction between 5M d^6-acetone and 0.1M **12** at 25 °C in DMSO: ratio between peaks at 5.82 ppm and 4.8 ppm is equalled to 1:1.

Interestingly the imidazolidine type species were also observed between acetone and other proline derivative by Gryko's group.[110, 111] However such species have not been implicated in the interaction between acetone and proline-tetrazole earlier in the investigations by Arvidsson and co-workers.[108] An additional support towards the imidazolidine type species formed by proline-tetrazole comes from the homonuclear coupling correlation analysis (COSY) which was carried out with the suppression of all singlets, such as methyl groups of acetone. ^{1}H-NMR spectrum of acetone produces a distinctive singlet at 2.09 ppm when measured in d^6-

DMSO, which is very strong due to the presence of six protons it accounts for. Hence these peaks reduce chances of observing coupling interaction between protons in species that are contained in only small amounts. When COSY with suppression of singlets was used to investigate the interaction between acetone (**1**) and proline-tetrazole (**12**), the spectrum showed a cross peak of coupling between two protons at 5.82 ppm and 4.15 ppm verifying the former implications that (*i*) both peaks belong to the same species and (*ii*) peak at 5.82 ppm is α-H of imidazolidine (Figure 5.15).

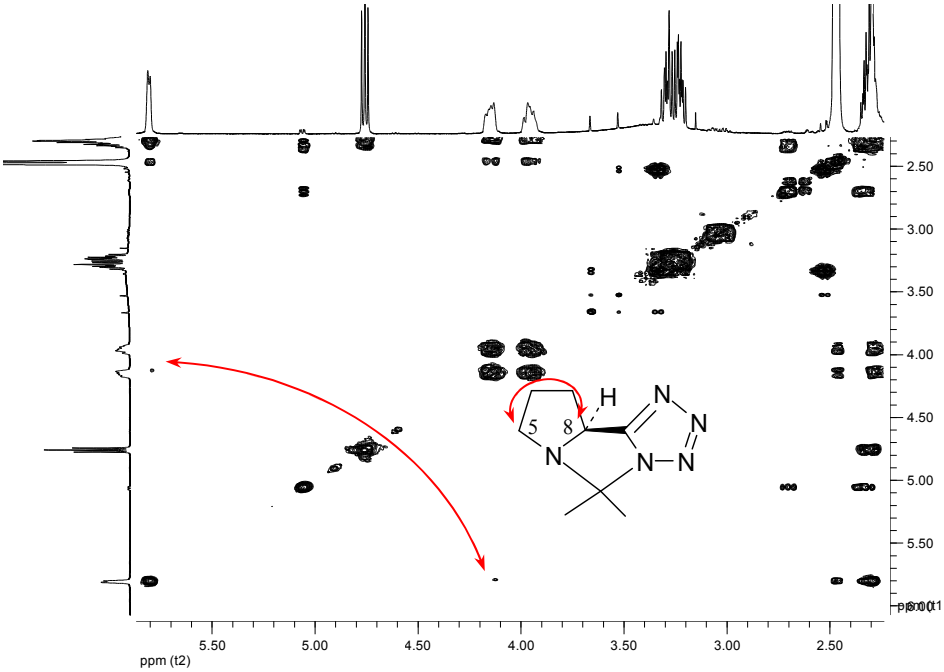

Figure 5.15 COSY spectrum of the species formed from the interaction between 1.5M d^6-acetone and 0.1M **12** at 25 °C in d^6-DMSO.

Although in section 5.1.2.2 was shown that proline reacts readily with aldehydes, ^{1}H-NMR investigation of the interaction between proline-tetrazole (**12**) and *o*-CBA (**2**) confirmed observation by Arvidsson and co-workers showing that there were no cyclic parasitic species similar to ones observed in the proline catalysed aldol reactions.[108] These species have not been observed by ^{1}H-NMR in the aldol reaction catalysed by other proline derivative, L-prolinethioamides. However when the same experiment was repeated in CH_2Cl_2, cyclic imidazolidinone species between their catalyst and an aromatic aldehyde were detected.[110]

5.2.3 Interaction between L-Proline-Tetrazole and the Reaction Product

Although the inhibition by the reaction product was not observed in the aldol reaction catalysed by proline-tetrazole, its interaction with the reaction product was nevertheless spectroscopically investigated. As expected within the time required for the aldol reaction to occur, there were no unknown species observed by ^{1}H-NMR. However when mixing of the product with the catalyst was carried out for a longer time (over a couple of hours) it was found by HPLC analysis that the enantiomeric excess of the product began to deplete while the amount of aldol dehydration product increases. This result suggests that the dehydration process may be enantioselective where only one enantiomer dehydrates or dehydration of one enantiomer occurs faster than dehydration of the other. After further investigation it was confirmed that kinetic resolution has taken place: both enantiomers of the aldol product form dehydration product however the *S*-product (which is minor, in case of L-proline-tetrazole catalysis) undergoes the dehydration process faster than the major enantiomer – *R*-product. Although this is an unfortunate event in the case of the reactions under study, such kinetic resolution might be utilised for the further enhancement of enantiomeric excess (for example, for the formation of *R*-product) at the end of a reaction, if L-proline-tetrazole is swapped with D-proline-tetrazole. Similar result was seen when the aldol product derived from various aromatic aldehydes was treated with that aldehyde in the presence of the proline derivative, L-prolinethioamide. However in this case instead of dehydration product, the increase in the amount of double addition product, product between the starting aldehyde and the cross-aldol product, was observed with concomitant depletion of the enantiomeric excess of the cross-aldol product.[111]

5.2.4 Additional Observation during L-Proline-tetrazole Catalysis

Double addition species **14** (Scheme 5.3) were also observed and identified in the aldol reaction of Scheme 4.1 catalysed by L-proline-tetrazole (see ^{1}H-NMR and ^{13}C-NMR in Appendix 3). Similar to aldol product **3**, the species **14** are also inclined to undergo dehydration.[111] The provisional results during the current investigation in addition to the study made by Gryko and co-workers provided a ground to propose the feasibility of a deactivation/ substrate inhibition route that involves the catalyst or, more specifically, the product iminium ion **15** as depicted in Scheme 5.3.[110, 111] This route may be responsible for the lost of aldehyde outside the catalytic cycle and, hence, the lack of overlay when the same *excess* protocol was applied (Figure 5.12). In addition such route could also potentially reduce the reaction yield.

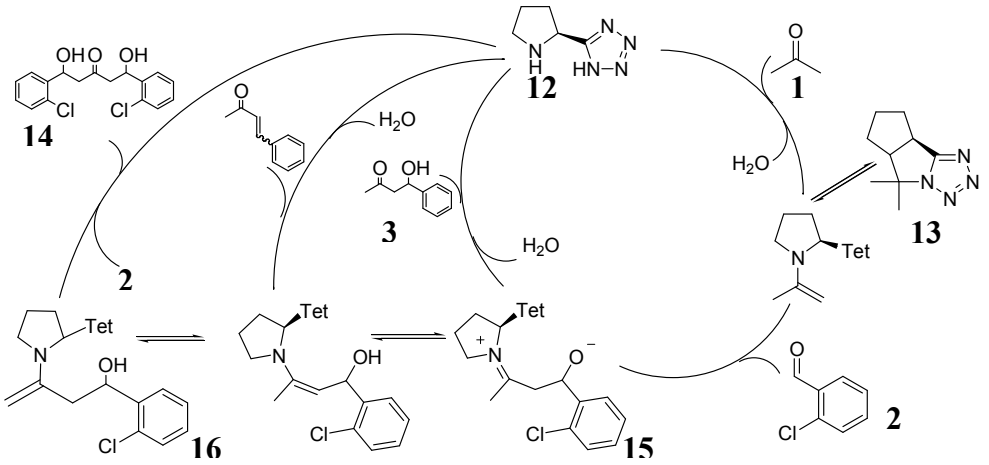

Scheme 5.3 Possible parallel reaction cycles occurring during the aldol reaction of Scheme 4.1 catalysed by L-proline-tetrazole ("Tet" – tetrazole ring abbreviation).

A deeper understanding of the implications of such a pathway in the loss of aldehyde requires further quantitative investigation. However if this route plays a more significant role in the L-proline-tetrazole catalysis than in the L-proline case, then it is likely that the hydrolysis step occurs much slower during the L-proline-tetrazole catalysis than it was observed in the case of the L-proline. Therefore iminium ion of the product may have more time to

equilibrate with the less stable product enamine species **16** and hence increase the chance to form the undesired double addition product **14**.

Interestingly, that the addition of water had much lesser effect on the rate of the aldol reactions catalysed by L-proline-tetrazole than it was observed during L-proline catalysis. Provisional experiments showed that 0.2-0.4 M of water had none or slightly accelerating effect on the rate, while further increase in the amount of water starts to suppress the rate. Unfortunately, it was not possible to find the conditions which would allow performing the reaction under steady-state catalyst concentration. Therefore for more quantitative investigation, such as modelling of the mathematical rate expression, the process of the formation of double addition product **14** should be investigated more closely and quantitatively.

5.3 Concluding Remarks

The study reported in the current chapter aimed to clarify the various roles water plays in the proline catalysed aldol reactions. It was shown that water embraces the complex and opposing tasks during proline catalysis, both on and off the catalytic cycle. On the cycle, the addition of water suppresses the intrinsic kinetic rate for the reaction of aromatic aldehydes, which may be rationalised by a shift in the relative concentration of the key intermediates. However, on the other hand, addition of water increases the total available catalyst concentration within the cycle due to suppression of the spectator species, and hence allowing the catalyst concentration to remain stable over the course of the reaction. Deconvoluting the processes occurring on and off the cycle will allow using the observed kinetic role of water as a mechanistic probe in obtaining true mechanistic understanding of this reaction.

Preliminary results concerning L-proline derivative, L-proline-tetrazole, showed that water does not have such a striking effect on the rate of the aldol reaction catalysed by this proline derivative. Even contrarily, small amounts of water promoted slight rate acceleration. Therefore a change in the rate-limiting step in the mechanism is possible. However conclusions

cannot be drawn from this observation before the true cause of observed reaction instability is entirely understood. Hence more work needs to be done to understand the L-proline-tetrazole catalysed system.

Chapter 6

Kinetic Analysis of the Aldol Reaction Catalysed by L-Proline

In the previous chapter it has been shown that catalyst stability over the course of the reaction can be achieved in proline catalysis of the aldol reaction by addition of water. The influence water has on the spectator species that are outside of catalytic cycle may be separated from the effect of water on the intrinsic kinetics. Investigation of the catalytic cycle's driving forces under the broad range of conditions in the absence of catalyst deactivation may now be undertaken. Therefore this chapter will probe the intrinsic kinetics of the proline catalysed aldol reaction. First of all, the power law will be used to quantify the magnitude of concentration dependencies using the graphical approach of manipulation kinetic data. Thereafter a more detailed kinetic analysis will be performed in order to confirm the validity of the proposed mechanism for proline catalysed reactions. The observed in the previous chapter kinetic role of water in the L-proline catalysed aldol reaction will also be used as a mechanistic probe to contribute to the overall mechanistic understanding.

6.1 The Global Kinetics of the Aldol Reactions: Power Law

Before going into detailed kinetic modelling, first, the global kinetics of the aldol reaction will be considered, to provide a general overview of the

reaction kinetics without considering the elementary steps and reaction intermediates. This investigation allows assessing the relative magnitude of the driving forces in the reactions, and thereafter providing clues for derivation of the mechanistic kinetic model to use for further detailed analysis.

The experimental protocol for this study involves reactions carried out with different values of *excess* ([**e**]) as described in section 2.1.2. All reactions were carried in the reaction calorimeter as discussed in section 4.2. The set of initial conditions employed for each reaction is provided in Table 6.1. Under each set of conditions the reactions were checked for the lack of catalyst deactivation using the "same *excess*" protocol (see section 2.1.1).

Table 6.1 Initial conditions (IC) employed during the experiments.

Experiments	Solvent	[**1**]	[**2**]	[**e**]	[**4**]
E6.1: IC		2.76 M	0.5 M	2.26 M	0.1/0.5 M
6.2: IC	DMSO	1.99 M	0.5 M	1.50 M	0.1 M
6.3: IC		1.25 M	0.5 M	0.75 M	0.1/0.5 M

The main approach of the current investigation is based on the graphical manipulation of obtained kinetic data. Assuming the power law form of the aldol reaction rate, its expression can be written as in equation 6.1.

$$rate = k \cdot [\mathbf{1}]^x \cdot [\mathbf{2}]^y \cdot [\mathbf{4}]^z \qquad \text{(eq 6.1)}$$

Equation 6.1 indicates that the rate is proportional to the concentration of the substrates **1**, **2** and **4** raised to the power, which refers to the reaction orders in each of these substrates, respectively x, y and z. The overall reaction order is equal to the sum of these orders. Although often orders in substrates are postulated from the theory and correlate with the stoichiometric coefficients of the reaction, it is not always the case. This in particular is true when reactions are catalytic and involve active intermediates and the series of sequential reactions. Hence the rate law must be confirmed by experimental observations.

6.1.1 The Proline Saturation Concentration

NMR investigations in section 5.1.2.1 revealed the relationship between the concentration of solution phase proline and added water concentration. It suggested that a saturated solution of proline exists in equilibrium with solid proline and in the presence of acetone proline's solubility limit in DMSO is ca 0.01M. Observation of solution proline being in equilibrium with solid proline was also supported by experiments showing that reactions carried out above the saturation limit exhibit zero order kinetics in the total amount of proline (**4**) added. Four aldol reactions under conditions displayed in Table 6.1 (E6.1 and E6.3) with two different amounts of catalysts **4** were performed in order to check this phenomenon. Each reaction was also tested for catalyst deactivation using the same *excess* protocol (see Appendix 7). The graphical rate equations obtained from four sets of experimental data as shown in Figure 6.1 confirm that the rates of the reactions under the same conditions are not dependent on the concentration of the catalyst.

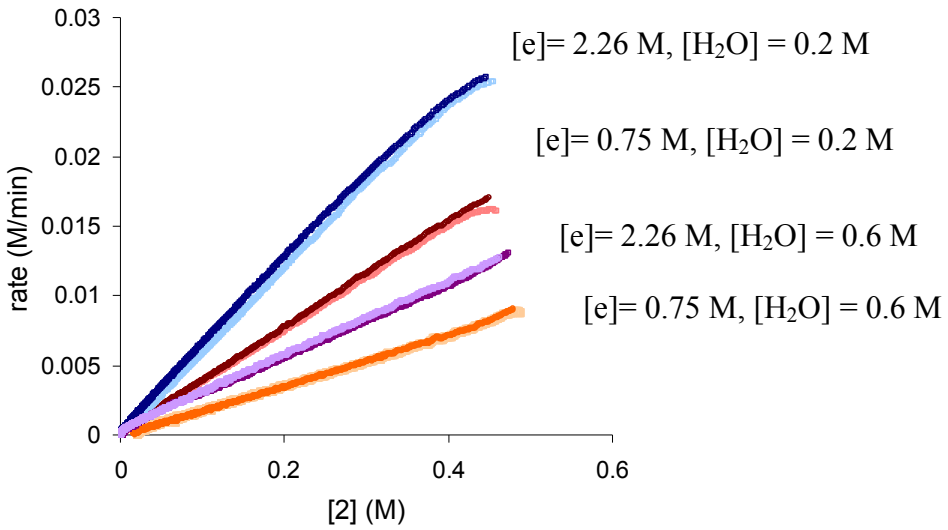

Figure 6.1 Plot of the rate of the aldol reaction of Scheme 4.1 in DMSO versus concentration of substrate [**2**]. Initial reaction conditions are as displayed in Table 6.1 for E6.1 and E6.3: $[\mathbf{2}]_0 = 0.5$ M. Overlay between experiments performed under the same conditions but different amounts of proline (**4**) (0.05 M and 0.1 M) shows zero order kinetics in **4**.

Figure 6.1 also illustrates the rate-concentration relationship in the aldol reaction. The reaction exhibits overall close to first order concentration dependency under all employed conditions, with positive order kinetics in the concentration of both substrates **1** and **2**, revealed from the fact that the experiments with different excess showed no overlay in graphical rate equations plotted as rate vs. $[\mathbf{2}]$.

6.1.2 Magnitudes of the Driving Forces

Taking into the account the observation about proline concentration, the power law rate expression (equation 6.1) can be simplified to probe the kinetic dependencies in substrates **1** and **2,** in cases the total employed catalyst concentration is higher its solubility limit. Catalyst concentration remains at its solubility limit under the particular conditions of water concentration and hence may be considered a constant lumped into an apparent rate constant.

The graphical methodology of reaction progress kinetic analysis may now be employed to find a kinetic order separately for each substrate of the reaction. First, both sides of the equation 6.1 are divided by the substrate $[\mathbf{1}]$ to the power of *x* providing a normalised rate equation 6.2.

$$normalised\ \ rate = \frac{rate}{[\mathbf{1}]^x} = k \cdot [\mathbf{2}]^y \qquad \text{(eq 6.2)}$$

Equation 6.2 gives a formula for a straight line with overlay between experiments carried out at different excess, if the function of rate and $[\mathbf{1}]$ on the left side is plotted on the Y-axis, and the function of $[\mathbf{2}]$ on the right is plotted on the X-axis and the correct powers *x* and *y* are employed. Thus the magnitude of the driving forces attributed to $[\mathbf{1}]$ and $[\mathbf{2}]$ may be assessed via this graphical manipulation.

When *x* and *y* are not correctly chosen, three experimental data sets do not overlay and do not exhibit linearity as it can be seen from Figure 6.2a for the arbitrarily chosen *x* and *y*. This graph shows a complex kinetic

behaviour in the normalized substrate concentration [**1**]. However it was found by trial and error that overlay can be found for $x \approx 0.5$ as shown in Figure 6.2b. It can also be noted that at this value of x, the curves become close to straight lines, meaning that $y \approx 1$. Thus a reasonable description of the reaction's driving forces is given by the equation 6.1 with $x \approx 0.5$ and $y \approx 1$ (when catalyst concentration is higher its solubility limit: z = 0). Positive order kinetics in [**2**] suggests that the rate-limiting step could be addition of aldehyde or formation of a new C-C bond but confirms that enamine formation cannot be rate limiting.

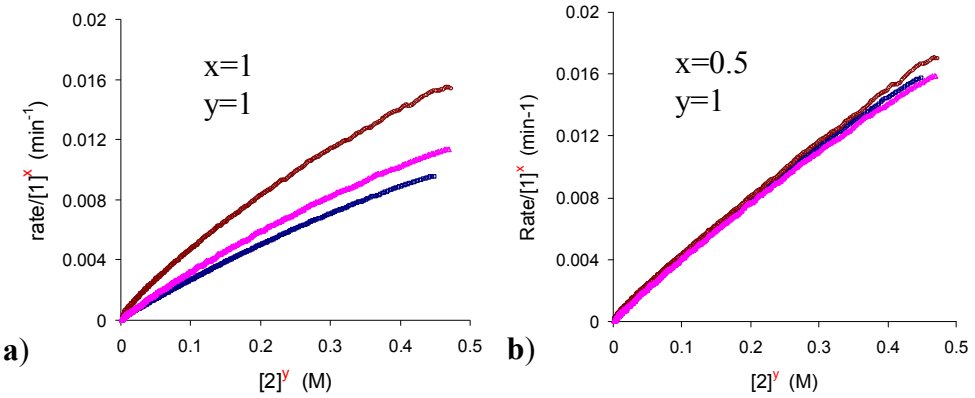

Figure 6.2 Plot of the normalized aldol reaction rate as in Equation 6.2 versus concentration of substrate $[\mathbf{2}]^y$. Blue squares: $[\mathbf{1}]_0$ = 2.75 M; $[\mathbf{2}]_0$ = 0.5 M; pink triangles: $[\mathbf{1}]_0$ = 2.00 M; $[\mathbf{2}]_0$ = 0.5 M; brown circles $[\mathbf{1}]_0$ = 1.25 M; $[\mathbf{2}]_0$ = 0.5 M; reaction carried in DMSO and 0.2 M H_2O with 0.1 M of total proline (**4**) concentration: a) $x = 1$ and $y = 1$; b) $x = 0.5$ and $y = 1$.

These results obtained from the graphical manipulations may be compared to the values of x and y obtained from solving them by nonlinear regression analysis of the experimental rate curves fitted to the power law form of equation 6.1. Carrying out this fitting using the curve-fitting Solver program[100] incorporated in Excel® for Chemists and the SolvStat.xls macro for statistical calculations, it was found $x = 0.46 \pm 0.002$ and $y = 0.91 \pm 0.001$. This reasonable agreement between the graphical methodology and the more mathematically rigorous approach lends support to the concept that kinetic information from experimental data sets may be extracted accurately by graphical as well as mathematical means. Thus this graphical methodology provides a user-friendly version of kinetic analysis, by

offering graphical manipulations of the kinetic data to establish the catalytic robustness and "visual nonlinear regression" analysis to acquire the necessary concentration dependencies.

6.2 Detailed Kinetic Investigation

6.2.1 Rate-limiting Step

The values of $x = 0.5$ and $y = 1$ for the kinetic orders in acetone [**1**] and *o*-CBA [**2**] are not intrinsic kinetic orders for the aldol reaction. Rather, these values represent the power-law compromise for a catalytic reaction with a more complex catalytic rate law. Our task is to find a mechanistically-based rate law for a steady-state catalytic cycle that can accommodate the power law form. The enamine mechanism, which was discussed previously is shown in Scheme 6.1.[56]

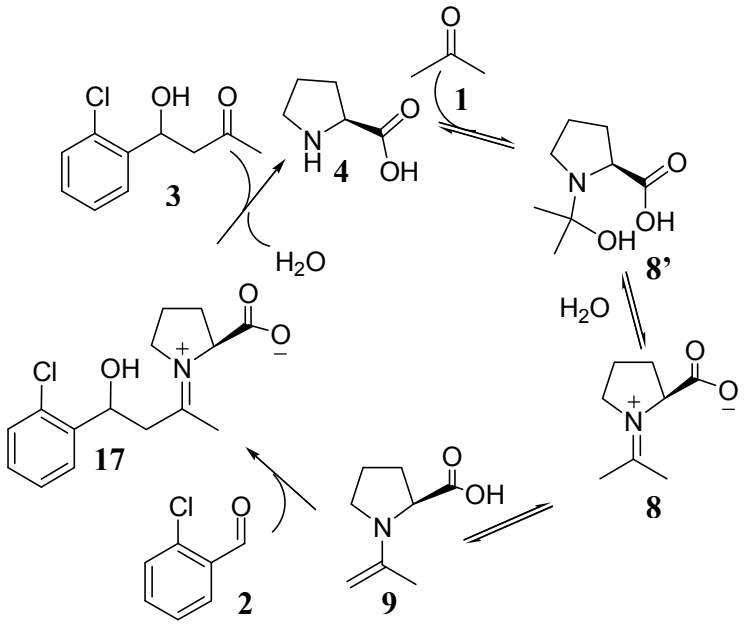

Scheme 6.1 Enamine mechanism proposed for the aldol reaction of Scheme 4.1.

The generally accepted mechanism for the intramolecular aldol reaction states that proline (**4**) reacts with ketone **1** to form enamine **9** via the formation of tetrahedral hemiaminal **8'** and iminium ion **8**. Enamine **9** then attacks the aldehyde substrate **2**, which then followed by the hydrolysis of the product iminium ion **17** to release the product **3**. Kinetically the steps between **8'**, **8** and enamine **9** cannot be separated and have to be lumped

together. Therefore Scheme 6.2 presents the overall mechanism of Scheme 6.1 combined into three kinetically distinguishable elementary steps, where the rate of each one is expressed through the rate constants k_1, k_{-1}, k_2, k_{-2} and k_3 and includes only active species **4**, **9** and **17**.

$$[\mathbf{1}]+[\mathbf{4}] \underset{k_{-1}}{\overset{k_1}{\rightleftharpoons}} [\mathbf{9}]+[H_2O]$$

$$[\mathbf{9}]+[\mathbf{2}] \underset{k_{-2}}{\overset{k_2}{\rightleftharpoons}} [\mathbf{17}]$$

$$[\mathbf{17}]+[H_2O] \xrightarrow{k_3} [\mathbf{3}]+[\mathbf{4}]$$

Scheme 6.2 Kinetically distinguishable elementary steps for the mechanism of the aldol reaction of Scheme 4.1.

Which of these steps is rate limiting? Different opinions have prevailed, none of which was based on the in-depth kinetic reasoning. Cordova and co-workers suggested that addition of water improves catalyst turnover due to the faster hydrolysis of the product iminium ion which would assume hydrolysis step rate-limiting.[112] Rate limiting formation of enamine was suggested in analogy to class I aldolases.[29] The theoretical calculations provided grounds to believe that formation of C-C bond is rate-limiting.[65, 67]

The full steady-state rate equation 6.1 was derived for the catalytic network in Scheme 6.2: total catalyst $[\mathbf{4}]_{total}$ partitions within three main species **4**, **9** and **17** ($[\mathbf{4}]_{total} = [\mathbf{4}] + [\mathbf{9}] + [\mathbf{17}]$, derivation of equation 6.1 can be found in Appendix 4). It is clear from this equation that the intrinsic kinetic role of water in this reaction network can be complex. The same is true for the reaction order in each substrate. The steady state reaction rate law in equation 6.1 can be simplified by assuming different limiting cases in which the rate-limiting step and catalyst resting state differ. The reaction rate laws for three cases are presented in equations 6.2-6.4.

$$r = \frac{k_1 k_2 k_3 [\mathbf{1}][\mathbf{2}][H_2O][\mathbf{4}]_{total}}{[H_2O](k_{-1}k_{-2} + k_{-1}k_3[H_2O] + k_3k_2[\mathbf{2}]) + k_1k_{-2}[\mathbf{1}] + k_1k_3[\mathbf{1}][H_2O] + k_1k_2[\mathbf{1}][\mathbf{2}]}$$

(eq 6.1)

Case I is when enamine **9** formation is rate-limiting with a resting state being in free proline **4**:

$$[\mathbf{1}] + [\mathbf{4}] \xrightarrow{k_1} [\mathbf{9}] + [H_2O]$$

Hence, in case I, $[\mathbf{4}]_{total} = [\mathbf{4}]$ and the rate will be only influenced by substrate **1** concentration and is represented by equation 6.2.

$$rate_I = k_1[\mathbf{1}][\mathbf{4}]_{total} \qquad \text{(eq 6.2)}$$

The rate-limiting electrophilic addition of aldehyde **2** or formation of product iminium ion **17** presents case II:

$$[\mathbf{9}] + [\mathbf{2}] \xrightarrow{k_2} [\mathbf{17}]$$

The enamine **9** is the resting state in the mechanism and therefore $[\mathbf{4}]_{total} = [\mathbf{9}]$. Rate should be influenced by the concentrations of **4** and **2** and relationship is presented by equation 6.3.

$$rate_{II} = k_2[\mathbf{2}][\mathbf{4}]_{total} \qquad \text{(eq 6.3)}$$

Limiting case III occurs when product hydrolysis is rate-limiting with product iminium ion **17** being the resting state:

$$[\mathbf{17}] + [H_2O] \xrightarrow{k_3} [\mathbf{3}] + [\mathbf{4}]$$

Hence, in this case $[\mathbf{4}]_{total} = [\mathbf{17}]$ and rate is only dependent on **4** and H_2O, which corresponds to rate in equation 6.4.

$$rate_{III} = k_3[H_2O][\mathbf{4}]_{total} \qquad \text{(eq 6.4)}$$

Clearly none of these liming cases describes the positive order kinetics in the concentration of both substrates **1** and **2**, as well as the rate suppression by addition of water. This indicates that if the mechanism in Scheme 6.1 holds, there is no single dominant resting state and the catalyst partitions itself between more intermediate species. The kinetic observation is consistent with the addition of aldehyde or C-C bond formation being rate-limiting step. In this model the catalyst is not fully saturated within enamine **9**, as in equation 6.3, and instead it partitions between free proline **4** and enamine **9**: $[\mathbf{4}]_{total} = [\mathbf{4}] + [\mathbf{9}]$ and therefore both substrate concentrations **1** and **2** should influence the rate of the aldol reaction. The rate law for such case is shown in equation 6.5.

$$rate = \frac{k_1 k_2 [\mathbf{1}][\mathbf{2}][\mathbf{4}]_{total}}{k_{-1}[H_2O] + k_2[\mathbf{2}] + k_1[\mathbf{1}]} \qquad \text{(eq 6.5)}$$

The form of equation 6.5 rationalizes the rate suppression by increasing amount of water, as it was observed during the investigation presented in section 5.1. The equilibrium position for enamine **9** is driven back towards unoccupied proline sites as water is increased, resulting in a decrease in the driving force of the rate-limiting step. The positive orders in both substrates **1** and **2** are also rationalized qualitatively by this equation.

6.2.2 Kinetic Isotope Effect

In order to enhance our mechanistic understanding, isotopic labelling studies were carried out. A Kinetic Isotope Effect (*KIE*) comes about when the ratio of rates of two reactants that only differ in isotopic composition is not equal to one: such as in Equation 6.6, rate of the reaction carried out with protonated components (k_H) versus rate of the reaction carried out with deuterated components (k_D). This ratio of rates between light and heavy isotopes is a characteristic of the reaction and the nature of the transition states. Kinetic isotope effect studies could aid in elucidating a reaction mechanism and also provide knowledge of the transition state.[113-115] There

are two possible kinetic isotope effects: (*i*) the primary effect occurs when a bond involving isotopic substituent is broken during the reaction; and (*ii*) the secondary occurs when isotopically substituted atoms are not directly involved in the bond breaking or forming step but still influences the vibrational energy of a system.

$$KIE = \frac{k_H}{k_D} \qquad \text{(eq 6.6)}$$

The difference in the rate of two isotopes is often explained by the difference in their zero point energy E_0, which is a minimal vibrational energy of the bond.[116] Considering isotopic substitution in C-H(D) bond, zero point energy E_0 is ca. 1.15 kcal/mol lower for a C-D bond than for a C-H bond, due to the greater mass of deuterium. The lower zero point energy indicates that a C-D bond has higher activation energy E_a and is stronger than a C-H. The rate constant for C-H(D) dissociation may be described by the equation 6.7.

$$k_{H(D)} = A_{H(D)} e^{(-E_{aH(D)}/RT)} \qquad \text{(eq 6.7)}$$

The exponential factor $A_{H(D)}$ is often assumed identical for both H and D atoms.[114] The activation energy $E_{aH(D)}$ consists of electronic energy, E_e, and vibrational energy, E_{vib}. Since E_e should be the same for both isotopic atoms, the difference in activation energy will be equal to the difference in vibrational energy or zero point energy that is 1.15 kcal/mol. Hence the primary *KIE* calculated for the C-H(D) cleavage at 25 °C in this case is equal to 7. Thus in a reaction where a C-H bond is broken or formed in the rate limiting step, a reaction involving a deuterium-substituted compound should show a significantly lower rate. The secondary kinetic isotope effect (*SKIE*) is usually lower in magnitude, but may still provide mechanistic information. For example, depending on the carbon hybridisation a secondary kinetic isotope effect can be of "normal" (*SKIE* $\geq$1) or "inverse" (*SKIE* < 1) magnitude. When reaction undergoes a change in carbon hybridisation from sp^2 to sp^3 then the inverse isotope effect occurs. This is due to the asymmetry of the sp^2 hybridised carbon, the force constant at the

transition state is stronger as it is developing sp^3 character. The force constant is weaker when a change in carbon hybridisation from sp^3 to sp^2 occurs and therefore normal secondary isotope effect is observed.[113, 116]

6.2.2.1 Investigation of Kinetic Isotope Effect in the Aldol Reaction

In the current study the kinetic isotope effect was examined for C-H(D) bond by comparing the rates between reaction employing deuterium labelled acetone versus normal acetone. Also the kinetic isotope effect was studied for OH(D) bond using deuterium oxide versus water. The reaction conditions employed during these experiments was as those used in the experiments E6.1 and E6.3 (Table 6.1).

All possible scenarios of the kinetic isotope effect that may be envisioned to take place in the enamine catalysis are associated with the chosen rate limiting step. If the formation of enamine **9** [scheme 6.3, (*1*)] is the rate limiting step, one should expect the primary kinetic isotope effect to take place with a theoretical value around 7. This is due to the breakage of the C-H(D) bond when one of the methyl hydrogens of the acetone is transferred to form enamine C=C double bond. If addition of *o*-CBA **2** to the enamine **9** [scheme 6.3, (*2*)] is rate limiting, one should anticipate an inverse secondary isotope effect due to formation of C-C bond between the carbonyl carbon of **2** and the terminal carbon of enamine **9**.[67]

NMR and FTIR studies revealed rapid exchange between protons of acetone and water, and acetone and product –OH in the presence of the proline, therefore it is expected that the presence of heavier deuterons in all molecules will be a weighted average of their initial concentrations in acetone and water.

The experimental results using deuterium labelled acetone revealed that the value of kinetic isotope value at 15 % conversion of aldehyde was varying from 1.94 to 2.17 while changing the amount of acetone between 1.25 M and 2.75 M. This changing kinetic isotope value is not completely

straightforward, however, implying proton scrambling that was also observed by NMR and FTIR spectroscopy and could be utilised in proton inventory study, which will be discussed shortly (see Section 6.2.2.2). Nevertheless the observed value of ca. 2 is much lower than the predicted magnitude for the enamine formation (step *1* in Scheme 6.3) as rate-limiting, which should be around 7, and hence suggests that the rate-limiting step takes place later after the enamine formation.

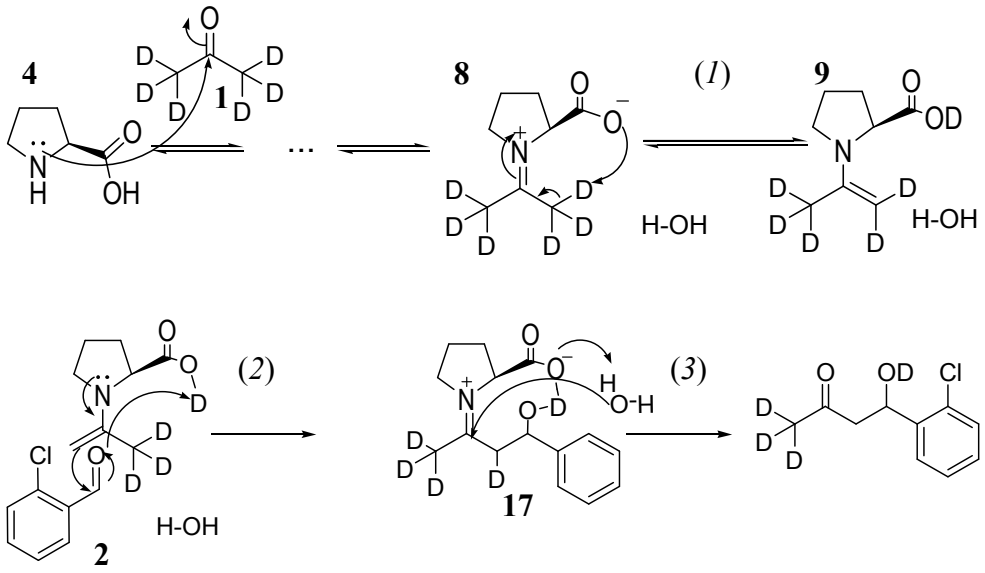

Scheme 6.3 Mechanism of three possible rate-limiting steps in the proline catalysed aldol reaction, showing contributions for the overall kinetic isotope effect: (*1*) cleavage of the C-D bond of iminium ion **8**. Formation of a tetrahedral intermediate was omitted for simplicity; (*2*) formation of C-C bond from the attack by enamine **9** on **2**; (*3*) hydrolysis of iminium ion **17**.

As discussed earlier, the formation of C-C bond should exhibit the inverse kinetic isotope effect with a value less than one. Therefore to rationalise the obtained experimental value it may be proposed that the rate-limiting step is the formation of C-C bond that is aided by the protonation of carbonyl oxygen of electrophile by the carboxylic group of the enamine, which exhibit normal kinetic isotope effect. Therefore the contribution of both effects may result in the observed value of ca 2. Additional reinforcement towards acquired value comes from the quantum chemical calculations which were carried out by Broadbelt to assess the isotope effect of the addition of the *o*-CBA to the enamine and afforded a value of 1.97.[1]

The reliability of the obtained magnitude of kinetic isotope effect was also considered by Broadbelt.[1] Her results showed that in the reaction where the transformation of an sp^2 carbon atom to an sp^3 occurs, such as addition of methyl radical to 1-propene, kinetic isotope value is indeed less than unity: 0.72 (Table 6.2: entry 1). Hydroxy proton transfer was also assessed by these computations using reactions with methoxy radicals (Table 6.2: entries 2 and 3). The predicted values for such kinetic isotope effect were 4.83 and 3.85. Assuming that in the enamine mechanism, those two motions occur in one step, one could expect a combined kinetic isotope effect where the value is greater than unity but suppressed compared to the typical proton transfer value due to the presence of an inverse α-secondary isotope effect.

Table 6.2 Rate constants and kinetic isotope effect (*KIE*) calculated using density functional theory (B3LYP/6-31G(d) in CPCM solvent of DMSO) for different reactions with hydrogen and deuterium.[1]

Entry	Reaction	k_H	k_D	*KIE*
		L mol^{-1} s^{-1}	L mol^{-1} s^{-1}	
1	1-propene + methyl radical → 2-butyl radical	$1.39 \cdot 10^2$	$1.94 \cdot 10^2$	0.72
2	Methoxy radical + acetaldehyde → methanol + acetoxy radical	$1.93 \cdot 10^{12}$	$3.99 \cdot 10^{11}$	4.83
3	Methoxy radical + hydrogen chloride → methanol + chloride radical	$7.91 \cdot 10^{12}$	$2.05 \cdot 10^{12}$	3.85

When iminium ion hydrolysis is rate limiting [Scheme 6.3, (3)] one should expect the effect from deuterium oxide on the rate of a reaction. However due to observed scrambling between protons of acetone and deuterium oxide, and higher amount of protons in acetone compared to deuterium oxide/water, the effect from altering the composition of water (H/D) is not necessarily be well manifested, which can be described as a concentration effect. As expected, experiments where water was replaced with deuterium oxide (0.2 M – 0.6 M) did not show any pronounced effect on the rate of aldol reaction, even with the lowest amount of acetone (1.25 M) and highest

[1] Professor L. J. Broadbelt final report (EPSRC grant)

employed amount of water (0.6 M), where one out of 6 protons originates in added water. Therefore the results from investigating the effect of deuterium oxide cannot be conclusive.

6.2.2.2 Proton Inventory Study

Observed proton scrambling between the acetone and water, along with the changing kinetic isotope value signified that the kinetic isotope effect depends on the amount of deuterium atoms present in the system. Therefore it was decided to carry out a "proton inventory" measurement. This technique is often used in the aqueous chemical systems to establish the number of exchanging proton sites involved in a transition state and contribution of an individual site, or fractionation factor, to the total isotope effect.[115, 117]

In these experiments the total amount of acetone was kept constant at 2.75 M and 1.25 M as in experiments E6.1 and E6.3 (Table 6.1, at $[H_2O]$ = 0.4 M) while the fraction of deuterium was changed from 0 to unity. All experiments were carried out in the reaction calorimeter following the procedures described in section 4.3. The Figure 6.3 presents the plot of observed rate at 15% conversion of *o*-CBA (**2**) versus increasing atom fraction of deuterium. As can be seen the dependency is linear (R=0.99) indicating involvement of one proton transfer within the transition state.[117] This result is consistent with the proposed one proton transfer between carboxylic group of the enamine and carbonyl oxygen of aldehyde. The data from both experiments with different total amount of acetone (2.75 M and 1.25 M) was fitted by using curve-fitting Solver program[100] simultaneously to the simplified expression of the Gross-Butler Equation 6.8 to provide the fractionation factor ϕ^*_{TS} of 0.46±0.02.

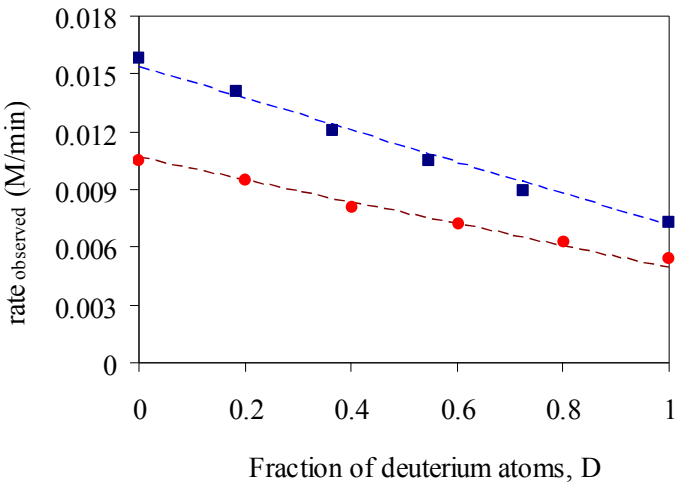

Figure 6.3 The effect on the rate by the present deuterium fraction in the aldol reaction of Scheme 4.1 carried out at constant overall concentration of acetone [**1**] and varying fraction of d^6-acetone. Initial overall $[\mathbf{1}]_0$: 2.75 M (blue squares); 1.25 M (red circles). Dotted lines: rate predicted by model in equation 6.8.

The fractionation factor can be thought of as representing the hypothetical process where reactant and transition state sites interpose equilibrium for proton exchange with water. This process is presented in Scheme 6.4.

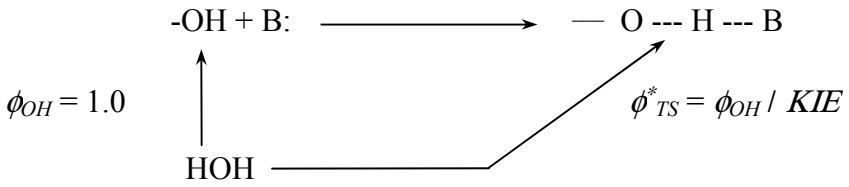

Scheme 6.4 Hypothetical equilibrium for exchange with water.[117]

The fractionation factor for the hypothetical exchange between hydroxyl group and water (ϕ_{OH}) could be assumed equal 1.[117, 118] Hence knowing the overall kinetic isotope value, the fractionation factor for the hydrogen transfer in the transition state, ϕ^*_{TS}, can be calculated as a ratio between ϕ_{OH} and kinetic isotope value. The calculated magnitude of ϕ^*_{TS} in such case is equalled to 0.48 and is in a good correlation with a value obtained from experimental data fitted to one transition-state hydrogen transfer model (Equation 6.8). The fractionation factor below unity implies that hydrogen binding in the transition state is less restricted to motions than the hydrogen motion in a water site.[117]

$$rate_{observed} = rate_H \cdot D \cdot (\phi^*_{TS} - 1) + rate_H \qquad \text{(eq 6.8)}$$

6.2.3 Detailed Kinetic Modelling

The purpose of detailed kinetic modelling is to assess quantitatively the viability of the Equation 6.5 and in addition to refine the mechanism of the aldol reaction of Scheme 4.1. Also it can assist in considering other factors that potentially may affect the reaction.

Firstly, Equation 6.5, which contains 3 adjustable parameters, was tested using kinetic data obtained from carrying out 18 reactions (including 9 same *excess* experiments) at three fixed water levels: 0.2 M, 0.4 M and 0.6 M; all other initial conditions are as it was provided in Table 6.1. As a standard procedure each experiment in Table 6.1 was performed using the "same *excess*" protocol (see section 2.1.1) in order to confirm the reproducibility and lack of catalyst instability. Although the total amount of the employed proline was 0.1 M, the $[\mathbf{4}]_{total}$ in the Equation 6.5 was different for each water concentration as determined in section 5.1.2.1: 0.0127 M, 0.0132 M and 0.0149 M respectively for 0.2 M, 0.4 M and 0.6 M H_2O. In order to avoid uncertainties, such as potential induction period or error arising from the correction of heat of mixing at the beginning of the reaction and the high number of data at high conversion, experimental data between 10-85 % conversion was only regressed and statistically analysed (Figure 6.4).

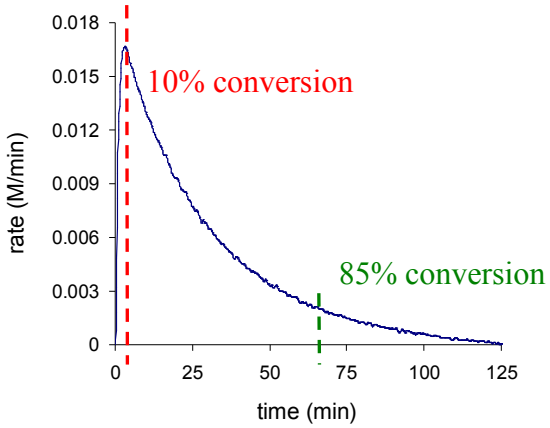

Figure 6.4 Temporal rate profile of the aldol reaction of Scheme 4.1. Data between dashed lines was used for the regression and statistical analysis.

The simulations of the enamine mechanism of scheme 6.1 qualitatively captured the general features of the substrate concentration dependencies and the rate suppression by increasing amount of water as can be seen in

Figure 6.5 and Table 6.3. However quantitative fitting of the data to the rate equation results in ambiguous conclusions. The rate is overestimated at the highest water concentration and underestimated at the lowest water concentration. Equation 6.5 was unable to reproduce quantitatively the important kinetic features, including the shape of the rate/concentration profile, which is particularly pronounced at 0.6 M water level and the highest acetone concentration studied (2.75 M). Equation 6.5 demands that rate should be most affected at lower water and acetone **1** concentration, as the term k_1[1] will have a more dramatic impact on the magnitude of the denominator when added to the lower value of [H_2O] at a given concentration of *o*-CBA **2**. However the experimental results show the opposite behaviour where rate is more suppressed at higher water and acetone concentration. This could indicate that additional inhibiting role for water may exist in the mechanism. Although modelling results for reactions in DMF are not presented here, a similar outcome was observed (see Appendix 7).

6.2.3.1 Additional Considerations in Assessing the Mechanism

The lack of quantitative fit of the data to the overall rate equation suggests that the proposed mechanism fails to take into account some features of the reaction chemistry. Thus it is useful to propose additional possibilities that may affect the mechanism of the aldol reaction:

(i) Water forms an off-cycle species via interaction with the catalyst that further influences the rate of the aldol reaction. (new species)

(ii) Water effectively changes the medium of the reaction and hence affects all rate constants differently at different amounts of water. (separate rate constants for different water concentrations)

(iii) Water effectively changes the medium of the reaction however the enamine equilibrium is less affected than the irreversible rate-

limiting step of the reaction. (fixing some but not all of the rate constants for different water concentrations)

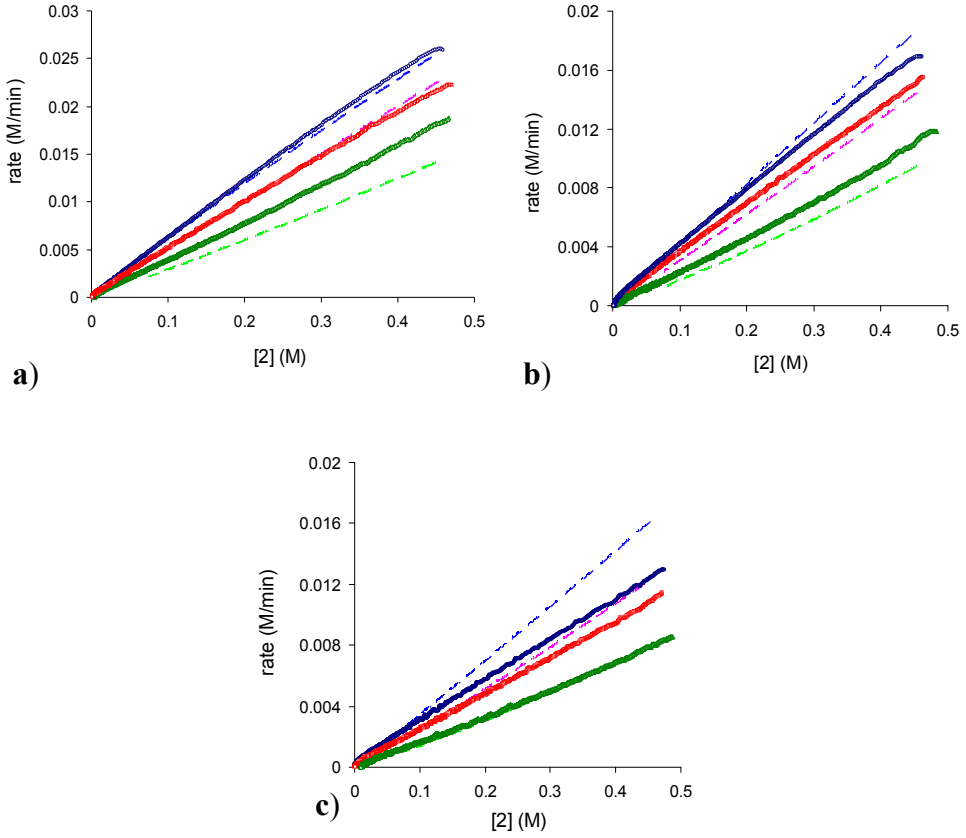

Figure 6.5 Kinetic modelling of the aldol reaction progress data according to the model of Scheme 6.1. Blue circles: $[\mathbf{1}]_0$ = 2.75 M; $[\mathbf{2}]_0$ = 0.5 M; red squares: $[\mathbf{1}]_0$ = 2.00 M; $[\mathbf{2}]_0$ = 0.5 M; green triangles $[\mathbf{1}]_0$ = 1.25 M; $[\mathbf{2}]_0$ = 0.5 M; reaction carried out at 25 °C in DMSO with 0.1 M of total proline concentration. Added water concentrations are: a) 0.2 M; b) 0.4 M; c) 0.6 M. Dotted lines represent the calculated rate values.

Proposal *(i)*. ^{1}H-NMR spectroscopy showed that addition of water results in the slight increase in the solution concentration of proline (see Section 5.2.1). Despite this observation the reaction rate is suppressed by the increasing concentration of water to a greater extent than may be accounted for by the enamine mechanism in Equation 6.5. However, if an interaction between water and proline exists which precludes a portion of the proline from taking part in the catalytic cycle then the total proline available for the catalytic cycle may decrease as water increases. It is known that proline exists as a zwitterion in water and can interact with water, acting as both acid and base.[76] Hence hydrogen bonding between proline and water may result in a portion of proline being sequestered by water outside the catalytic

cycle. In addition the ^{17}O-NMR investigations by Spisni and co-workers indicated the possibility of the formation of dimer complexes in DMSO between L-proline and water.[119] The authors suggested that proline is hydrogen bonded to at least two water molecules through the oxygen atom at the carboxylate group. Such process may be represented as equilibrium between proline and a putative inactive proline-water complex depicted as **18** in Scheme 6.5.

The steady-state rate Equation 6.5 modified to include the effect of the proline-water interaction to form **18** (Scheme 6.5) is given in Equation 6.10 and possesses an additional adjustable parameter. The stronger inhibiting role of water in this rate expression is evident from the squared term in water concentration in the denominator. The fit of 18 reaction data sets to this model provided a better picture than the previous model without putative species **18** as can be seen in Figure 6.6 and Table 6.3.

$$[\mathbf{4}]+[H_2O] \overset{K_W}{\rightleftharpoons} [\mathbf{18}]$$

$$[\mathbf{1}]+[\mathbf{4}] \underset{k_{-1}}{\overset{k_1}{\rightleftharpoons}} [\mathbf{9}]+[H_2O]$$

$$[\mathbf{5}]+[\mathbf{2}] \underset{k_{-2}}{\overset{k_2}{\rightleftharpoons}} [\mathbf{17}]$$

$$[\mathbf{17}]+[H_2O] \overset{k_3}{\longrightarrow} [\mathbf{3}]+[\mathbf{4}]$$

Scheme 6.5 Elementary steps for the mechanism of the aldol reaction in Scheme 4.1 including the additional proline sequestering by water (step 1).

$$rate = \frac{k_1 k_2 [\mathbf{1}][\mathbf{2}][\mathbf{4}]_{total}}{k_{-1}K_W[H_2O]^2 + k_{-1}[H_2O] + k_2 K_W [\mathbf{2}][H_2O] + k_1[\mathbf{1}] + k_2[\mathbf{2}]}$$

(eq. 6.10)

It is known that carbonyl compounds such as aldehyde and ketones are susceptible towards hydration forming various hydrates or 1,1-diols.[6] This phenomenon could also affect the rate of the reaction by introducing additional equilibria similar to that considered in the case of the proline hydration (Scheme 6.5). The position of the equilibrium mainly depends on

the structure of the carbonyl compounds where steric and electronic factors may play roles. Sterically congested carbonyls are not prone to hydrate easily while electronegative atoms such as halogens attached to the carbon next to the carbonyl group can increase the potential to hydration. In view of the aldol reaction between acetone and *o*-CBA of Scheme 4.1 it is viable to expect that hydration of neither carbonyl will exhibit a large equilibrium constant. In addition the study carried out by Hilal and co-workers on the calculation of equilibrium hydration constants (K_{eq}) provided hydration equilibrium constant for acetone: $K_{eq} = 0.002$, while for *m*-chlorobenzaldehyde and *p*-chlorobenzaldehyde, isomeric compounds of *o*-CBA, $K_{eq} = 0.016\text{-}0.020$.[120] Hence for this reason the possible equilibria between water and carbonyl compounds were not considered here.

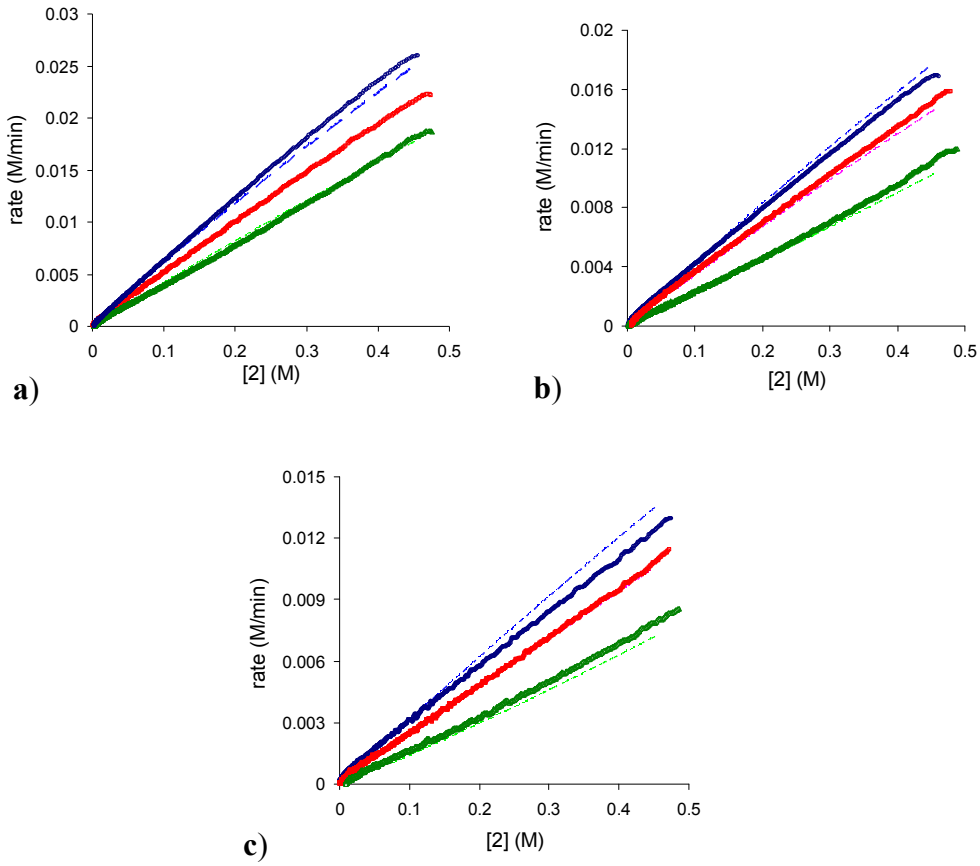

Figure 6.6 Kinetic modelling of the aldol reaction progress data according to Proposal *i*. Blue circles: $[\mathbf{1}]_0 = 2.75$ M; $[\mathbf{2}]_0 = 0.5$ M; red squares: $[\mathbf{1}]_0 = 2.00$ M; $[\mathbf{2}]_0 = 0.5$ M; green triangles $[\mathbf{1}]_0 = 1.25$ M; $[\mathbf{2}]_0 = 0.5$ M; reaction carried out in DMSO with 0.1 M of total proline concentration. Added water concentrations are: a) 0.2 M; b) 0.4 M; c) 0.6 M. Dotted lines represent the calculated rate values.

Proposal (ii). The inhibiting influence of water on the rate of the aldol reaction could also be regarded as an effect of the hydrogen bonding interaction between water molecules and aprotic solvent, DMSO.[121] In such case the increasing amount of water may change solvating properties of the medium and hence affect the rate constants of all elementary steps of the reaction.[122] Separate simulation of each set of experimental kinetic data obtained with different fixed amount of water could provide the sense for how good/bad the experimental data represents the proposed enamine mechanism described by the Equation 6.5 when possible media effect is not taken on account. As expected, the separate regression of different water levels resulted in excellent agreement between experimental data sets and the model values as can be seen in Figure 6.7 and Table 6.3. Although water increasingly suppresses each of the obtained regression parameters, the rate parameter defining the reversible formation of proline from enamine species, k_{-1}, was the most affected by water (Figure 6.8). Therefore it was decided again to fit all the experimental data to the Equation 6.5, albeit keeping the most adjusted parameter k_{-1} constant for all experimental sets while changing the least adjusted parameter k_2 (Proposal iii).

This assumption suggests that the magnitude of the equilibrium constant for the formation of enamine is essentially independent of the surrounding media, albeit the rate constant for C-C bond forming step is different for each water level. Figure 6.9 and Table 6.3 demonstrates that with this assumption it was possible to obtain an excellent fit of all experimental data sets to the Equation 6.5.

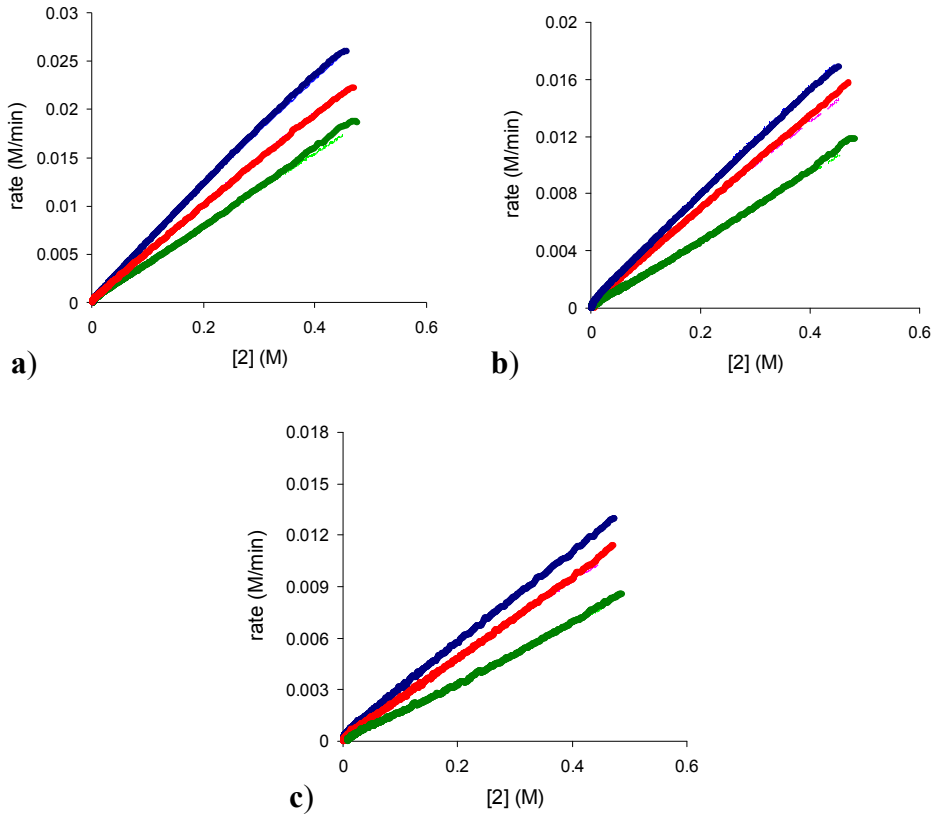

Figure 6.7 Kinetic modelling of the aldol reaction progress data according to Proposal *ii*. Blue circles: $[\mathbf{1}]_0$ = 2.75 M; $[\mathbf{2}]_0$ = 0.5 M; red squares: $[\mathbf{1}]_0$ = 2.00 M; $[\mathbf{2}]_0$ = 0.5 M; green triangles $[\mathbf{1}]_0$ = 1.25 M; $[\mathbf{2}]_0$ = 0.5 M; reaction carried out in DMSO with 0.1 M of total proline concentration. Added water concentrations are: a) 0.2 M; b) 0.4 M; c) 0.6 M. Dotted lines represent the calculated rate values.

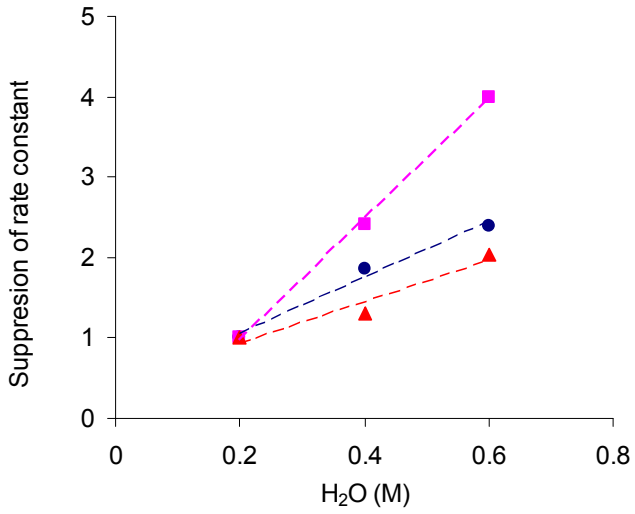

Figure 6.8 The effect of water on the rate constants of the aldol reaction obtained from simulating each set of experimental data separately for each water level. Blue circles: k_1; pink squares: k_{-1}; red triangles: k_2.

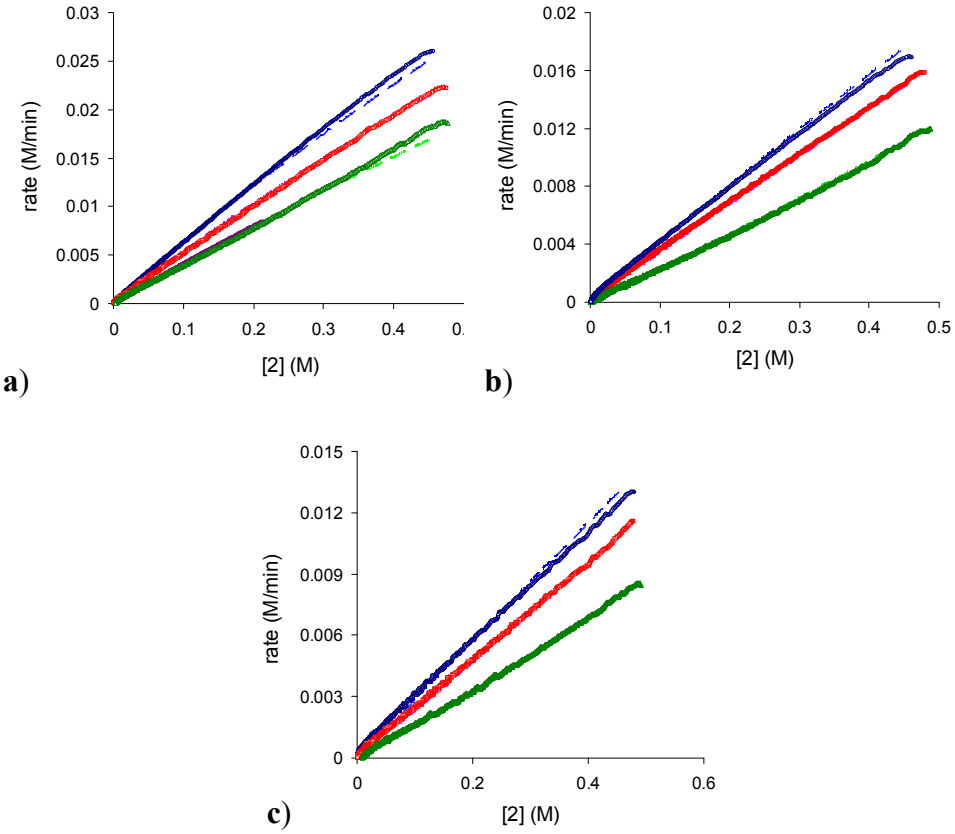

Figure 6.9 Kinetic modelling of the aldol reaction progress data according to Proposal *iii*. Blue circles: $[\mathbf{1}]_0$ = 2.75 M; $[\mathbf{2}]_0$ = 0.5 M; red squares: $[\mathbf{1}]_0$ = 2.00 M; $[\mathbf{2}]_0$ = 0.5 M; green triangles $[\mathbf{1}]_0$ = 1.25 M; $[\mathbf{2}]_0$ = 0.5 M; reaction carried out in DMSO with 0.1 M of total proline concentration. Added water concentrations are: a) 0.2 M; b) 0.4 M; c) 0.6 M. Dotted lines represent the calculated rate values.

6.2.4 Summary of Detailed Kinetic Modelling: Regressed Kinetic Parameters and Statistics

Four potential kinetic models based on the enamine mechanism of Scheme 6.1 were examined and discussed. Here their statistical considerations are provided. All adjustable parameters (rate constants), which were obtained from fitting experimental data to the investigated models using Solver curve-fitting program, are summarised in Appendix 5.[100] The statistical parameters were calculated by SolvStat.xls macro and equations used to calculate the correlation parameter, R^2, and root mean square deviation, SE (y) are provided in Appendix 5.

Table 6.3 Best fit kinetic parameters for the aldol reaction simulations shown in Figures 6.4-6.8.[1]

Model	# of parameters	R^2	SE (y)	Remarks
1: Scheme 6.1, Equation 6.5 Figure 6.5	3	0.952072	0.000853	Poor fit, lowest number of parameters
(*i*):Scheme 6.5, Equation 6.10 Figure 6.6	4	0.991959	0.000338	Reasonable fit, low number of adjustable parameters
(*ii*):Scheme 6.1 Equation 6.5 Figure 6.7	9	0.996232	0.000229	Excellent fit, high number of adjustable parameters
(*iii*)Scheme 6.1 Equation 6.5 Figure 6.9	5	0.994922	0.000268	Reasonable fit

As can be seen from Table 6.3 models ***i-iii*** have high R^2 and low SE (y) values which suggest that all of these models could provide a meaningful prediction of the reaction rates. Although R^2 in model ***1*** is the lowest, 3 adjustable parameters may justify application of this model. The highest R^2 value and lowest SE (y) was obtained for model ***iii*** although incorporation of 9 adjustable parameters makes it less compelling, regardless of its good correlation with experimental data. Nevertheless the goodness of this model supports the enamine mechanism with rate-limiting C-C bond formation as described by Equation 6.5 with additional complications of catalyst-water interactions. It is difficult to distinguish the likelihood between model ***ii*** and ***iii*** because both models have similar R^2 and SE (y) and number of adjustable parameters. In addition both factors discussed in section 6.2.3, hydrogen bonding between proline and water, and medium effect, equally may affect the rate of the reaction. Therefore in this research neither of

[1] Data from 10-85% conversion used in fitting and statistical analysis

these two models could be discriminated but both are offered as chemically and physically reasonable working models. Additional testing of these possibilities awaits further experimental results.

6.3 Concluding Remarks

Kinetic analysis of the aldol reaction catalysed by proline of the Scheme 4.1 showed positive order kinetics in both substrates and rate suppression by water. This is consistent with the model where the rate-limiting step follows formation of enamine but precedes the hydrolysis step. This implies attack on the enamine, where the C-C bond is formed, as rate-limiting, also supported by the kinetic isotope effects. Detailed kinetic modelling offered additional suggestions regarding the role that water may play in the proline catalysis.

Chapter 7

Origin of Autoinductive Behaviour in α-Aminoxylation Reaction

In the previous chapters a comprehensive mechanistic picture for the proline catalysed aldol reaction was developed. It has been shown that attack of enamine on an electrophile for C-C bond formation is rate-limiting. This was supported by both detailed kinetic modelling and kinetic isotope effects. This chapter will discuss the differences that exist between aldol and α-aminoxylation reactions. The aldol reaction exhibits positive order behaviour, where rate decreases with decrease in the substrate concentration. However α-aminoxylation reaction shows unusual behaviour, with the rate increasing while substrates are being consumed.[123, 124]

7.1 Initial Investigations of α-Aminoxylation reaction

The great potential of the proline catalysed α-aminoxylation reaction lies in its ease of α-oxygenating of various carbonyl compounds.[17, 55] This is the first direct chemical method to afford α-oxygenated products, which previously were accessed with the aid of chiral auxiliaries. Initial studies showed that L-proline catalysed α-aminoxylation reactions between propionaldehyde and nitrosobenzene (Scheme 7.1) exhibit dramatically higher activity than proline catalysed aldol reactions, even with a lower amount of the catalyst and lower reaction temperature, and in solvents

where proline solubility is lowest.[26, 79] When continuous monitoring of the reaction progress was undertaken by reaction calorimetry by our group, it was observed that the rate of α-aminoxylation in chloroform rose steadily through the course of the reaction.[123] This behaviour suggests that catalyst improves over the course of a reaction in the manner of an autocatalytic or autoinductive reaction. In these reactions the product either acts itself as a catalyst (autocatalytic reactions) or promotes the formation of a more efficient catalyst (autoinductive reactions).

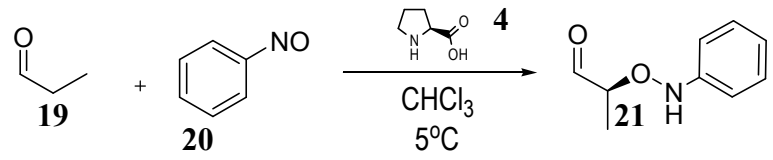

Scheme 7.1 α-Aminoxylation reaction between propionaldehyde (**19**) and nitrosobenzene (**20**).

When the reaction product was added to the fresh reaction substrates in the absence of proline, the reaction did not occur, suggesting that the rising rate in α-aminoxylation could not be explained by an autocatalytic effect.[123] Interestingly, however, when a fresh dose of substrates were added to the crude reaction mixture containing catalysts and reaction product from the first reaction, the new reaction was initiated with the initial rate as high as the rate at the end of the first reaction. This result provided grounds to suggests an autoinductive cause of the rising rate in α-aminoxylation reaction where the proline-product adduct formed over the course of the reaction serves as a more active catalyst.[123, 125] These early experimental investigations implied that the α-aminoxylation reaction occurs via dual pathway, where the activated product-proline species catalyses the fastest pathway.

7.2 Does Product of α-Aminoxylation Reaction Possess a Unique Property of Accelerating its own Reaction?

Investigations were undertaken to assess the generality of the rate-enhancing effect in the α-aminoxylation reaction of Scheme 7.1 by monitoring the effects of various additives other than the reaction's own product. Due to

the fact that proline solubility is low in all organic solvents (in chloroform, for example, its solubility is measured in thousands parts of a mole per litre: $0.51 \cdot 10^{-3}$[126]), a particular reaction preparation protocol was employed to insure that the phenomenon of the proline in a hetereogeneous mixture being solubilised throughout the reaction can be excluded. A mixture of L-proline (**4**) and the additive employed was stirred in the chloroform at room temperature for 1 hour and filtered through 0.45 μm filter to remove any remaining solid proline. The filtrate containing only solution phase was used as a catalyst in the series of α-aminoxylation reactions. Additional amount of additive was added directly into each reaction vial. The reactions were initiated by injecting the propionaldehyde (**19**) and monitored by the reaction calorimetry using set up similar to that described in section 4.2 for aldol reaction. The validity of observed kinetic data was ensured by correlating data between FTIR and HPLC measurements, which are presented in the Appendix 2.

The study was initiated by exploring the effect that the aldol product (**3**) has on the rate of the α-aminoxylation reaction. When the α-aminoxylation reaction was carried out with addition of the aldol product (**3**), the rate was enhanced by increasing amount of product in such a way that the rate gradually shifted from the autoinductive behaviour toward positive order kinetics as the concentration of aldol product was increasing from 0.1 M to 0.7M (Figure 7.1a). The rate constants obtained by fitting the linear tredline to the initial temporal concentration profiles can be seen in Figure 7.1b. It shows that the rate of the α-aminoxylation reaction is proportional to the added amount of aldol product (**3**).

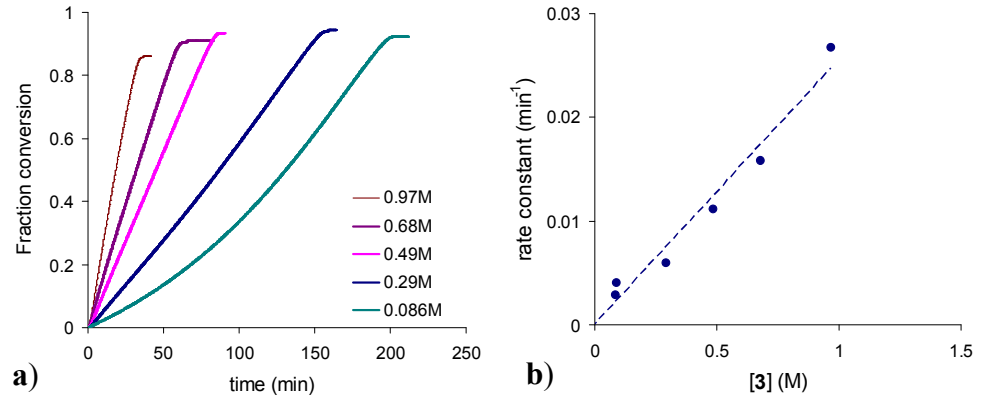

Figure 7.1 The α-aminoxylation reaction of Scheme 7.1 using 2 M **19**, 0.5 M **20** and the filtrate from the mixture of 0.04 M **4** and 0.1 M **3** in $CHCl_3$: a) fraction conversion versus time for aldol product **3** as noted; b) rate constants as a function of added aldol product **3**. Reaction product *ee* 97-98 % in all cases.

Thus the source of the rate enhancement in the α-aminoxylation reaction is not limited to its own product **21**; the aldol product **3** is also capable of accelerating the rate. In addition, the similar rate acceleration was observed by other additives including acetic acid and methanol (Figure 7.2).

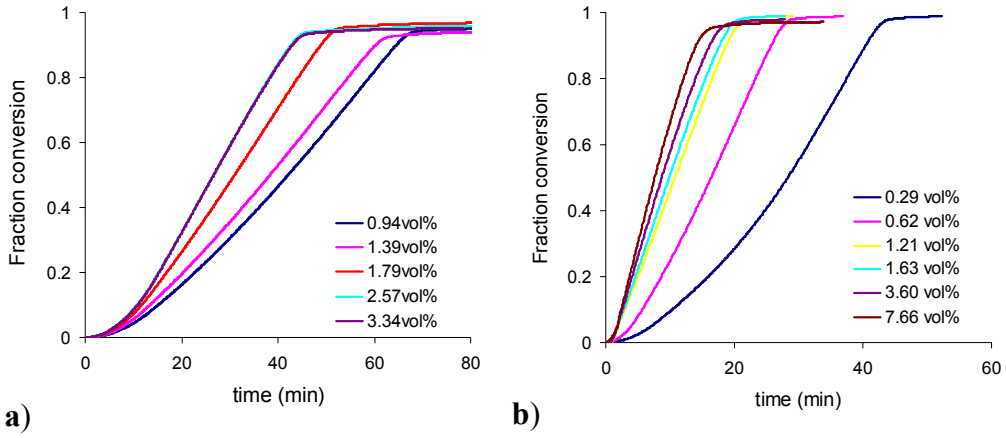

Figure 7.2 The α-aminoxylation reaction of Scheme 7.1 using 2 M **19**, 0.5 M **20** and the filtrate from the mixture of 0.04 M **4** and CH_3OH or CH_3COOH in $CHCl_3$. a) fraction conversion versus time for CH_3OH; b) fraction conversion versus time for CH_3COOH.

Interestingly, in agreement with the results obtained in Figure 7.1, the shift from autoinductive behaviour towards positive order kinetics was already observed previously for the α-aminoxylation reaction with addition of 5 vol % of methanol.[127] However in that this effect was attributed simply

proline solubilisation, and studies with lower methanol concentration were not carried out. The results of the current study showed that at low concentration of additives (0.1M aldol product, 0.1-2 vol % acetic acid and methanol) the rising rate still prevails (Figure 7.1 and 7.2) indicating that the reaction product concentration dominates the mechanism. With the higher amount of additives the dominance of additive concentration can be seen from the shift away from the autoinductive behaviour. It is also interesting to note, that rate appears to saturate for acetic acid and methanol, which can be seen in Figure 7.3, indicating that the binding for these additive could be stronger.

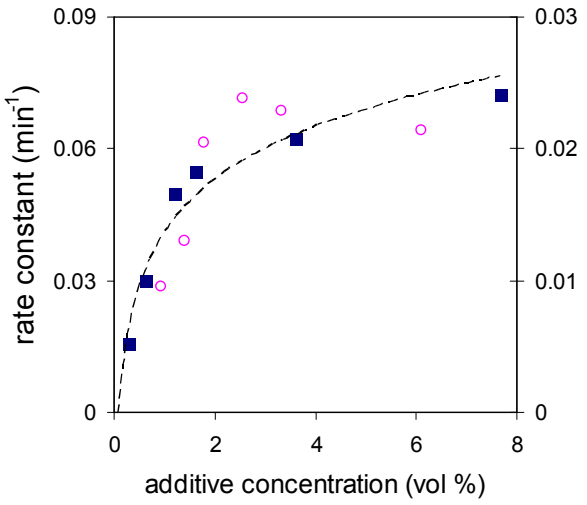

Figure 7.3 Rate constant versus additive concentration for the α-aminoxylation reaction of Scheme 7.1 using 2 M **19**, 0.5 M **20** and the filtrate from the mixture of 0.04 M **4** and CH_3OH or CH_3COOH in $CHCl_3$. Left ordinate: squares for CH_3COOH; Right ordinate: empty circles for CH_3OH. Dotted line is a guide to eye.

While the rate of α-aminoxylation reaction was enhanced by all additives, the aldol reaction carried out in chloroform with addition of aldol product, propionic acid and methanol showed neither pronounced rate acceleration nor a change in the kinetic profile upon addition of any of these additives (Figure 7.4). In all these experiments the experimental filtering protocol described earlier was also used in order to avoid effect due to proline solubilisation. The reactions were carried out using FTIR spectrometer and validity of the experimental tool was ensured by comparing the fractional

conversion with HPLC over the course of the reaction prior initiating the addition experiments (see Appendix 7).

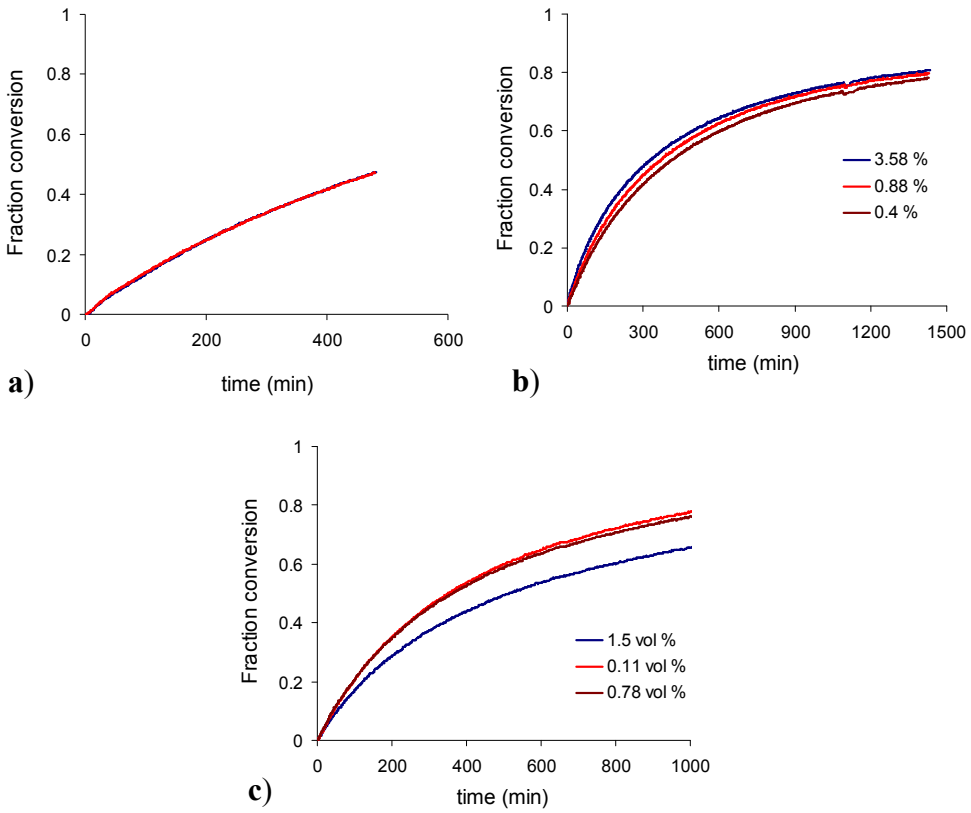

Figure 7.4 The fraction conversion versus time for the aldol reaction of Scheme 4.1 using 2 M **1**, 0.5 M **2** and the filtrate in $CHCl_3$ from the mixture of 0.04 M **4** and a) aldol product (**3**); b) CH_3OH; c) CH_3CH_2COOH.

7.3 Rationalisation of the Observed Differences between Aldol and the α-Aminoxylation Reactions

Rationalization of the observed results lies in considering mechanistic differences between the aldol and α-aminoxylation reactions. Both reactions are catalysed by the same catalyst and therefore thought to follow the general pathway. However kinetic analysis, which was carried out for both the aldol and α-aminoxylation reactions using reaction progress kinetic analysis, showed different concentration dependencies.[25, 38] The α-aminoxylation reaction exhibits positive order kinetics in the concentrations of the reaction product (**21**) and aldehyde (nucleophile **19**) and zero order kinetics in the concentration of nitrosobenzene (electrophile **20**).[125, 128]

Assuming that the α-aminoxylation reaction proceeds through the same steps of enamine catalysis as an aldol reaction (see section 6.2), zero order kinetics in nitrosobenzene (**20**) implies the occurrence of the limiting case I discussed in section 6.2.1. This limiting case is possible when addition of a donor substrate is rate limiting with the resting state being the free proline species.

Thus this outcome suggests that two reactions have different rate limiting steps: addition of the donor aldehyde **19** to the catalyst **4** is the rate limiting step for the α-aminoxylation reaction, while electrophilic addition of **2** to enamine **9** is rate limiting for the aldol reaction, as described in Chapter 6. This is depicted in Scheme 7.2. If the role of additives is to enhance the rate of addition to the catalyst **4**, this therefore will be seen as an increase in the rate of α-aminoxylation reaction. For the aldol reaction the enhanced rate of nucleophilic addition to the catalyst **4** will not necessarily change the steady-state concentration of enamine **5**, which provides a rate-determining driving force.

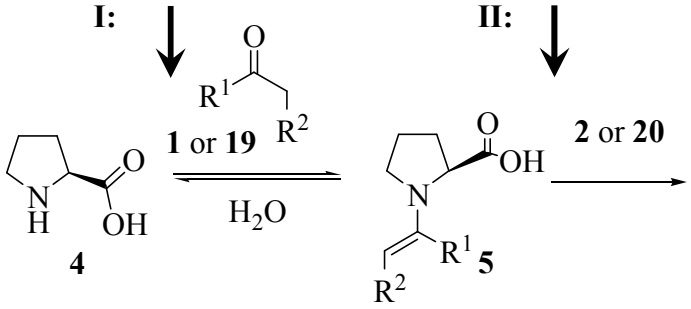

Scheme 7.2 Simplified scheme presenting first two steps of the aldol of Scheme 4.1 and α-aminoxylation of Scheme 7.1. **I**: Rate-limiting step for α-aminoxylation; **II:** Rate-limiting step for aldol reaction.

Though the kinetic role of additives may be similar for both reactions, it will appear as a rate enhancement only when the activation affects the rate limiting step. The important consideration as well is the stereochemical control of the aldol and α-aminoxylation reactions, which was not affected by the addition of additives. This may be explained by the fact that the stereochemistry determining step, which is for both reactions considered to be the enamine attack on the electrophile,[66, 69] occurs after the influence of additives.

7.3.1 The Nature of Rate-Enhancing Interactions

Although, the nature of the rate-enhancing interaction is not revealed unambiguously by the kinetic analysis, the possible formation of hydrogen-bonding species between the proline (**4**) and the α-aminoxylation product (**21**) was already proposed on the basis of DFT calculations.[128] The calculations implied that the external hydrogen bonding interactions between the proline and the reaction product may suppress the internal proline interaction occurring between lone pair of its nitrogen and its carboxylic proton. Such internal interaction makes proline less nucleophilic by forming an optimal "closed" proline conformation, where the lone pair of nitrogen is less available for attack. When proline is exposed to external hydrogen bonding via the carboxyl proton and the reaction product, it may "open" and therefore be more ready to initiate nucleophilic addition.[67, 128]

Similarly, hydrogen bonding interactions can be proposed between the carboxyl and/or amine proton of the proline (**4**) and additives, such as the aldol product, acetic acid and methanol. The ^{1}H-NMR spectrum of proline in chloroform with methanol or acetic acid at concentrations where the rate profile shifts from autoinductive behaviour, begin to resemble the spectrum of proline in pure methanol or acetic acid, where hydrogen bonding with amino acids readily occurs (see Appendix 6).

Hydrogen-bonding activation of substrates leading to enhanced reactivity and/ or enantioselectivity has also been reported and became an important consideration in organocatalytic design and rationalisation of catalytic behaviour.[44, 129] Therefore it may also be proposed that the reactivity of substrate can be affected by the addition of these additives. Hence the interaction between propionaldehyde (**19**) and the aldol product (**3**) was studied by ^{1}H-NMR spectroscopy, carrying out a so-called NMR titration experiment in the absence of the proline catalyst.[130, 131] When increasing amounts of the aldol product (0.1 M – 2 M) were added to 2 M propionaldehyde mixture in chloroform, a proton upfield shift next to the carbonyl oxygen was observed indicating possible formation of the hydrogen bonded complex (Figure 7.5). At the same time a downfield shift

of the proton of the aldol product (**3**) hydroxyl group was also observed, indicating the decrease in the electron density around this proton. This can be explained by assuming that this proton formed additional hydrogen bonding with the carbonyl oxygen of the propionaldehyde (**19**) which deshielded its nucleus. Hence the slight upfield shift of the proton in **19** may be explained by a shielding effect, which could occur due to the carbonyl oxygen interacting with the hydroxy proton of the aldol product **3**.

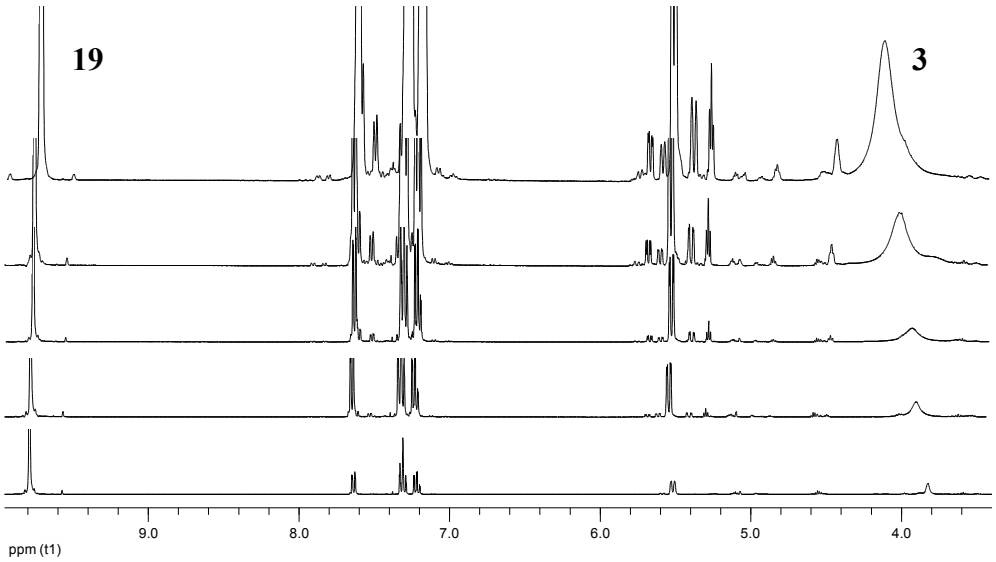

Figure 7.5 Interaction between carbonyl proton of 2 M **19** and hydroxy proton of **3**. From bottom to top: 0.1 M **3**, 0.3 M **3**, 0.5 M **3**, 1 M **3**, 2 M **3**.

Further analysis of the observed chemical shifts as a function of the additive concentration may provide the binding constant K' for the hydrogen bonded species. The methodology of the used calculations is given in the Appendix 6.[130] It was assumed that the binding stoichiometry is 1:1, meaning that one molecule of each substrate produces one molecule of hydrogen bonded complex. Hence the binding constant for the complexation of propionaldehyde (**19**) with the aldol product **3** was estimated to $K' = 0.05\ M^{-1}$ ($\Delta G = 3.3$ kJ/mol), which is comparable with the typical value for the strength of hydrogen bonding between hydroxyl group and lone pair of oxygen.[1]

[1] IUPAC Compendium of Chemical Terminology, Electronic version, http://goldbook.iupac.org/H02899.html.

Such activation of the proline (**4**) and propionaldehyde (**19**) is represented in the Scheme 7.3. Since both species are being the driving forces for the α-aminoxylation reaction both mechanisms are possible and it is not straightforward to distinguish between them for the present case.

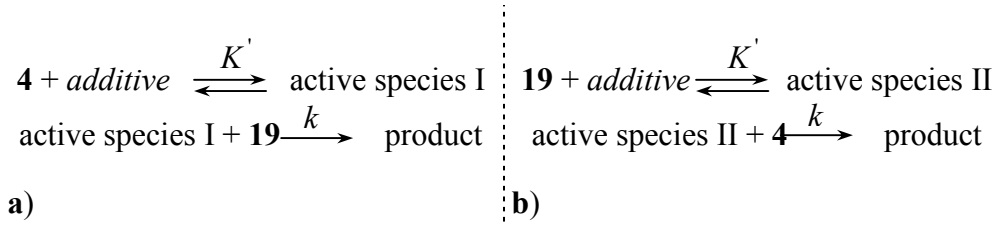

Scheme 7.3 Two models representing α-aminoxylation reaction with the activation by additives of: a) L-proline (**4**); b) propionaldehyde (**19**).

Scheme 7.3a represents the proline (**4**) activation via active species I, where activation by additives outweighs substrate activation by the reaction product as the additive concentration increased. In Scheme 6.3b analogous substrate activation by additives is represented via active species II. A rate law describing reaction product formation via the two activated pathways as in Scheme 7.3 may be written as in equation 7.1.

$$rate = \frac{k[\mathbf{19}]_t \cdot [additive] \cdot [\mathbf{4}]_t}{1 + K'[additive]} \qquad \text{(eq 7.1)}$$

This equation is consistent with both types of activation and assumes quasi-equilibrium applied on activated species I and II.[1] This equation implies that at high additive concentration the reaction should exhibit saturation kinetics in additives, as was observed in methanol and acetic acid, and positive order kinetics in **19**.

7.3.2 Simulation of the Kinetic Behaviour in α-Aminoxylation and Aldol Reactions

Proposed proline and substrate activation models (model I and model II) were also used to simulate the behaviour of the aldol and α-aminoxylation reactions, using COPASI 4.2 simulator for biochemical networks.[132]

[1] $[\mathbf{4}]_t = [\mathbf{4}] + [\text{active species I}]$
$[\mathbf{19}]_t = [\mathbf{19}] + [\text{active species II}]$

COPASI is versatile, easy to use program incorporating deterministic and stochastic simulation methods. In the current work the deterministic approach was applied and reaction equations for both models were automatically converted to the appropriate mathematical equations. Each model was described entirely, showing each kinetically meaningful step of the proline catalysed enamine mechanism, in addition to four steps representing the activation by the reaction product and other additives (Scheme 7.4 and 7.5). It was hoped that the simulation could provide a ground for selecting between two models.

$$Nu^- + \mathbf{4} \underset{k_{-1}}{\overset{k_1}{\rightleftharpoons}} \mathbf{9} + H_2O$$

$$\mathbf{9} + E^+ \xrightarrow{k_2} \text{iminium}$$

$$\text{iminium} + H_2O \xrightarrow{k_3} \textit{product} + \mathbf{4}$$

$$\mathbf{4} + \textit{product} \underset{k_{-4}}{\overset{k_4}{\rightleftharpoons}} \text{active species*}$$

$$\mathbf{4} + \textit{additive} \underset{k_{-5}}{\overset{k_5}{\rightleftharpoons}} \text{active species I}$$

$$\text{active species*} + Nu^- \underset{k_{-6}}{\overset{k_6}{\rightleftharpoons}} \mathbf{9} + H_2O + \textit{product}$$

$$\text{active species I} + Nu^- \underset{k_7}{\overset{k_{-7}}{\rightleftharpoons}} \mathbf{9} + H_2O + \textit{additive}$$

Scheme 7.4 Kinetic scheme of the enamine mechanism involving activation of the proline (**4**) by the reaction product and additives (model I).

The cycle was initiated in each case by the reversible nucleophilic addition of the L-proline (**4**) to the carbonyl substrate Nu^- to form enamine **9** and molecule of water and described by the equilibrium constant $\frac{k_1}{k_{-1}}$. This was followed by enamine attack on the electrophile E^+ where product iminium is formed. In the employed steady-state treatment of the mechanism, this step was considered to be irreversible due to being the rate-limiting step for the aldol reaction. It is also considered to be kinetically inconsequential for α-

aminoxylation because it comes after the rate-limiting step in this case. Therefore for the purpose of simulations of the kinetic behaviour of the α-aminoxylation reaction, the rate constant (k_2) for this step was assumed to be very large (10000), while in case of the aldol reaction, k_2 was much smaller (0.001). The next step - the product hydrolysis, is kinetically meaningless for both reactions and therefore the rate constant k_3 is selected to be 10000 for both models. Four further steps for two models depend on the mode of the activation: proline activation or carbonyl substrate Nu^- activation.

$$Nu^- + \mathbf{4} \underset{k_{-1}}{\overset{k_1}{\rightleftharpoons}} \mathbf{9} + H_2O$$

$$\mathbf{9} + E^+ \xrightarrow{k_2} \text{iminium}$$

$$\text{iminium} + H_2O \xrightarrow{k_3} \textit{product} + \mathbf{4}$$

$$Nu^- + \textit{product} \underset{k_{-4}}{\overset{k_4}{\rightleftharpoons}} \text{active species}$$

$$Nu^- + \textit{additive} \underset{k_{-5}}{\overset{k_5}{\rightleftharpoons}} \text{active species II}$$

$$\text{active species} + \mathbf{4} \underset{k_{-6}}{\overset{k_6}{\rightleftharpoons}} \mathbf{9} + H_2O + \textit{product}$$

$$\text{active species II} + \mathbf{4} \underset{k_{-7}}{\overset{k_7}{\rightleftharpoons}} \mathbf{9} + H_2O + \textit{additive}$$

Scheme 7.5 Kinetic scheme of the enamine mechanism involving activation of a carbonyl substrate (Nu^-) by the reaction product and additives (model II).

In each case two types of active species could be formed from the activation by the various additives and the reaction product, as was evident from the earlier experiments showing that additives as well as the reaction products of the aldol and α-aminoxylation reactions are capable to accelerate the rate of α-aminoxylation. Hence the following step in both models represents the reversible formation of the active species from the interaction with the reaction product, described by the equilibrium constant $\frac{k_4}{k_{-4}}$. The reversible formation of the actives species from the interaction with additives is

represented in the fifth step via the equilibrium constant $\frac{k_5}{k_{-5}}$. Both activated species take part in the formation of the enamine **9**, water and a molecule of the reaction product/additive, which are shown in the sixth and seventh steps and presented as the reversible steps with equilibrium constants $\frac{k_6}{k_{-6}}$ and $\frac{k_7}{k_{-7}}$, respectively for the species activated by the reaction product and the additives.

By exploiting these two activation models it was possible to verify the observed effect by additives on the behaviour of the α-aminoxylation and aldol reactions shown in Figure 7.6. The increasing amount of reaction product and additives (0-2M) did not influence the behaviour of the simulated aldol reaction under any activation mode. However simulation of the α-aminoxylation reaction, as expected, showed rate enhancement by the reaction product: the autoinductive behaviour. Increasing additive concentration also shifted the kinetic profile from autoinductive behaviour towards positive order kinetics during both activation models.

Table 7.1 summarises the rate constants used to simulate the effect of reaction product and additives. Two sets of the rate constants were used to simulate the activation behaviour: 1) equilibrium constants, K_4 and K_5, are on the side of the formed active species ($k_4 > k_{-4}$ and $k_5 > k_{-5}$); 2) equilibrium is on the opposite side ($k_4 < k_{-4}$ and $k_5 < k_{-5}$). In both cases, in order to observe the rate acceleration by additives, the rate of the formation of active species should be higher than initial formation of enamine species **9** ($k_1 << k_4$ and/or k_5). While formation of **9** from active species in reactions 4 and 5 (Scheme 7.4 and 7.5) should be equal or faster to the initial formation of active species ($k_6 \geq k_4$ and $k_7 \geq k_5$). Applying the quasi-equilibrium approximation on the steps 4, 5, 6 and 7, the relationship between equilibrium constants K_1, K_4, K_5, K_6 and K_7 may be defined as $K_1 = K_4 \cdot K_6 = K_5 \cdot K_7$.

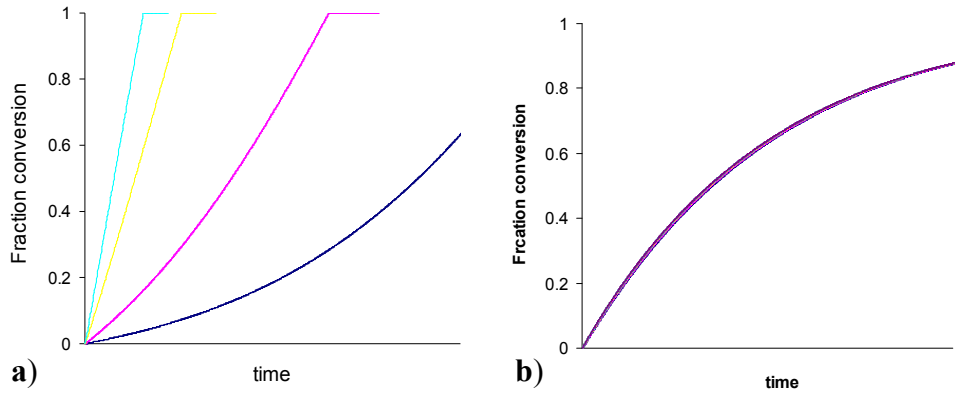

Figure 7.6 The simulation (COPASI 4.2) of the fractional conversion of the reactions that follow the steps of Schemes 7.4 and 7.5 using 2 M **Nu**$^-$, 0.7 M **E**$^+$ and 0.04M **4** and varying additive concentration from 0 to 1M: a) $k_1 << k_2$; b) $k_1 > k_2$.

Table 7.1 Rate constants used in simulation of aldol (k_2 = 0.001; k_3 = 10000) and α-aminoxylation behaviour (k_2 = 10000; k_3 = 10000).

	k_1, $M^{-1}s^{-1}$	k_{-1}, $M^{-1}s^{-1}$	k_4, $M^{-1}s^{-1}$	k_{-4}, s^{-1}	k_5, $M^{-1}s^{-1}$	k_{-5}, s^{-1}	k_6, $M^{-1}s^{-1}$	k_{-6}, $M^{-2}s^{-1}$	k_7, $M^{-1}s^{-1}$	k_{-7}, $M^{-2}s^{-1}$
Set 1	0.005	0.001	0.05	0.01	0.06	0.015	0.1	0.1	0.125	0.1
Set 2	0.005	0.001	0.1	2	0.5	1	1	0.01	1	0.1

Both sets of rate constants when used with model *I* (proline activation) provided rate acceleration by additives in α-aminoxylation and no effect in the aldol reaction. However model *II* (substrate activation) is only possible when used with a second set of rate constants. When set 1 was used, most of product was bound as activated species and only a small amount of a free product was obtained.

Although applying simulations does not help to discern between two activation models, these simulations of hydrogen bonded interactions contributed to the better understanding of the relative rates of individual steps in the catalytic cycle and the general mechanism of the proline catalysed reactions. These simulations supported the mechanism proposed for α-aminoxylation reaction, where the activation of proline/carbonyl substrate is able to enhance the rate of the reaction. In the aldol reaction addition of electrophile to the enamine **9** is the slowest step; therefore the

steady state concentration of **9** is not influenced by the additives over the course of the reaction. However, if the electrophilic addition takes place only a fraction slower than the formation of **9**, then the initial rate of the reaction may be influenced by additives. Also it must be remembered that solvent could also influence the rate constants to different extent at each step of a reaction.[133] Hence depending on the nature of the solvent employed, the rising rate behaviour may be disguised due to the perturbation of the rate constant values.

7.4 Concluding Remarks

This chapter showed that in both aldol and α-aminoxylation reactions the presence of hydrogen-bonding species is possible. However due to the difference in rate-limiting steps in those reactions the observed effects from the hydrogen-bonded species are different. This phenomenon was also supported by the simulation carried out using COPASI biochemical network simulator.

Chapter 8

Summary and Conclusions

This chapter summarises the main contributions of this thesis and outlines future work directions.

8.1 Summary

Mechanistic analysis of catalytic reactions is a concern of chemists, where spectroscopic analysis is most often the primary experimental tool employed.[22] Despite the fact that catalysis is essentially a kinetic phenomenon, kinetics is not always considered as an imperative component of a mechanistic study.[23] Therefore here we endeavour to demonstrate the importance of kinetic analysis in the mechanistic investigation of complex catalytic reactions. However, generally, the limiting feature of a kinetic analysis as typically carried out by organic chemists is that it often involves pseudo-zero order conditions that are removed far from real environment and also implicates a large number of separate experiments. Reaction progress kinetic analysis methodology recently developed by our group allows these issues to be overcome, and the obtained kinetic information may be used to streamline the process development and the process scale up.[25, 128] The important components of this methodology were discussed and compared to the conventional kinetic analysis method in Chapter 2.

The useful implementation of this methodology has been demonstrated through the mechanistic investigation of two organocatalytic reactions, aldol

and α-aminoxylation, which are both important for the formation of chiral building blocks. Relevant aspects concerning existing mechanistic knowledge of the organocatalytic reactions were presented in Chapter 3. The method of experimental data acquisition and first initial kinetic investigations indicating to the catalyst instability in the aldol reaction are presented in Chapter 4.

A particular merit of the employed kinetic methodology is its ease in discerning the features of a reaction that cannot be explained by the direct rate/substrate concentration dependency. Hence it enabled us to separate the processes occurring on the catalytic cycle of the L-proline catalysed aldol reaction from those occurring off the cycle. This study was disclosed in Chapter 5, where, furthermore, as a result of the synergetic contribution between the kinetic methodology and a traditional NMR spectroscopy, an implication of water in the intrinsic kinetics of the L-proline catalysed aldol reaction was exposed. In addition the catalyst deactivation pathway was also proposed.

Intrinsic kinetic analysis of the aldol reaction was performed in Chapter 6. A power law driving force analysis gave a broad picture that allowed proposal of a detailed elementary step reactions mechanism. The observed rate/concentration dependency was rationalised by the steady-state rate expression which was derived on basis of enamine mechanism with the rate-limiting C-C bond formation. The rate-limiting step was also supported by the kinetic isotope effect and by quantitative kinetic modelling where kinetic parameters were estimated. Interestingly, kinetic modelling hinted that water may possess additional roles in the enamine catalysis, such as formation of hydrogen bonded putative proline-water species.

The mechanism of aldol reaction was compared to α-aminoxylation reaction in Chapter 7. While the two reactions exhibit very different kinetic profiles, our analysis showed that in fact the same general enamine mechanism proposed for the aldol reaction may also be proposed for the α-aminoxylation reaction. Here the study showed that formation of hydrogen bonded species between the reaction products and catalyst and/or substrate

is very likely to occur in both reactions. However due to the difference in the rate-limiting steps, kinetic consequences of this interaction are not observable in the aldol reaction. The implication of the rate limiting step in the explanation of the kinetic differences of these two reactions was also supported by the simulation performed using COPASI simulation software.

In conclusion, this work has shown the importance of kinetic analysis and provided the mechanistic information that could be missed if kinetics of the catalytic reactions is not considered: for example, kinetic analysis implicitly provided clues for the nature of the catalytic species. Furthermore, this study led to the elaboration of the application of the methodology of *reaction progress kinetic analysis*.

8.2 Future research directions

Regarding the reactions under study the future research could be focused on the spectroscopic investigation in order to confirm or dismiss the proposals that were deduced from the kinetic study concerning the nature of the various species. Also the L-proline-tetrazole system requires better understanding of both the deactivation pathway, which was not possible to explain explicitly, and its reactivity within the cycle.

Bibliography

1. I. Chorkendorff, J. W. Niemanstsverdriet, *Concepts of Modern Catalysis and Kinetics*, Wiley-VCH, Weinheim, **2007**.
2. G. Centi, R. A. van Santen, Wiley-VCH, Weinheim, **2007**, p. 424.
3. J. Wagner, R. A. Lerner, C. F. Barbas, III, *Science* **1995**, *270*, 1797.
4. T. D. Machajewski, C. H. Wong, *Angew. Chem. Int. Ed.* **2000**, *39*, 1352.
5. R. Noyori, *Adv. Synth. Catal.* **2003**, *345*.
6. J. Clayden, N. Greeves, S. Warren, P. Wothers, *Organic Chemistry*, Oxford University Press Inc., New York, **2001**.
7. A. M. Thayer, *Chemical & Engineering News* **2007**, *85*, 11.
8. J. Halpern, B. M. Trost, *PNAS* **2004**, *101*, 5347.
9. J. M. Keith, J. F. Larrow, E. N. Jacobsen, *Adv. Synth. Catal.* **2001**, *343*, 5.
10. M. Braun, R. Devant, *Tetrahedron Letters* **1984**, *25*, 5031.
11. D. A. Evans, J. M. Takacs, *Tetrahedron Letters* **1980**, *21*, 4233.
12. B. M. Trost, *Angew. Chem. Int. Ed.* **1995**, *34*, 259.
13. A. M. Thayer, *Chemical & Engineering News* **2005**, *83*, 40.
14. B. M. Trost, *PNAS* **2004**, *101*, 5348.
15. A. Berkessel, H. Groger, *Asymmetric Organocatalysis - From Biomimetic Concepts to Applications in Asymmetric Synthesis*, Wiley-VCH Verlag GmbH & Co., Weinheim, **2005**; H. Pellissier, *Tetrahedron* **2007**, *63*, 9267; P. I. Dalko, L. Moisan, *Angew. Chem. Int. Ed.* **2004**, *43*, 5138.
16. B. List, *Chem. Rev.* **2007**, *107*, 5413.
17. J. M. Janey, *Angew. Chem. Int. Ed.* **2005**, *44*, 2.
18. R. O. Duthaler, *Angew. Chem. Int. Ed.* **2003**, *42*, 975.
19. A. M. Thayer, *Chemical & Engineering News* **2005**, *83*, 55.
20. S. Jaroch, H. Weinmann, K. Zeitler, *ChemMedChem* **2007**, *2*, 1261.
21. H. Scott Fogler, *Elements of Chemical Reaction Engineering*, 4th ed., Prentice Hall PTR, **2006**.
22. K. Laidler, *Chemical kinetics*, Harper & Row, New York, **1987**.
23. J. Halpern, *Inorganica Chimica Acta-Articles* **1981**, *50*, 11.
24. A. Cornish-Bowden, *Fundamentals of Enzyme Kinetics*, Portland Press Ltd, London, **2004**.
25. D. G. Blackmond, *Angew. Chem. Int. Ed.* **2005**, *44*, 4302.
26. G. F. Zhong, *Angew. Chem. Int. Ed.* **2003**, *42*, 4247.
27. B. List, R. A. Lerner, C. F. Barbas, *J. Am. Chem. Soc.* **2000**, *122*, 2395.
28. C. F. I. Barbas, A. Heine, G. Zhong, T. Hoffmann, S. Gramatikova, R. Bjornestedt, B. List, J. Anderson, E. A. Stura, I. A. Wilson, R. A. Lerner, *Science* **1997**, *278*, 2085.
29. T. Hoffmann, G. Zhong, B. List, D. Shabat, J. Anderson, S. Gramatikova, R. A. Lerner, C. F. Barbas III, *J. Am. Chem. Soc.* **1998**, *120*, 2768.
30. D. T. Lynch, G. Emig, *Chemical Engineering Science* **1989**, *44*, 1275.

31. D. G. Blackmond, T. Schultz, J. S. Mathew, C. Loew, A. Pfaltz, *Synlett* **2006**, *18*, 3135.
32. A. E. Rubin, *Chem. Rev.* **2006**, *106*, 2794.
33. C. LeBlond, J. Wang, R. D. Larsen, C. J. Orella, A. L. Forman, R. N. Landau, J. Laquidara, J. R. Sowa, D. G. Blackmond, Y.-K. Sun, *Thermochimica Acta* **1996**, *289*, 189.
34. R. N. Landau, *Thermochimica Acta* **1996**, *289*, 101.
35. M. T. DeCrosta, J. B. Schwartz, R. J. Wigent, K. Marshall, *Int. J. Pharm.* **2000**, *198*, 113; S. E. Evon, S. Chervin, G. T. Bodman, A. J. Torres, *Process Safety Progress* **1999**, *18*, 1; W. J. Sun, X. W. Yang, H. G. Zhang, X. Y. Wang, S. L. Gao, *Journal of Rare Earths* **2006**, *24*, 423.
36. W. L. Duan, H. Iwamura, R. Shintani, T. Hayashi, *J. Am. Chem. Soc.,* **2007**, *129*, 2130.
37. C. LeBlond, J. Wang, R. D. Larsen, C. J. Orella, A. L. Forman, R. N. Landau, J. Laquidara, J. R. Sowa, D. G. Blackmond, Y.-K. Sun, *Thermochimica ActaReaction Calorimetry* **1996**, *289*, 189.
38. J. S. Mathew, M. Klussmann, H. Iwamura, F. Valera, A. Futran, E. A. C. Emanuelsson, D. G. Blackmond, *J. Org. Chem.* **2006**, *71*, 4711.
39. M. Milosevic, D. Sting, A. Rein, *Spectroscopy* **1995**, *10*, 44.
40. P. W. Atkins, *Physical Chemistry*, Oxford University Press, Oxford, **1994**.
41. M. Movassaghi, E. N. Jacobsen, *Science* **2002**, *298*, 1904.
42. M. Shibasaki, M. Kanai, K. Funabashi, *Chem. Commun.* **2002**, 1989.
43. J. Seayad, B. List, *Org. Biomol. Chem.* **2005**, *3*, 719.
44. M. S. Taylor, E. N. Jacobsen, *Angew. Chem. Int. Ed.* **2006**, *45*, 1520.
45. K. Tanaka, A. Mori, S. Inoue, *J. Org. Chem.* **1990**, *55*, 181.
46. E. J. Corey, M. J. Grogan, *Org. Lett.* **1999**, *1*, 157; M. S. Iyer, K. M. Gigstad, N. D. Namdev, M. Lipton, *J. Am. Chem. Soc.* **1996**, *118*, 4910.
47. A. G. Doyle, E. N. Jacobsen, *Chem. Rev.* **2007**, *107*, 5713; T. Akiyama, *Chem. Rev.* **2007**, *107*, 5744.
48. M. S. Sigman, P. Vachal, E. N. Jacobsen, *Angew. Chem. Int. Ed.* **2000**, *39*, 1279; A. G. Wenzel, E. N. Jacobsen, *J. Am. Chem. Soc.* **2002**, *124*, 12964; T. Okino, Y. Hoashi, Y. Takemoto, *J. Am. Chem. Soc.* **2003**, *125*, 12672.
49. T. Hashimoto, K. Maruoka, *Chem. Rev.* **2007**, *107*, 5656.
50. C. L. Liotta, in *The Sahem Phase transfer catalysis review* (Ed.: S. McCoy), SACHEM, Inc., Austin, **1997**, p. 16.
51. E. J. Corey, F. Xu, M. C. Noe, *J. Am. Chem. Soc.* **1997**, *119*, 12414; B. Lygo, P. G. Wainwright, *Tetrahedron Letters* **1997**, *38*, 8595.
52. E. J. Corey, F.-Y. Zhang, *Org. Lett.* **1999**, *1*, 1287.
53. M. J. Gaunt, C. C. C. Johansson, *Chem. Rev.* **2007**, *107*, 5596.
54. A. Erkkila, I. Majander, P. M. Pihko, *Chem. Rev.* **2007**, *107*, 5416.
55. S. Mukherjee, J. W. Yang, S. Hoffmann, B. List, *Chem. Rev.* **2007**, *107*, 5471.
56. B. List, *Acc. Chem. Res.* **2005**, *37*, 548.

57. K. A. Ahrendt, C. J. Borths, D. W. C. MacMillan, *J. Am. Chem. Soc.* **2000**, *122*, 4243; J. L. Cavill, J.-U. Petersb, N. C. O. Tomkinson, *Chem. Commun.* **2003**, 728.
58. W. Notz, S. Watanabe, N. S. Chowdari, G. Zhong, J. M. Betancort, F. Tanaka, C. F. Barbas, *Adv. Synth. Catal.* **2004**, *346*, 1131; W. Notz, F. Tanaka, S. Watanabe, N. S. Chowdari, J. M. Turner, R. Thayumanavan, C. F. Barbas III, *J. Org. Chem.* **2003**, *68*, 9624.
59. Z. G. Hajos, D. R. J. Parrish, *J. Org. Chem.* **1974**, *39*, 1615.
60. U. Eder, G. Sauer, R. Wiechert, *Angew. Chem. Int. Ed.* **1971**, *10*, 496.
61. A. J. Morris, D. R. Tolan, *Biochemistry* **1994**, *33*, 12291.
62. Z. G. Hajos, http://preprint.chemweb.com/orgchem/0209001, **2002**.
63. D. Rajagopal, M. S. Moni, S. Subramanian, S. Swaminathan, *Tetrahedron: Asymmetry* **1999**, *10*, 1631.
64. C. Allemann, R. Gordillo, F. R. Clemente, P. H. Y. Cheong, K. N. Houk, *Acc. Chem. Res.* **2004**, *37*, 558.
65. F. R. Clemente, K. N. Houk, *Angew. Chem. Int. Ed.* **2004**, *43*, 5766.
66. S. Bahmanyar, K. N. Houk, *J. Am. Chem. Soc.* **2001**, *123*, 11273.
67. K. N. Rankin, J. W. Gauld, R. J. Boyd, *J. Phys. Chem* **2004**, *106*, 5155.
68. S. Bahmanyar, K. N. Houk, *Org. Lett* **2003**, *5*, 1249.
69. S. Bahmanyar, K. N. Houk, H. J. Martin, B. List, *J. Am. Chem. Soc.* **2003**, *125*, 2475.
70. C. Marquez, J. O. Metzger, *Chem. commun.* **2006**, 1539.
71. B. List, L. Hoang, H. J. Martin, *PNAS* **2004**, *101*, 5839.
72. D. Gryko, M. Zimnicka, R. Lipinski, *J. Org. Chem.* **2007**, *72*, 964.
73. D. Seebach, A. K. Beck, D. M. Badine, M. Limbach, A. Eschenmoser, A. M. Treasurywala, R. Hobi, W. Prikoszovich, B. Linder, *Helvetica Chimica Acta* **2007**, *90*, 425.
74. P. M. Pihko, K. M. Laurikainen, A. Usano, A. I. Nyberg, J. A. Kaavi, *Tetrahedron* **2006**, *62*, 317.
75. A. I. Nyberg, A. Usano, P. M. Pihko, *Synlett* **2004**, *11*, 1891.
76. A. P. Brogan, T. J. Dickerson, K. D. Janda, *Angew. Chem. Int. Ed.* **2006**, *45*, 2.
77. T. J. Dickerson, T. Lovell, M. M. Meijler, L. Noodleman, K. D. Janda, *J. Org. Chem.* **2004**, *69*, 6603.
78. N. S. Chowdari, C. F. Barbas, *Org. Lett.* **2005**, *7*, 867.
79. S. P. Brown, M. P. Brochu, C. J. Sinz, D. W. C. MacMilan, *J. Am. Chem. Soc.* **2003**, *125*, 10808.
80. A. Bøgevig, K. Juhl, N. Kumaragurubaran, W. Zhuang, K. A. Jørgensen, *Angew. Chem. Int. Ed.* **2002**, *41*, 1790; H. Vogt, S. Vanderheidena, S. Bräse, *Chem. Commun.* **2003**, 2448.
81. B. List, *J. Am. Chem. Soc.* **2002**, *124*, 5656.
82. D. E. Ward, V. Jheengut, O. T. Akinnusi, *Org. Lett.* **2005**, *7*, 1181.
83. D. E. Ward, V. Jheengut, *Tetrahedron Letters* **2004**, *45*, 8347.
84. D. Enders, C. Grondal, *Angew. Chem. Int. Ed.* **2005**, *44*, 1210.
85. C. Grondal, D. Enders, *Tetrahedron* **2006**, *62*, 329; D. Enders, J. Palecek, C. Grondal, *Chem. Commun.* **2006**, 655.
86. J. T. Suri, D. B. Ramachary, C. F. Barbas, *Org. Lett.* **2005**, *7*, 1383.

87. A. B. Northrup, I. K. Mangion, F. Hettche, D. W. C. MacMillan, *Angew. Chem. Int. Ed.* **2004**, *43*, 2152; A. B. Northrup, D. W. C. MacMillan, *Science* **2004**, *305*, 1752.
88. J. Casas, M. Engqvist, I. Ibrahem, B. Kaynak, A. Cordova, *Angew. Chem. Int. Ed.* **2005**, *44*, 1343.
89. Y. J. Wang, Z. X. Shen, B. Li, Y. W. Zhang, *Chinese journal of chemistry* **2006**, *24*, 1196; C. Garcia, V. S. Martin, *Current Organic Chemistry* **2006**, *10*, 1849.
90. S. Samanta, C. G. Zhao, *J. Am. Chem. Soc.* **2006**, *128*, 7442.
91. K. Sakthivel, W. Notz, T. Bui, I. K. F. Barbas, *J. Am. Chem. Soc.* **2001**, *123*, 5260; B. List, *Tetrahedron* **2002**, *58*, 5573.
92. Y. S. Zheng, M. A. Avery, *Tetrahedron* **2004**, *60*, 2091.
93. B. List, P. Pojarliev, C. Castello, *Org. Lett.* **2001**, *3*, 573.
94. O. Tokuda, T. Kano, W. G. Gao, T. Ikemoto, K. Maruoka, *Org. Lett.* **2005**, *7*, 5103; S. Samanta, C. G. Zhao, *Tetrahedron Letters* **2006**, *47*, 3383.
95. W. Notz, B. List, *J. Am. Chem. Soc.* **2000**, *122*, 7386.
96. A. Bogevig, N. Kumaragurubaran, K. A. Jorgensen, *Chem. Commun.* **2002**, 620.
97. A. B. Northrup, D. W. C. MacMillan, *J. Am. Chem. Soc.* **2002**, *124*, 6798.
98. J. Coates, in *Encyclopedia of Analytical Chemistry* (Ed.: R. A. Meyers), John Wiley & Sons Ltd., Chichester, **2000**, pp. 10815.
99. D. G. Blackmond, A. Armstrong, V. Coombe, A. Wells, *Angew. Chem. Int. Ed.* **2007**, *46*, 3798.
100. J. E. Billo, *Excesl for Chemists*, 2nd ed., John Wiley & Sons, Inc., New York, **2001**.
101. K. Hiroi, S. Yamada, *Chemical & Pharmaceutical Bulletin* **1974**, *21*, 47; K. Hiroi, K. Achiwa, S. Yamada, *Chemical & Pharmaceutical Bulletin* **1972**, *20*, 246.
102. H. E. Ferran, D. A. Drake, T. A. Spencer, *J. Org. Chem.* **1975**, *40*, 2017.
103. D. Seebach, M. Boes, R. Naef, W. B. Schweizer, *J. Am. Chem. Soc.* **1983**, *105*, 5390.
104. F. Orsini, F. Pelizzoni, M. Forte, R. Destro, P. Gariboldi, *Tetrahedron* **1988**, *44*, 519.
105. T. Kano, J. Takai, O. Tokuda, K. Maruoka, *Angew. Chem. Int. Ed.* **2005**, *44*, 3055; P. Dambruoso, A. Massi, A. Dondoni, *Org. Lett.* **2005**, *7*, 4657.
106. A. J. A. Cobb, D. M. Shaw, S. V. Ley, *Synlett* **2004**, 558.
107. A. Hartikka, P. I. Arvidsson, *Tetrahedron: Asymmetry* **2004**, *15*, 1831.
108. A. Hartikka, P. I. Arvidsson, *Eur. J. Org. Chem.* **2005**, 4287.
109. R. G. Almquist, W.-R. Chao, C. Jennings-White, *Journal of medicinal chemistry* **1985**, *28*, 1067; A. J. A. Cobb, D. M. Shaw, D. A. Longbottom, J. B. Gold, S. V. Ley, *Organic & Biomolecular Chemistry* **2005**, *3*, 84.
110. D. Gryko, R. Lipinski, *Adv. Synth. Catal.* **2005**, *347*, 1948.
111. D. Gryko, R. Lipinski, *Eur. J. Org. Chem.* **2006**, 3864.

112. A. Cordova, W. B. Zou, P. Dziedzic, I. Ibrahem, E. Reyes, Y. M. Xu, *Chemistry-a European Journal* **2006**, *12*, 5383.
113. R. E. Weston, *Annu. Rev. Nucl. Sci* **1961**, *11*, 439.
114. L. Melander, W. H. Saunders, *Reaction Rates of Isotpic Molecules*, John Wiley & Sons, New York, **1980**.
115. D. Pollard-Knight, A. Cornish-Bowden, *Eur. J. Biochem.* **1983**, *141*, 157.
116. F. A. Carrol, in *Perspectives on Structure and Mechanism in Organic Chemistry*, Brooks, Pacific Groove, **1998**, p. 919.
117. K. B. Schowen, R. L. Schowen, *Methods in enzymology* **1982**, *87*, 551.
118. M. Karpefors, P. Adelroth, P. Brzezinski, *Biochemistry* **2000**, *39*, 6850.
119. A. Spisni, E. D. Gotsis, D. Fiat, *Biochemical and Biophysical Research Communications* **1986**, *135*, 363.
120. S. Hilal, L. L. Bornander, L. A. Carreira, *QSAR & combinatorial science* **2005**, *24*, 631.
121. O. El Seoud, *Pure Appl. Chem.* **2007**, *79*, 1135.
122. E. S. Amis, *Solvents effects on reaction rates and mechanism*, Academic Press Inc., New York, **1966**.
123. S. P. Mathew, H. Iwamura, D. G. Blackmond, *Angew. Chem. Int. Ed.* **2004**, *43*, 3317.
124. H. Iwamura, D. H. Wells, S. P. Mathew, M. Klussmann, A. Armstrong, D. G. Blackmond, *J. Am. Chem. Soc.* **2004**, *126*, 16312.
125. H. Iwamura, S. P. Mathew, D. G. Blackmond, *J. Am. Chem. Soc.* **2004**, *126*, 11770.
126. M. Klussmann, A. J. P. White, A. Armstrong, D. Blackmond, *Angew. Chem. Int. Ed.* **2006**, *45*, 7985.
127. S. P. Brown, PhD Thesis, California Institute of Technology (Pasadena), **2005**.
128. S. P. Mathew, M. Klussmann, H. Iwamura, D. H. Wells, A. Armstrong, D. G. Blackmond, *Chem. Commun.* **2006**, 4291.
129. P. M. Pihko, *Angew. Chem. Int. Ed.* **2004**, *43*, 2062.
130. K. Hirose, *J Incl Phenom Macrocyclic Chem* **2001**, *39*, 193.
131. L. Fielding, *Tetrahedron* **2000**, *56*, 6151.
132. S. Hoops, S. Sahle, R. Gauges, C. Lee, J. Pahle, N. Simus, M. Singhal, L. Xu, P. Mendes, U. Kummer, *Bioinformatics* **2006**, *22*, 3067.
133. C. Reichardt, *Solvents and Solvent effects in organic chemistry*, VCH, New York, **1990**.
134. A. C. Ferretti, J. S. Mathew, D. G. Blackmond, *Ind. Eng. Chem. Res.* **2007**, *46*, 8584.

APPENDIX 1: CORRECTION AND PROCESSING OF RAW EXPERIMENTAL DATA

A1.1 Evaluation of Heat of Mixing

The heat of mixing was evaluated in separate experiment by imitating the real experimental set up albeit without the catalyst. Figure A1.1 and A1.2 display the heats of mixing observed for the aldol and α-aminoxylation reactions. In case of the aldol reaction the endothermic signal was observed, while for of α-aminoxylation this heat is exothermic.

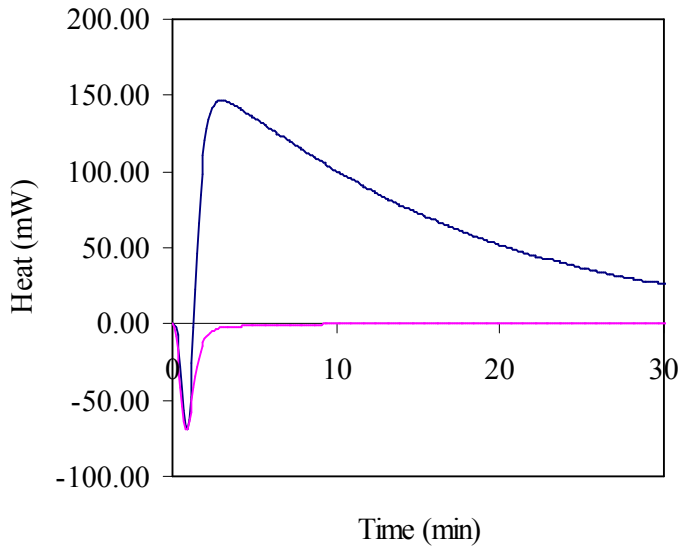

Figure A1.1 Endothermic heat of mix observed in aldol reaction. Curve in pink: separate experiment to determine the heat of mixing; curve in blue: heat flow observed during the experiment.

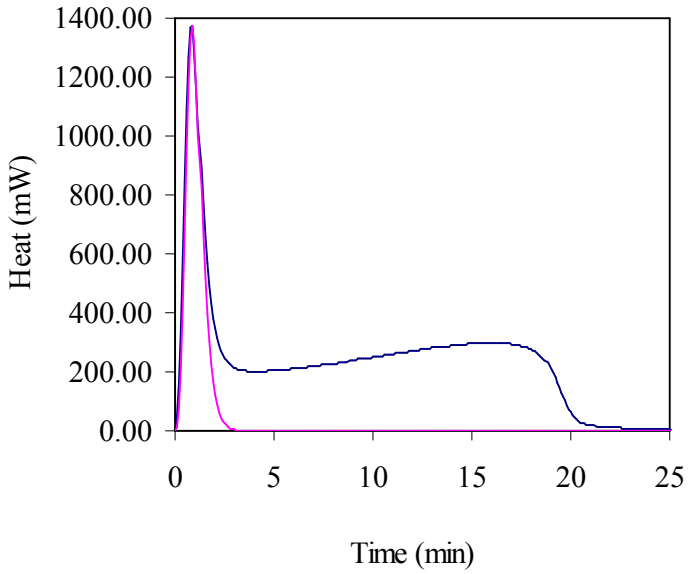

Figure A1.2 Exothermic heat of mix observed in α-aminoxylation reaction. Curve in pink: separate experiment to determine the heat of mixing; curve in blue: heat flow observed during the experiment.

A1.2 Acquisition of Kinetic Data from Heat Flow Data

When heat flow data is acquired and adjusted for the lag time (Section 4.2.2) and heat of mixing reaction rate, fractional conversion and concentrations can be calculated.[134]

The reaction rate is proportional to the heat flow in accordance to the Equation 2.6 of the main text via thermodynamic heat of the reaction ΔH_{rxn} (in kJ/mol). This heat is calculated as the total heat flow released by a reaction per number of moles of a limiting substrate at the end of the reaction (eq. A1.1). Number of moles is usually obtained from the initial number of moles of limiting substrate fed into reactor and the final fractional conversion which is measured by the independent technique, such as HPLC, at the end of each reaction.

$$\Delta H_{rxn} = \frac{\sum_{0}^{end} q \cdot \Delta t}{number\ of\ moles} \qquad \text{(eq. A1.1)}$$

Since reactions are carried out in the batch systems the fractional conversion is the function of time that reactants spend in the reactor. Therefore the

fraction of heat released in a small amount of time will correspond to the fraction of conversion achieved at the same amount of time, which can be expressed as in Equation 2.7 in the main text. In order to obtain the conversion profile the final fractional conversion should be also known.

Once the temporal conversion is known the temporal concentration profiles of the substrates and product can be easily calculated from the Equation A1.2-A1.3.

$$[\mathbf{S}](t) = [\mathbf{S}]_o(1 - \text{conversion}(t)) \qquad \text{(eq. A1.2)}$$

$$[\mathbf{P}](t) = [\mathbf{S}]_o(\text{conversion}(t)) \qquad \text{(eq. A1.3)}$$

The concentration of the second substrate in case of two-substrate reaction can be calculated via *excess* (Section 2.1).

A 1.3 Acquisition of Kinetic Data from *in situ* FTIR or Similar Tools

Although Beer & Lambert law (equation 2.8 in the main text) can be used directly to obtain concentration profile during FTIR measurement, often peak height (Figure A1.3) data is used in order to remove the movement of a baseline. The change from initial value in the peak height (*PH*) at any time corresponds to the fractional conversion achieved at the same time as shown in Equation A1.4.

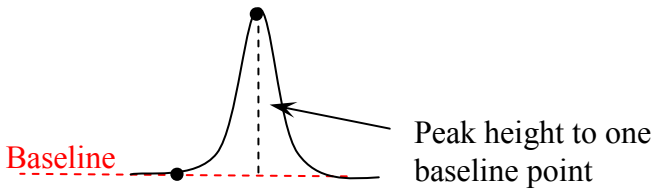

Figure A1.3 Peak height to one point baseline.

$$\frac{\text{conversion}(t)}{\text{conversion}_{end}} = \frac{PH_o - PH(t)}{PH_o - PH_{end}} \qquad \text{(eq. A1.4)}$$

In this case the final fractional conversion should also be known which as before is measured at the end of the reaction by an independent method such as HPLC.

The rate of a reaction is obtained as a derivative of the temporal concentration profile as shown in Equation 2.9 of the main text. This is done by fitting the concentration-time data to a polynomial of a most appropriate order. Once the constants of the polynomial were determined, the polynomial equation is differentiated with respect to time providing the rate values.

APPENDIX 2: ANALYTICAL METHODS

A2.1 Work up Procedure for the Aldol Reaction

Reaction work up and analysis were performed according to a literature procedure.[27] Typically a sample of the crude reaction mixture (0.05ml) were added to an NH_4Cl and extracted with ethyl acetate. The organic phase dried with $MgSO_4$ and used directly in HPLC analysis. For HPLC analysis Chiralpak AD chiral column (DAICEL) was employed. Mobile phase: hexane/ethanol (95:5), flow rate = 1 ml/min, wavelength = 210 nm.

Conversion was ascertained by determining the concentration of *o*-CBA remaining at the end of the reaction using Equation A2.1. In order to establish the relative composition of aldol reaction the response factor (RF) for each identified component of the reaction: *o*-CBA, aldol product, dehydration product was determined by correlating obtained area for aldol product (*A*3+*A*4) with other components (*A*1, *A*2).

$$conversion(\%) = \frac{[A1]\cdot RF_1 + [A2]\cdot RF_2 + [A3]\cdot RF_3 + [A4]\cdot RF_4}{[A2]\cdot RF_2 + [A3]\cdot RF_3 + [A4]\cdot RF_4}\cdot 100 \qquad \text{(eq. A2.1)}$$

Entry	Component	Area	RF	Time
1	*o*-CBA	*A*1	0.49	5.3
2	Dehydration product	*A*2	0.48	7.4
3	*R*-aldol product (minor)	*A*3	1	14.2
4	*S*-aldol product (major)	*A*4	1	16.4

The enantiomeric excess (*ee*) was calculated from the Equation A2.2.

$$ee(\%) = \frac{[A4]-[A4]}{[A3]+[A4]}\cdot 100 \qquad \text{(eq. A2.2)}$$

A2.2 Work up Procedure for α-Aminoxylation Reactions

Reaction work up and analysis were performed according to a literature procedure.[26] Typically a sample of the crude reaction mixture (0.05ml) were added added to an ethanol suspension of $NaBH_4$ at 0 °C to reduce the aldehyde group of the reaction product **21** quantitatively to give the corresponding primary alcohol. After 5 minutes, the mixture was treated with saturated aqueous $NaHCO_3$ and extracted with ethyl acetate. The sample was analysed by HPLC using Chiralpak AD chiral column (DAICEL), mobile phase: hexane/ethanol (90:10), flow rate = 1 ml/min, wavelength = 241 nm.

Conversion was ascertained by determining the concentration of nitrosobenzene remaining (in reduced and non reduced form) at the end of the reaction using approach similar to that decribed for the aldol reaction in Section A2.1. No significant side products were observed, with the alcohol product comprising > 98 area % of the product peaks. The enantiomeric excess was calculated using the Equation A2.2.

The relative composition of aldol reaction was established using the relative response factor (RF) for each identified component of the reaction: nitrobenzene, reduced nitrobenzene and α-aminoxylation product. Most leftover of nitrosobenzene was also reduced by $NaBH_4$ during work up and therefore it was calibrated from standards produced from pure nitrosobenzene in $CHCl_3$ reduced using the same procedure by $NaBH_4$)

Entry	Component	Area	RF	Time
1	Nitrosobenzene		12.18	4.66
2	Reduced nitrosobenzene		0.95	6.08
3	*R*-α-Aminoxylation product (minor)		1	13.9
4	*S*-α-Aminoxylation product (major)		1	16.3

APPENDIX 3: SPECTROSCOPIC ANALYSIS

A 3.1 Formation of Decarboxylated Species: Spectroscopic Analysis

(**a**) General: NMR spectra were recorded on a Bruker DRX-400 or AV400 (^{1}H 400 MHz, ^{13}C 100 MHz) spectrometer.

(**b**) Interaction between 2-CBA (**2**) and L-proline (**4**) – observation of **6a**/**6b** and **7a**/**7b**.

o-CBA (**2**, 142.7 mg, 1.015 mmol) was added to L-proline (**4**, 23.8 mg, 0.207 mmol) in d^{6}-DMSO (1.88 mL) stirred for 30 minutes. The sample was mixed for a few minutes at 25 °C, filtered through a 0.45 μm filter and investigated by NMR within the next five minutes. For the quantitative analysis the internal standard (**IS**), 2,5-dimethylfuran, was used. Figure A3.1 shows composition of the ^{1}H-NMR spectrum after 10 minutes of the interaction.

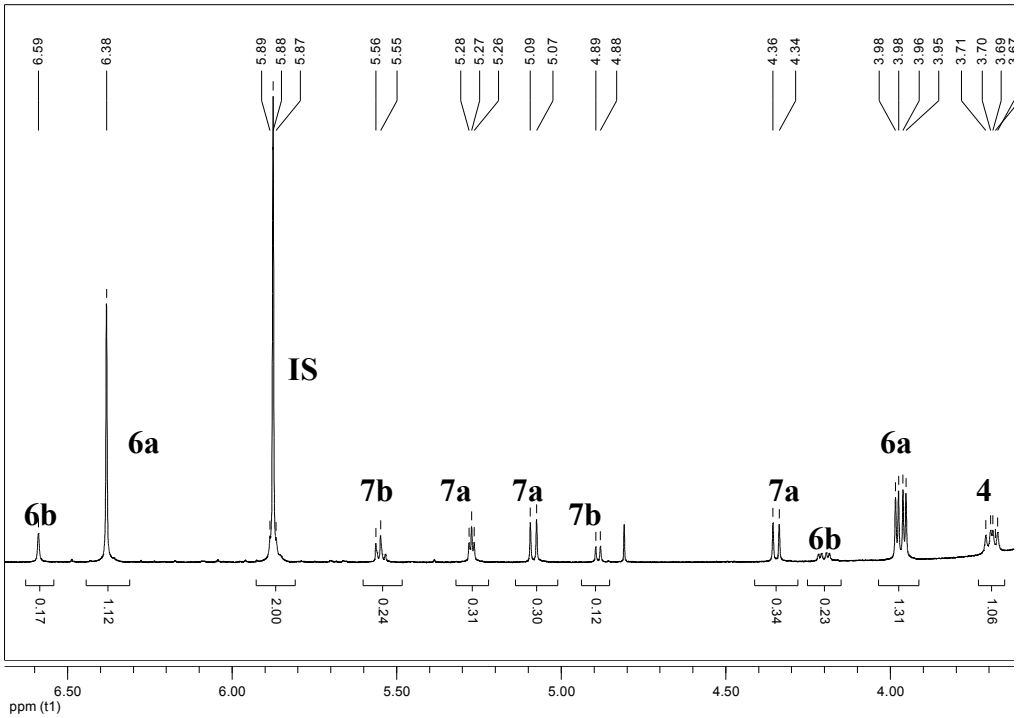

Figure A3.1. ^{1}H-NMR spectrum (400 MHz) in d^{6}-DMSO of the mixture of **6a**/**6b** and **7a**/**7b** (after 10 minutes of interaction between **2** and **4**).

6a: 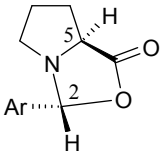

6a: δ6.38 (s, 1H, H-2), 3.97 (dd, J = 9.0, 3.5 Hz, 1H, H-5).

6b: 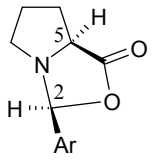

6b:δ6.59 (s, 1H, H-2), 4.20 (dd, J = 9.5, 3.7 Hz, 1H, H-5).

7a: 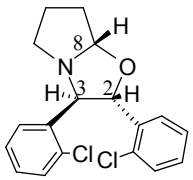

7a: δ5.27 (t, J = 3.2 Hz, 1H, H-8), 5.08 (d, J = 7.6 Hz, 1H, H-2), 4.35 (d, J = 7.5 Hz, 1H, H-3).

7b: 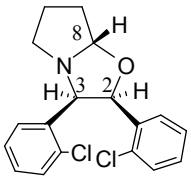

7b: δ5.57-5.52 (m, 2 H, H-2, H-8), 4.89 (d, J = 5.7 Hz, 1H, H-3).

(**c**) Characterization of **7a**/**7b**: First, **7a** and **7b** were identified from ^{1}H, ^{13}C, HMQC and HMBC spectra as the mixture in a ratio of 2.5:1. Figures A3.2 to A3.3 present ^{1}H and ^{13}C spectra of the **7a**/**7b** mixture in d^{6}-DMSO.

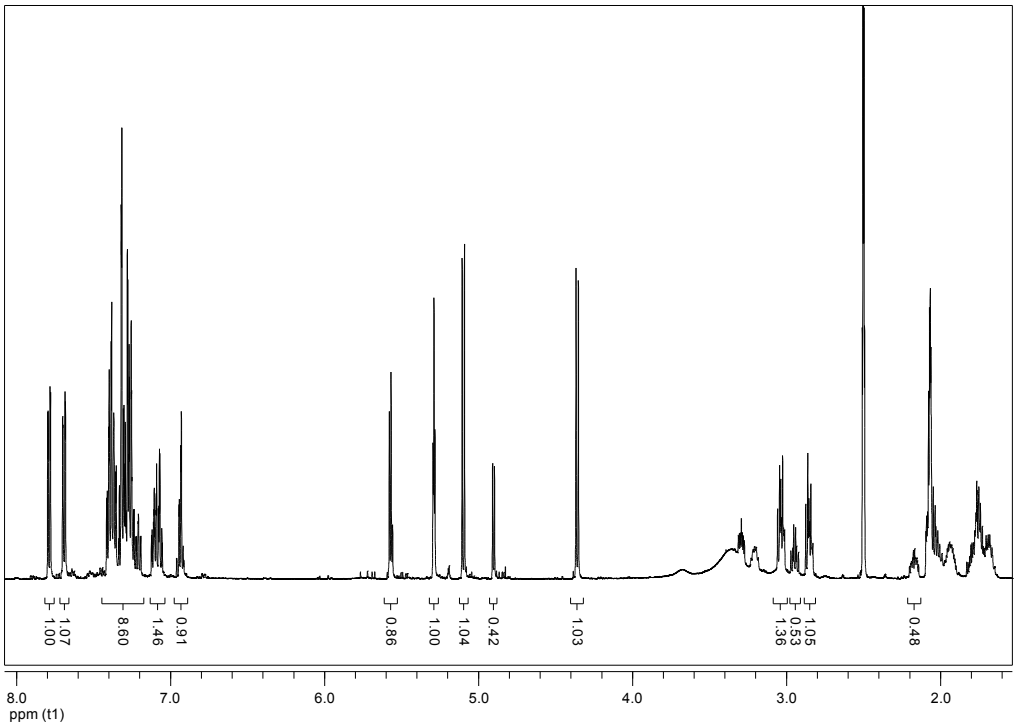

Figure A3.2 ^{1}H-NMR (400 MHz) spectrum of the 6a/6b mixture in d^{6}-DMSO.

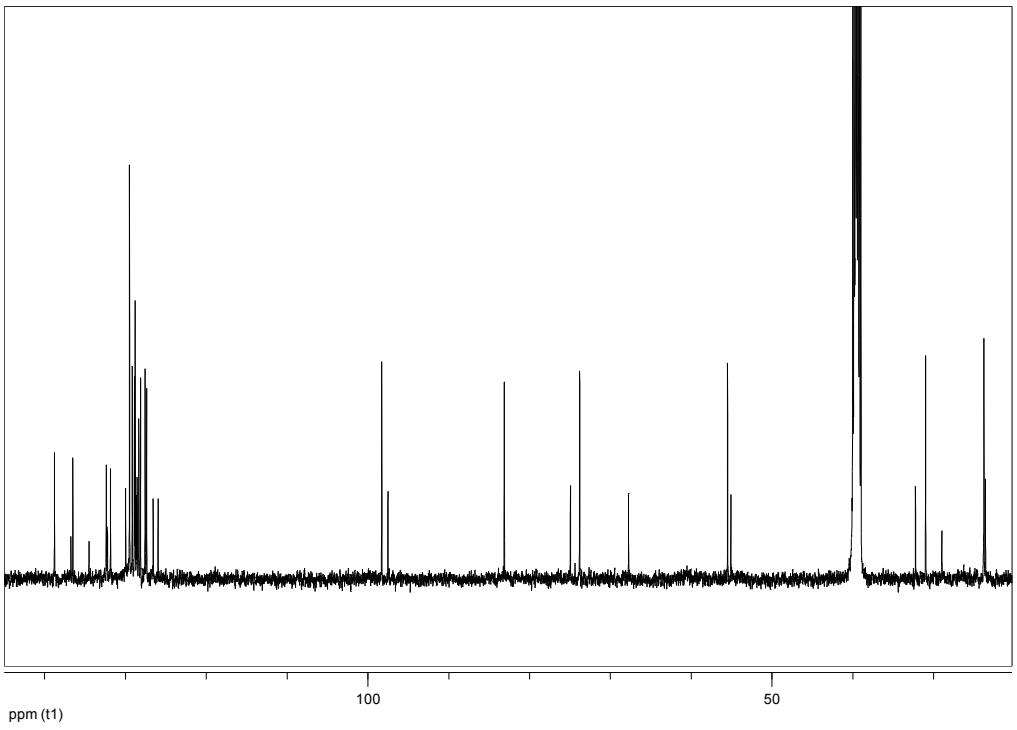

Figure A3.3 ^{13}C-NMR (100 MHz) spectrum of the 6a/6b mixture in d^{6}-DMSO.

(**d**) **7a** and **7b** were separated by flash column chromatography on silica gel using hexanes/EtOAc = 10:1 as the eluent. Minor diastereomer **7b** was not isolated completely and present in a 5:1 ratio of **7b**:**7a**. The NMR spectra

(^{1}H, ^{13}C, COSY, NOESY and HMQC) of both diastereomers were obtained in $CDCl_3$. The data for **7a** in $CDCl_3$ is given in Figures A3.4 to A3.6. In order to observe separated proton peaks for H-2 and H-8 of **7b** which overlap in $CDCl_3$ and d_6-DMSO the NMR spectra of **7b** are given in C_6D_6 (Figures A3.7 to A3.9).

7a: R_f = 0.28 (hexanes/EtOAc = 10:1).

^{1}H-NMR (400 MHz, $CDCl_3$): δ 7.77 (dd, J = 7.8, 1.5 Hz, 1H, Ar-H), 7.71 (dd, J = 7.8, 1.5 Hz, 1H, Ar-H), 7.36-7.16 (m, 6H, Ar-H), 5.38 (dd, J = 4.4, 2.0 Hz, 1H, H-8), 5.28 (d, J = 7.3 Hz, 1H, H-2), 4.53 (d, J = 7.3 Hz, 1H, H-3), 3.20 (dt, J = 10.3, 6.1 Hz, 1H, H-5), 2.95 (dt, J = 9.8, 6.6 Hz, 1H, H-5), 2.30-2.07 (m, 3H, H-7, H-6), 1.94-1.81 (m, 1H, H-6).

^{13}C-NMR (100 MHz, $CDCl_3$): δ 139.2 (Ar-C), 137.3 (Ar-C), 133.7 (Ar-C), 133.0 (Ar-C), 129.5 (Ar-CH), 129.4 (Ar-CH), 129.1 (Ar-CH), 129.0 (Ar-CH), 128.5 (Ar-CH), 127.7 (Ar-CH), 127.2 (Ar-CH), 127.2 (Ar-CH), 98.9 (C-8), 83.6 (C-2), 74.1 (C-3), 56.0 (C-5), 31.6 (C-7), 23.9 (C-6).

HRMS (ESI): *m/z* calc. for $C_{18}H_{18}NOCl_2$ $[M+H]^+$: 334.0765, found: 334.0762.

7b: R_f = 0.20 (hexanes/EtOAc = 10:1).

^{1}H-NMR (400 MHz, C_6D_6): δ 7.49 (dd, J = 7.8, 2.0 Hz, 1H, Ar-H), 7.20 (dd, J = 6.8, 2.4 Hz, 1H, Ar-H), 7.12-6.96 (m, 1H, Ar-H), 6.95-6.83 (m, 2H, Ar-H), 6.70-6.56 (m, 3H, Ar-H), 5.83 (d, J = 5.4 Hz, 1H, H-2), 5.48 (t, J = 5.1 Hz, 1H, H-8), 5.14 (d, J = 5.38 Hz, 1H, H-3), 3.09 (mc, 1H, H-5), 2.62 (td, J = 9.3, 6.1 Hz, 1H, H-5), 1.88-1.79 (m, 1H, H-7), 1.67-1.24 (m, 3H, H-7, H-6).

^{13}C-NMR (100 MHz, C_6D_6): δ 138.0 (Ar-C), 135.7 (Ar-C), 133.9 (Ar-C), 133.8 (Ar-C), 130.5 (Ar-CH), 129.5 (Ar-CH), 129.1 (Ar-CH), 129.0 (Ar-CH), 128.6 (Ar-CH), 126.3 (Ar-CH), 125.9 (Ar-CH), 98.2 (C-8), 76.4 (C-2), 68.7 (C-3), 55.4 (C-5), 32.9 (C-7), 23.9 (C-6). (The missing Ar-CH signal is hidden by the solvent.)

HRMS (ESI): m/z calc. for $C_{18}H_{18}NOCl_2$ $[M+H]^+$: 334.0765, found: 334.0771.

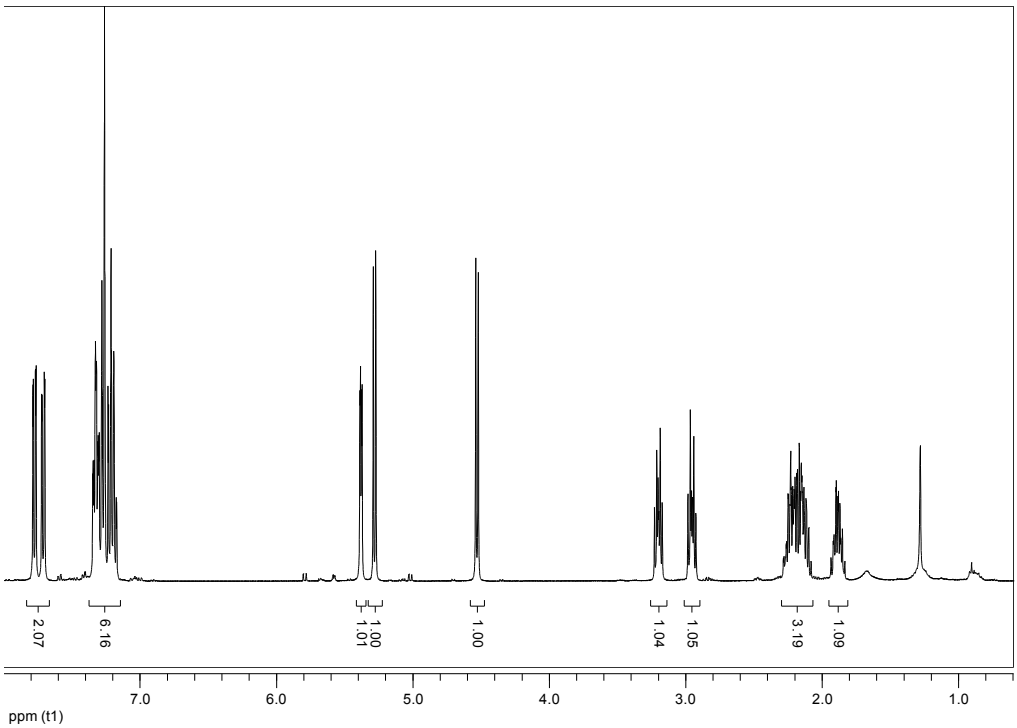

Figure A3.4 ^{1}H-NMR (400 MHz) spectrum of **7a** in $CDCl_3$.

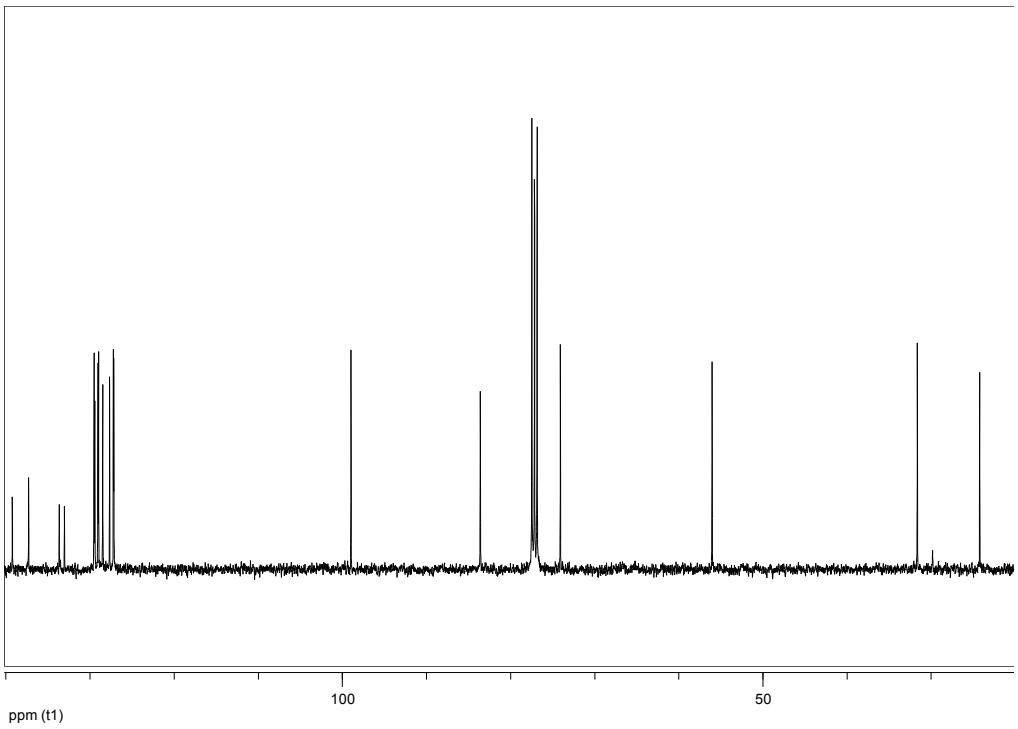

Figure A3.5 ^{13}C-NMR spectrum of **7a** in $CDCl_3$.

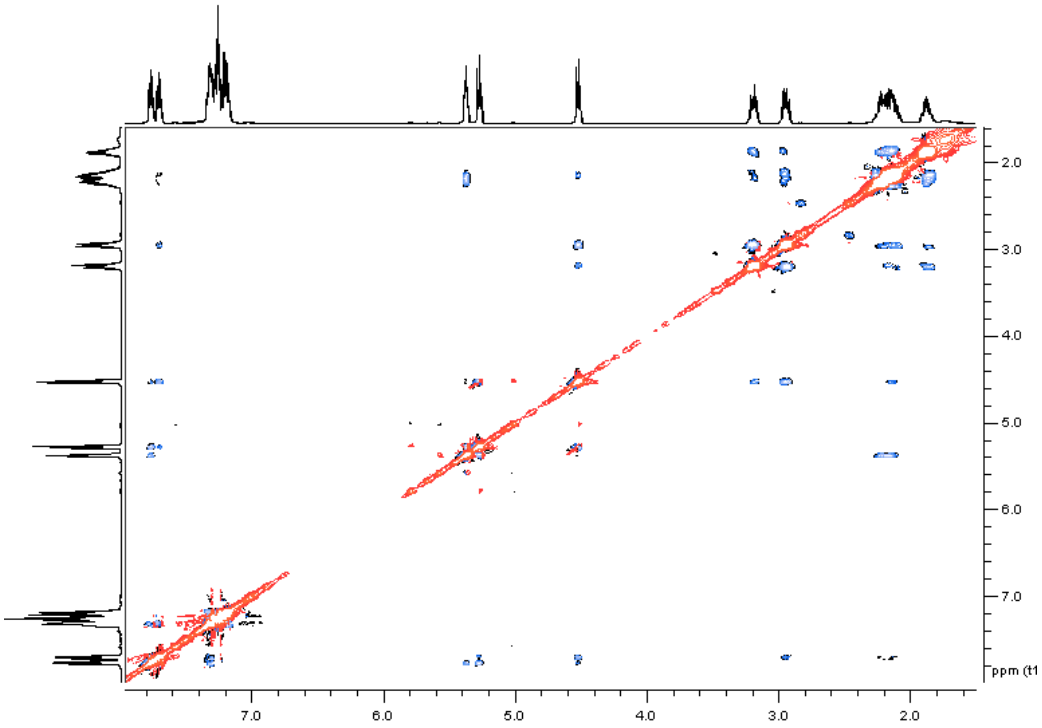

Figure A3.6 NOESY spectrum of **7a** in $CDCl_3$.

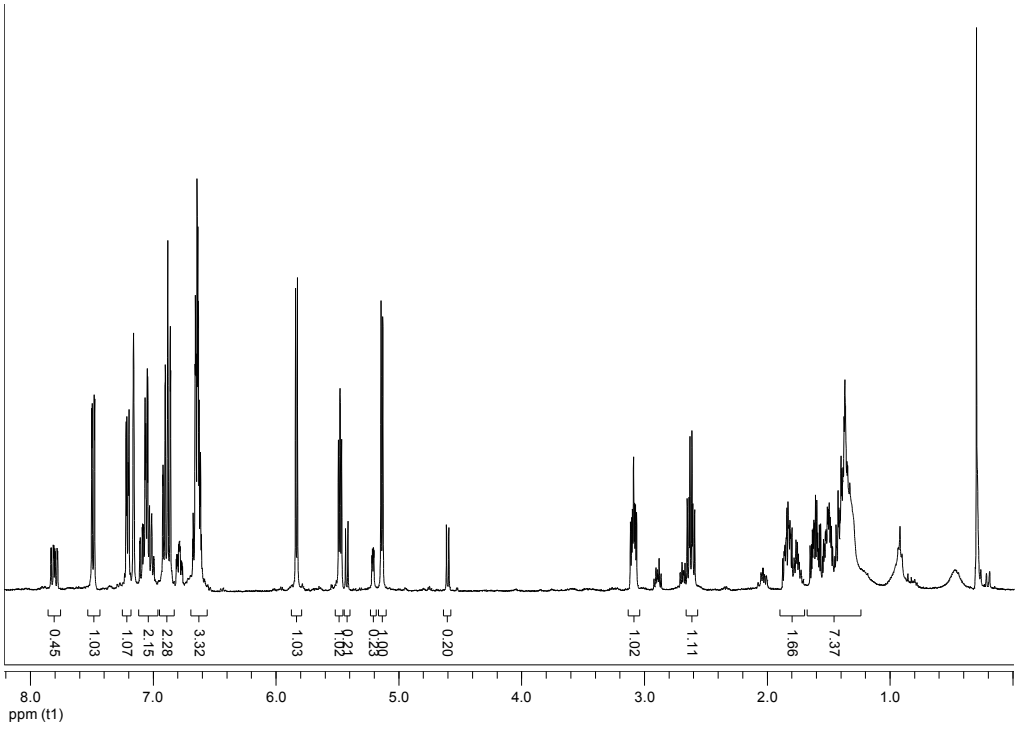

Figure A3.7 ^{1}H-NMR (400 MHz) spectrum of **7b** in C_6D_6.

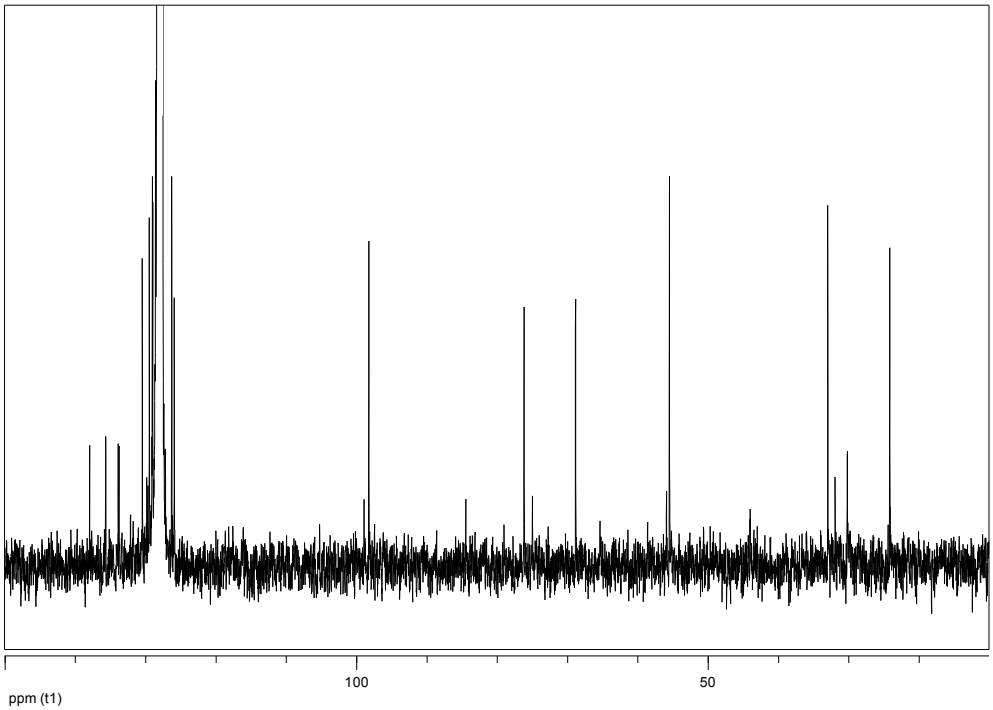

Figure A3.8 ^{13}C-NMR (100 MHz) spectrum of **7b** in C_6D_6.

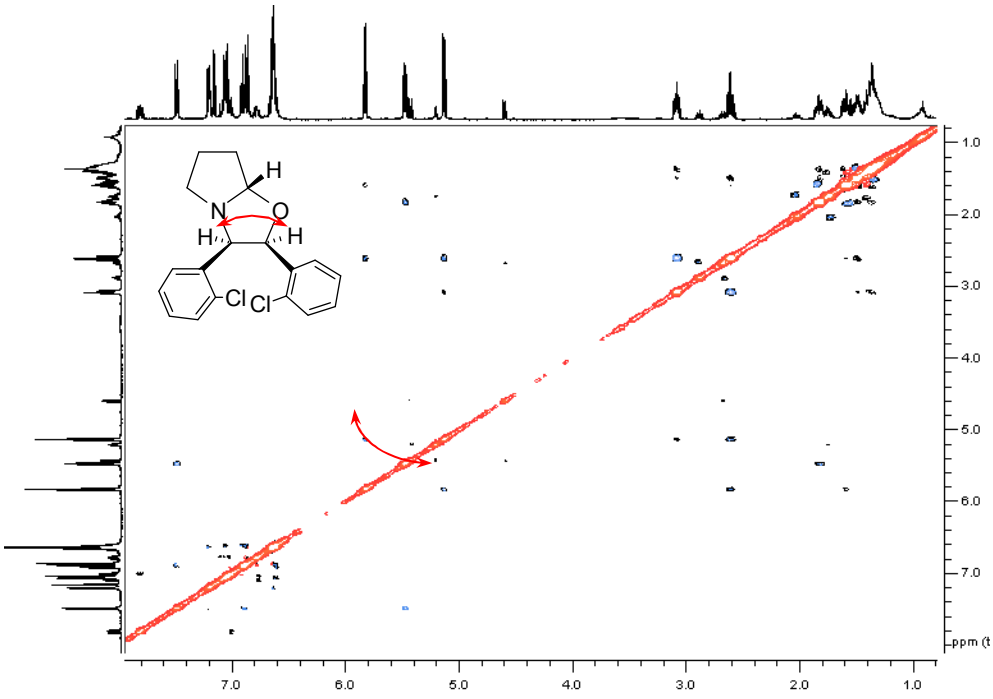

Figure A3.9 NOESY spectrum of **7b** in C_6D_6.

(**e**) NMR spectra of the separated diastereomers **7a** and **7b** were also measured in d^6-DMSO and showed identical shifts like their mixture in d^6-DMSO.

A3.2 Spectroscopic Analysis of the Synthesised L-Proline-Tetrazole

(**a**) ^{1}H-NMR and ^{13}C-NMR spectra of L-Proline-tetrazole **12** are displayed in Figures A3.10-A3.11.

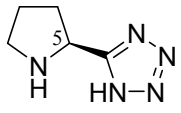

12

^{1}H-NMR (400 MHz, d^{6}-DMSO): δ4.77 (t, J = 8.3, 7.3 Hz, 1H, H-5), 3.34-3.15 (m, 2H, H-2), 2.39-2.27 (m, 1H, H-4), 2.21-1.91 (m, 3H, H-4, H-3).

^{13}C-NMR (100 MHz, d^{6}-DMSO): δ158.3 (C-6), 55.5 (C-5), 45.3 (C-2), 30.5 (C-4), 23.8 (C-3).

HRMS (ESI): *m/z* calc. for $C_5H_{10}N_5$ $[M+H]^+$: 140.0936, found: 140.0939.

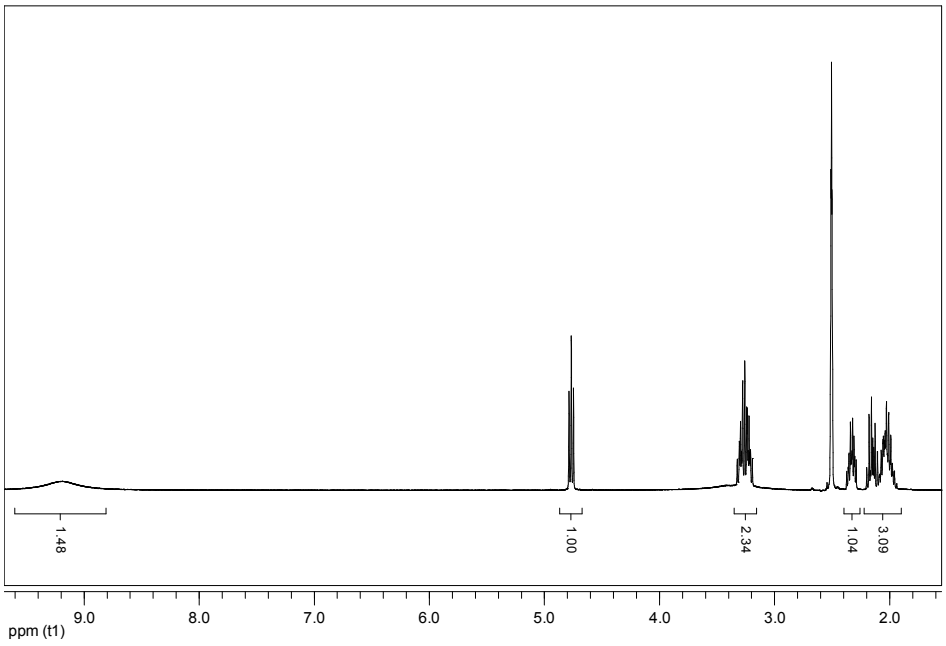

Figure A3.10 ^{1}H-NMR (400 MHz) spectrum of **12** in d^{6}-DMSO.

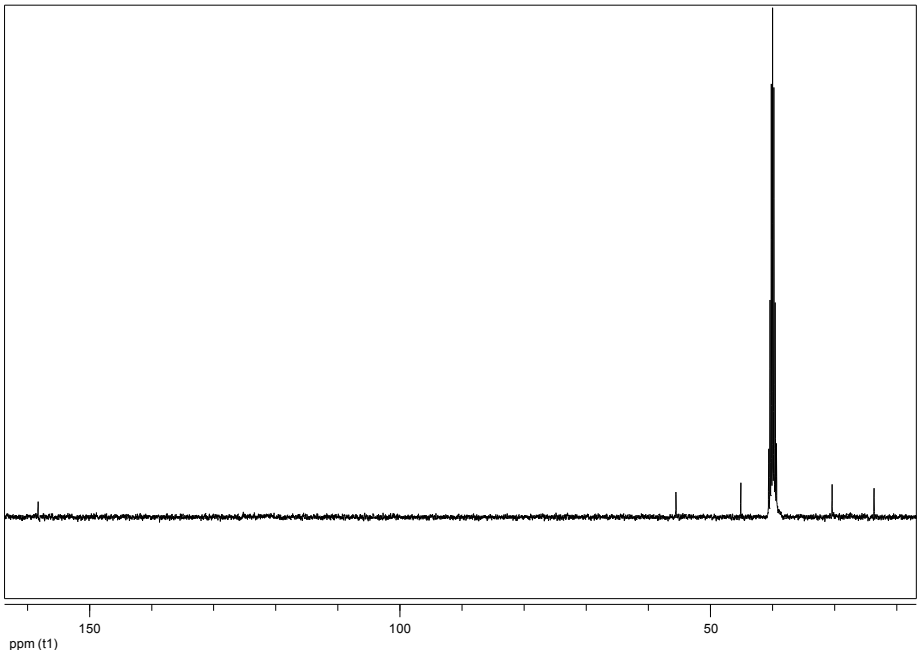

Figure A3.11 ^{13}C-NMR (100 MHz) spectrum of **12** in d^6-DMSO.

A 3.3 Spectroscopic Analysis of the Double Addition Species[1]

^{1}H-NMR and ^{13}C-NMR spectra of double addition species **14** are presented in Figures A3.13-A3.14.

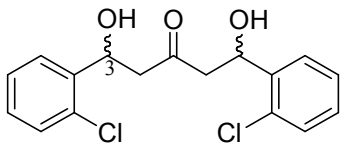

14

^{1}H-NMR (400 MHz, d^6-DMSO): δ7.62 (dd, J = 7.8, 1.5 Hz, 2H, Ar-H), 7.43 -7.22 (m, 6H, Ar-H), 5.57 (d, J = 4.4, 2H), 5.42 (dd, J = 11.2, 6.4Hz, 2H), 2.72 (d, J = 6.4 Hz, 4H, H-2).

^{13}C-NMR (100 MHz, d^6-DMSO): δ206.3 (C-1), 143.0 (Ar-C), 130.7 (Ar-C), 129.5 (Ar-C), 129.0 (Ar-C), 128.0 (Ar-C), 127.7 (Ar-C), 65.8 (C-3), 51.2 (C-2).

[1] Dr A. Franzke's unpublished results

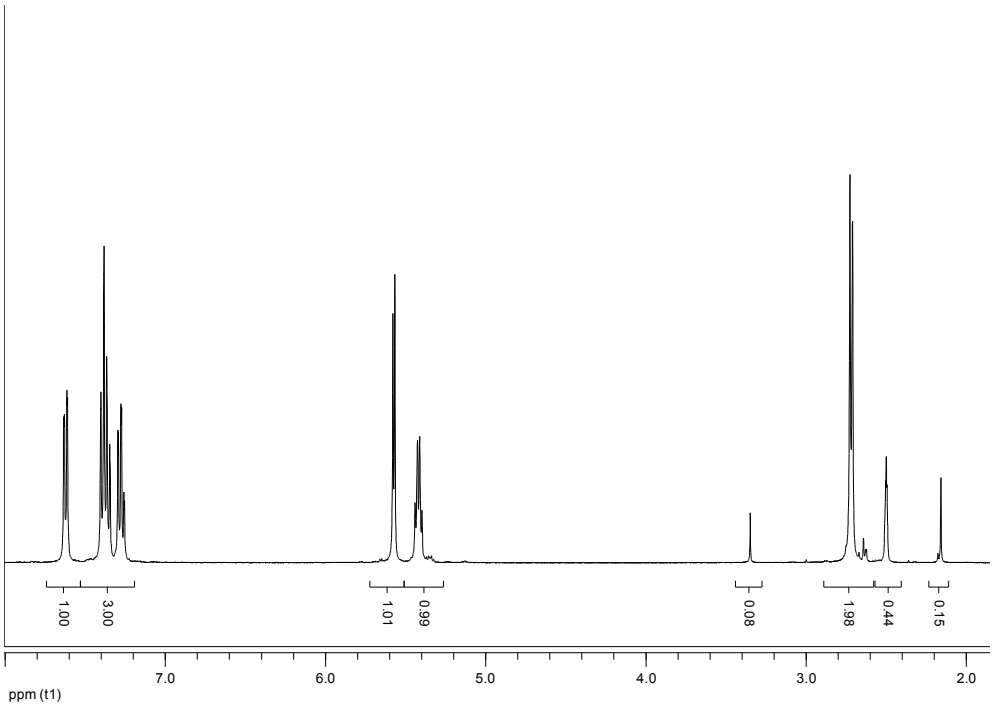

Figure A3.13 ^{1}H-NMR (400 MHz) spectrum of **14** in d^{6}-DMSO.

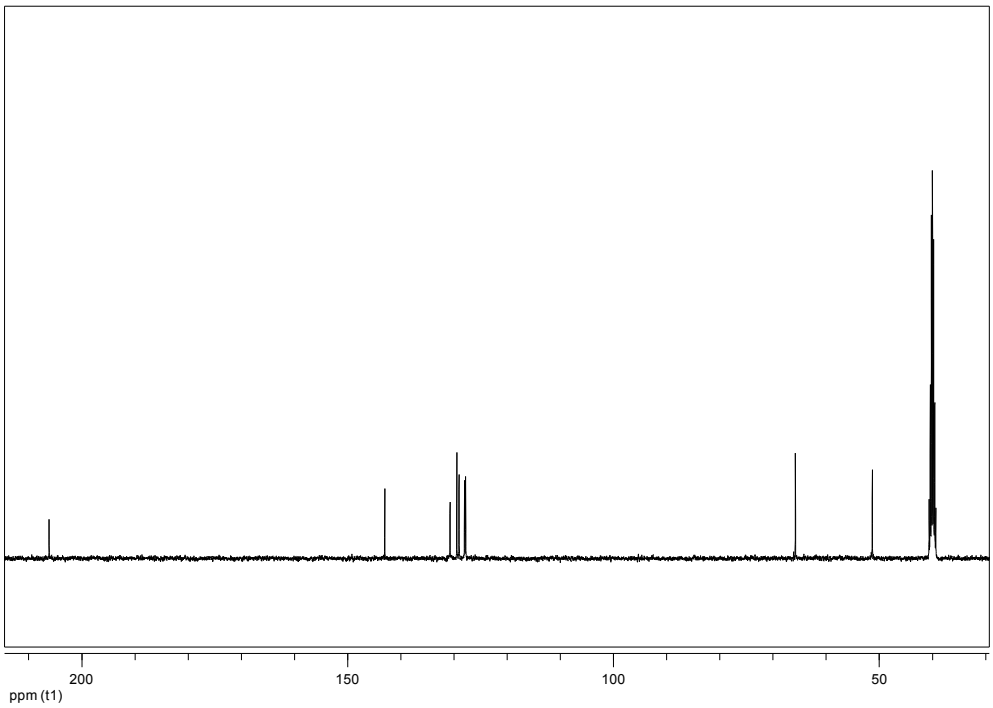

Figure A3.14 ^{13}C-NMR (100 MHz) spectrum of **14** in d^{6}-DMSO.

APPENDIX 4: DERIVATION OF STEADY-STATE RATE EQUATIONS

A 4.1 Derivation of the Steady-State Rate Equation 2.2 for Two-Substrate Catalytic Cycle of Scheme 2.1b

The mechanism of Scheme 2.1b of the main text can be represented in terms of elementary steps with the rate of each one as shown in equations A4.1-A4.3.

$$r_1 = k_1[\mathbf{S1}][\mathbf{C}] \qquad \text{(eq. A4.1)}$$

$$r_{-1} = k_{-1}[\mathbf{CS}] \qquad \text{(eq. A4.2)}$$

$$r_2 = k_2[\mathbf{S2}][\mathbf{CS}] \qquad \text{(eq. A4.3)}$$

The rate of the reaction with the mechanism of Scheme 2.1b of the main text is equal to the last irreversible elementary step (equation A4.3), which is the formation of the product. However the concentration of intermediate is not always possible to measure directly therefore the steady state (SS) approximation is often assumed. It suggests that the net rate of formation of intermediate species **CS** may be set to zero as in equation A4.4:

$$\frac{d[\mathbf{CS}]}{dt} \approx 0 = r_1 - r_{-1} - r_2 \qquad \text{(eq. A4.4)}$$

Hence the concentration of the intermediate can be solved by applying SS approximation as in equation A4.5:

$$[\mathbf{CS}] = \frac{k_1[\mathbf{S1}][\mathbf{C}]}{k_{-1} + k_2[\mathbf{S2}]} \qquad \text{(eq. A4.5)}$$

However the concentration of empty catalytic sites C which take part in the catalytic cycle is not exactly known but can be represented via the total amount of catalyst employed in the reaction and intermediate species CS as in equation A4.6:

$$[\mathbf{C}]_{total} = [\mathbf{C}] + [\mathbf{CS}] \qquad \text{(eq. A4.6)}$$

Substituting equation A4.5 for [**CS**] in equation A4.6 the concentration of empty cites can be obtained which is shown in equation A4.7.

$$[\mathbf{C}] = \frac{[\mathbf{C}]_{total}}{1 + \dfrac{k_1[\mathbf{S1}]}{k_{-1} + k_2[\mathbf{S2}]}} \qquad \text{(eq. A4.7)}$$

Substituting equation A4.7 of concentration of empty catalytic sites in equation A4.5 the concentration of intermediate species **CS** can be represented via the known catalyst amount as in equation A4.8.

$$[\mathbf{CS}] = \frac{k_1[\mathbf{S1}][\mathbf{C}]_{total}}{k_{-1} + k_2[\mathbf{S2}] + k_1[\mathbf{S1}]} \qquad \text{(eq. A4.8)}$$

Inserting the concentration of intermediate from equation A4.8 into the rate equation A4.3 the steady-state elementary rate law as in equation 2.2 can be derived.

A4.2 Derivation of the Steady-State Rate Equation 6.1 for the Enamine Mechanism of Scheme 6.1

In order to derive the rate equation 6.1 (in the main text), several assumptions again have to be considered. Firstly, formation of the product is the rate limiting and irreversible. Secondly, the concentration of each intermediate follows the steady-state approximation.

The concentration of enamine **9** that is solved applying steady-state (equation A4.9) is provided in equation A4.10.

$$\frac{d[\mathbf{9}]}{dt} \approx 0 \qquad k_1[\mathbf{1}][\mathbf{4}] - k_{-1}[\mathbf{9}][H_2O] - k_2[\mathbf{9}][\mathbf{2}] + k_{-2}[\mathbf{17}] = 0 \qquad \text{(eq. A4.9)}$$

$$[\mathbf{9}] = \frac{k_{-2}k_1[\mathbf{1}] + k_1k_3[\mathbf{1}][H_2O]}{k_{-1}k_{-2}[H_2O] + k_{-1}k_3[H_2O]^2 + k_3k_2[\mathbf{2}][H_2O]} \cdot [\mathbf{4}] \qquad \text{(eq. A4.10)}$$

The same approximation is applied for the iminium **17** as shown in equation A4.11.

$$\frac{d[\mathbf{17}]}{dt} \approx 0$$

$$k_2[\mathbf{9}][\mathbf{2}] - k_{-2}[\mathbf{17}] - k_3[\mathbf{17}][H_2O] = 0 \qquad \text{(eq. A4.11)}$$

Therefore the concentration of **17** is evaluated by equation A4.12.

$$[\mathbf{17}] = \frac{k_2[\mathbf{2}]}{k_{-2} + k_3[H_2O]} . [\mathbf{9}] \qquad \text{(eq. A4.12)}$$

The total concentration of catalyst **4** that takes part in the catalytic cycle equals to the sum of all kinetically meaningful intermediates and the empty sites is described by the equation A4.13.

$$[\mathbf{4}]_{total} = [\mathbf{9}] + [\mathbf{17}] + [\mathbf{4}] \qquad \text{(eq. A.13)}$$

Substituting equations A4.10 and A4.12 into equation A4.13 the concentration of empty catalyst sites $[\mathbf{4}]$ can be represented by the equation A4.14.

$$[4] = \frac{[\mathbf{4}]_{total}}{1 + \frac{k_{-2}k_1[\mathbf{1}] + k_1k_3[\mathbf{1}][H_2O]}{k_{-1}k_{-2}[H_2O] + k_{-1}k_3[H_2O]^2 + k_3k_2[\mathbf{2}][H_2O]} + \frac{k_1k_2[\mathbf{1}][\mathbf{2}]}{k_{-1}k_{-2}[H_2O] + k_{-1}k_3[H_2O]^2 + k_3k_2[\mathbf{2}][H_2O]}}$$

(eq. A4.14)

When the hydrolysis in Scheme 6.1 of the main text is rate limiting, then the rate of a reaction is proportional to the concentration of iminium ion $[17]$ and water as shown in equation A4.15.

$$r = k_3[\mathbf{17}][H_2O] \qquad \text{(eq. A4.15)}$$

In equation A4.15 concentration of water can be in a catalytic amount, $[H_2O]_{catalytic}$, when no additional water, $[H_2O]_{added}$, was added into reaction. However in order to prevent catalyst deactivation at least 0.2M water must be introduced in the reaction. Assuming steady state, this amount is much higher then the amount of water that was generated by the intermediates

therefore an assumption that $[H_2O]_{catalytic} << [H_2O]_{added}$ and that $[H_2O] = [H_2O]_{added}$ in equation A4.15 can be applied.

Re-arranging equations A4.10, A4.12 and A4.14 and substituting $[\mathbf{17}]$ in equation A4.15 the general steady-state rate equation A4.16 is obtained.

$$r = \frac{k_1 k_2 k_3 [\mathbf{1}][\mathbf{2}][H_2O][\mathbf{4}]_{total}}{k_{-1}k_{-2}[H_2O] + k_{-1}k_3[H_2O]^2 + k_3k_2[\mathbf{2}][H_2O] + k_1k_{-2}[\mathbf{1}] + k_1k_3[\mathbf{1}][H_2O] + k_1k_2[\mathbf{1}][\mathbf{2}]}$$

(eq. A4.16) = (eq. 6.1)

APPENDIX 5: KINETIC MODELLING

A 5.1 Summary of estimated rate constants

Four models of the enamine mechanism, which were discussed in Section 6.2.3 of the main text, were used to fit experimental kinetic data. All adjustable parameters (rate constants) were obtained from fitting experimental data to the investigated models using Solver curve-fitting program. The rate constants and the statistics are presented in Table A5.1.

Table A5.1 Best fit of rate constants from the simulations carried out for the aldol reaction of Scheme 4.1.[1]

Parameter	Model ***I*** Scheme 6.1, Eq. 6.5 Figure 6.4	Model *i* Scheme 6.5, Eq. 6.10 Figure 6.5	Model *ii* Scheme 6.1 Eq. 6.5 Figure 6.6	Model *iii* Scheme 6.1 Eq. 6.5 Figure 6.8
k_1 ($M^{-1}min^{-1}$)	3.96 (±0.01)	16.22(±0.42)	4.73(±0.05)	3.69(±0.03)
k_{-1} ($M^{-1}min^{-1}$)	61.27(±1.02)	13.63(±0.19)	22.64(±0.32)	14.35(±0.16)
k_2 ($M^{-1}min^{-1}$)	11.78(±0.15)	6.36(±0.02)	7.28(±0.02)	7.06(±0.02)
K_W (M^{-1})		12.70(±0.44)		
$k^{0.4}$ ($M^{-1}min^{-1}$)			2.54(±0.03)	
$k^{0.4}_{-1}$ ($M^{-1}min^{-1}$)			9.41(±0.14)	
$k^{0.4}_{2}$ ($M^{-1}min^{-1}$)			5.55(±0.02)	5.37(±0.02)
$k^{0.6}_{1}$ ($M^{-1}min^{-1}$)			1.98(±0.03)	
$k^{0.6}_{-1}$ ($M^{-1}min^{-1}$)			5.67(±0.12)	
$k^{0.6}_{2}$ ($M^{-1}min^{-1}$)			3.58(±0.02)	3.94(±0.01)
R^2	0.952072	0.991959	0.996232	0.994922
SE (y)	0.000853	0.000338	0.000229	0.000268

A5.2 Calculation of statistical parameters

Statistical parameters for each model were calculated using the equations A5.1-A5.4.

[1] Data from 10-85% conversion used in fitting and statistical analysis

For the calculation of correlation parameter equation A5.1 was used.

$$R^2 = 1 - \frac{SS_{resid}}{SS_{regr}} \qquad \text{(eq. A5.1)}$$

The value of squared errors is shown in equation A5.2.

$$SS_{resid} = \sum_i (y_i - f_i)^2 \quad \text{(eq. A5.2)}$$

y_i – value obtained from experiments

f_i – value predicted by the model

The regression sum of squared is shown in equation A5.3.

$$SS_{regr} = \sum_i (f_i - \bar{y})^2 \quad \text{(eq. A5.3)}$$

$\bar{y}$ – the average value of all y_i.

Calculation of root mean square deviation is shown in equation A5.4.

$$SE(y) = \sqrt{\left(\frac{SS_{resid}}{N-k}\right)} \quad \text{(eq. A5.4)}$$

N – number of experimental data points

k – number of adjustable parameters.

APPENDIX 6: CALCULATION OF EQUILIBRIUM CONSTANT FOR HYDROGEN BONDED COMPLEXATION

A6.1 Methodology

Equilibrium constant for hydrogen bonded species was calculation from the NMR titration experiments using nonlinear least square method based on the methodology described elsewhere.[130] When the equilibrium of hydrogen bond exchange between hydrogen bonded complex and starting component is much faster than the NMR time scale, then the observation of separate peaks for this complexed species is not possible. However in this case, the shift of the peaks which are assigned to the starting components in the complex is observed, in a way representing the weight average chemical shift as shown in Figure A6.1.

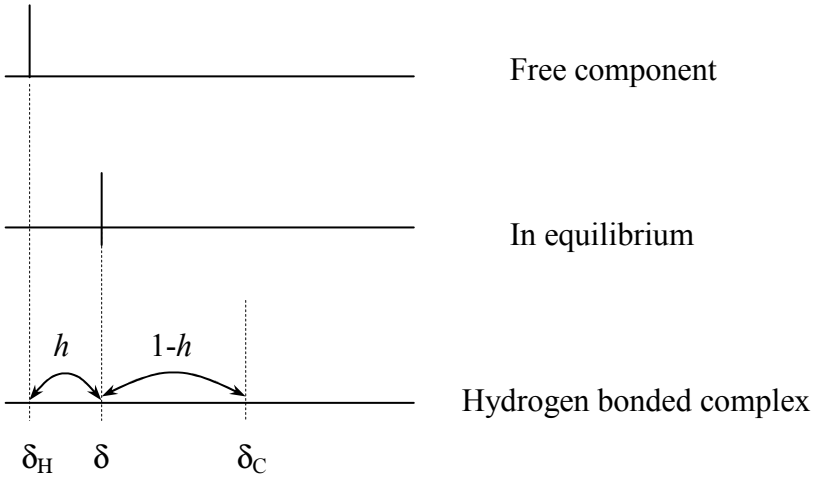

Figure A6.1 Representative NMR spectra for the fast exchange of complexation indicating a correlation of the complexation ratio x and each spectrum.[130]

The difference *h* between the shift observed during complexation and the shift of a peak in a free component is equalled to the ratio of complexed species at equilibrium with starting component (S) as in equation A6.1 (the stoichiometry of complexation is assumed 1:1). Therefore the observed chemical shift δ can be defined as the fractional composite of the chemical shifts of a free component δ_H and hydrogen bonded complex δ_C as in equation A6.2.

$$h = \frac{[complex]}{[\mathbf{S}]} \qquad \text{(eq. A6.1)}$$

$$\delta = \delta_H \cdot (1\text{-}h) + \delta_C \cdot h \qquad \text{(eq. A6.2)}$$

$$[complex] = \frac{\delta - \delta_H}{\delta_C - \delta_H} \cdot [\mathbf{S}] \qquad \text{(eq. A6.3)}$$

The amount of a formed complex ([*complex*]) can be expressed via equations A6.1 and A6.2 as shown in equation A6.3. The values of [*complex*] at each amount of starting free component calculated through the nonlinear regression analysis using Solver with δc as an adjustable parameter by minimising the error between *h* obtained from NMR data and the one calculated from equation A6.2. Then the equilibrium constant *K′* was calculated using equation A6.4.

$$K' = \frac{[complex]}{([\mathbf{19}] - [complex] \cdot [\mathbf{3}] - [complex])} \qquad \text{(eq. A6.4)}$$

A6.2 Experimental Procedure

The propionaldehyde **19** was carefully weighted in the NMR tube and known amount of $CDCl_3$ was added. The NMR spectrum of **19** in $CDCl_3$ was recorded. Then increasing amounts of aldol product was added while each time between additions recording the NMR spectrum. The obtained NMR data which is summarised in Table A6.1 was used for the calculation of equilibrium constant. The calculations were based on the NMR shift of propionaldehyde **19**.

The least square error, parameter δ_C and average equilibrium constant are presented in Table A6.

Table A6.1 Calculation of equilibrium constant using NMR data

[**19**]	[**3**]	δ_H	δ	$h = \delta - \delta_H$	h (eq.A6.2)	SS_{resid} $^{x}10^{-19}$	[*complex*] (eq. A6.3)	*K′* (eq. A6.4)
1.996	0.112	9.796	9.79	0.006	0.006	0.105	0.012	0.060
1.996	0.317	9.796	9.782	0.014	0.014	0.569	0.028	0.049
1.996	0.511	9.796	9.771	0.025	0.025	1.814	0.050	0.056
1.996	1.016	9.796	9.756	0.04	0.04	4.645	0.080	0.045
1.996	2.067	9.796	9.726	0.07	0.07	14.22	0.140	0.039

Table A6.2

ΣSS_{resid}	δ_C	*K'avrg*
$21.36^{x}10^{-19}$	8.796	0.050

APPENDIX 7: ADDITIONAL INFORMATION NOT PROVIDED IN THE MAIN TEXT

A7.1 The validation of aldol reaction carried out in chloroform

The validation of the aldol reaction carried out in chloroform (Fisher) and monitored by *in situ* FTIR is shown in Figure A7.1.

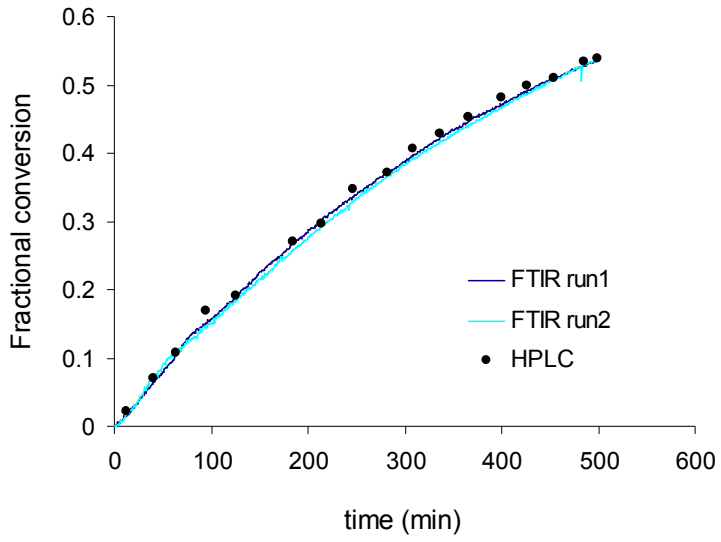

Figure A7.1 Fraction conversion vs. reaction time measured by FTIR and HPLC for aldol reaction of Scheme 4.1 carried out in $CHCl_3$. Reaction conditions are: $[1]_0 = 1.5M$, $[2]_0 = 0.4M$, $[4] = 0.04M$. Product enantiomeric excess = 54%.

A7.2 The validation of the α-aminoxylation reaction carried out in chloroform

The validation of the α-aminoxylation reaction carried out in chloroform (Fisher) and monitored by *in situ* FTIR is shown in Figure A7.2.

In case of α-aminoxylation reaction, disappearance of carbonyl peak of an aldehyde at 1729 cm^{-1} and appearance of C-O bond of the product at 1077 cm^{-1} were monitored by FTIR.

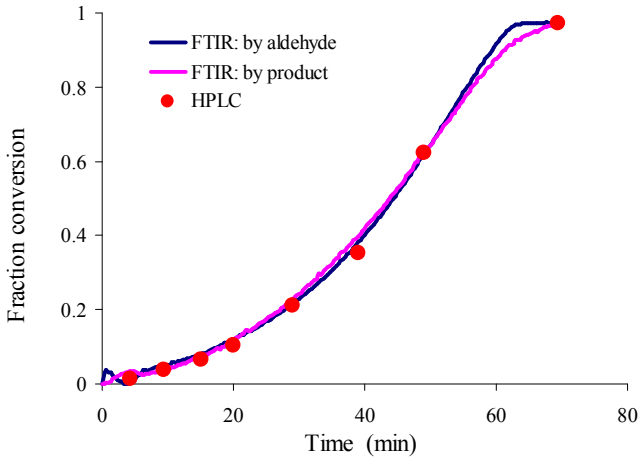

Figure A7.2 Fraction conversion vs. reaction time as measured by in situ FTIR, and sample analysis by HPLC for the α-aminoxylation reaction of Scheme 7.1 carried out in $CHCl_3$. Reaction conditions are: $[\mathbf{19}]_0 = 1.97M$, $[\mathbf{20}]_0 = 0.7M$, $[\mathbf{4}] = 0.07M$. Product enantiomeric excess = 99%.

A7.3 Catalytic stability in aldol reactions

(**a**) Plots confirming catalyst stability for the experiments E5.5-E5.6 carried out during the investigation of water effect in the aldol reaction of Scheme 4.1 (Chapter 5) are displayed in Figure A7.3.

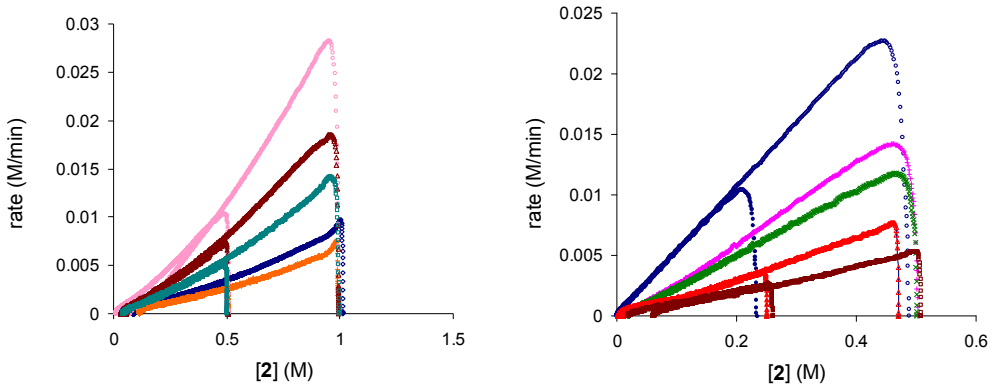

Figure A7.3 Same excess protocol for the experiments E5.5-E5.6. Added water from top to bottom: (a) 0.2, 0.4, 0.6, 1.0, 1.4, 1.8 M in E5.5; (b) 0.2, 0.4, 0.6, 1.0, 1.3 M in E5.6.

(b) Test of catalytic stability using the same *excess* protocol in the experiments carried out in order to confirm zero order kinetics in the proline (Section 6.1.1) is shown in Figure A7.4.

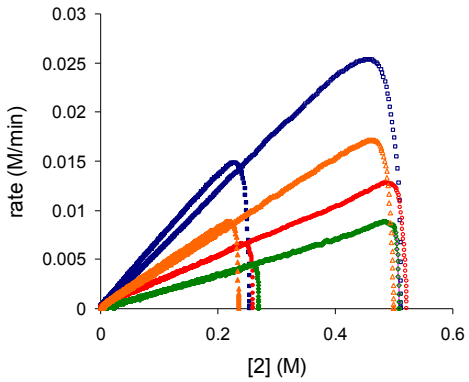

Figure A7.4 Same excess protocol for the experiments E6.1and E6.3 using 0.5M **4**. Experimental conditions from top to bottom: 2.26 M [**e**], 0.2M H_2O; 0.75 M [**e**], 0.2 M H_2O; 2.26 M [**e**], 0.6 M H_2O; 0.75 M [**e**], 0.6 M H_2O.

A7.4 Aldol Reaction Catalysed by L-Proline-Tetrazole: Product Addition

Comparison of fractional conversion versus time for the aldol reactions of Scheme 4.1 in main text catalysed by proline-tetrazole with/without addition of the aldol product **3** is displayed in Figure A7.5

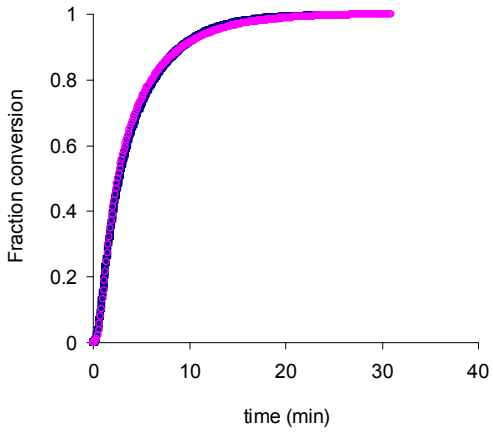

Figure A7.5 Fractional conversion versus time for the aldol reactions of Scheme 4.1 catalysed by proline-tetrazole with/without addition of the aldol product **3**. Reaction conditions are: $[1]_0 = 1.76$M, $[2]_0 = 0.23$M, [4] = 0.1M. Pink circles: [3] = 0.25M. Product enantiomeric excess = 66%.

A7.5 Aldol Reaction Catalysed by Proline in DMF: Catalytic Stability and Kinetic Modelling

All experiments of l-proline catalysed aldol reaction of Scheme 4.1 carried out in DMF were tested for catalytic stability using the same *excess* protocol. Then kinetic modelling using all sets of experimental data was

performed. Figure A7.6a presents the fitting of 8 sets of experimental data to the simplest three parameter model of Equation 6.5. Figure A7.6b displays fitting to four parameter model where formation of new proline-water species is assumed (Equation 6.10, proposal *i*).

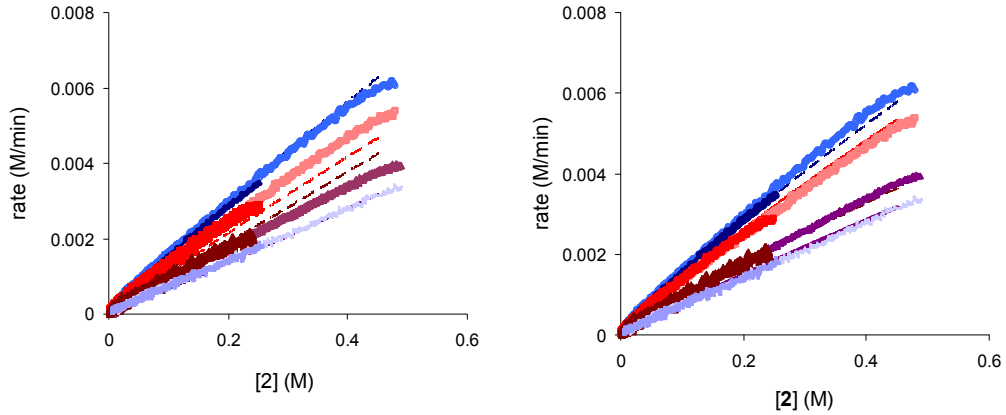

Figure A7.6 Kinetic modelling of the reaction progress data. Blue circles: [**e**] = 2.25 M; 0.2M H_2O; $[\mathbf{2}]_0$ = 0.5 M; red squares: [**e**] = 1.50 M; 0.2 M H_2O; purple triangles: [**e**] = 2.25 M; 0.4 M H_2O; lilac dash: [**e**] = 1.50 M; 0.4 M H_2O. All reactions were carried out at 25 °C in DMF with 0.1 M of total proline concentration. a) model according Eq. 6.5; b) model according Eq. 6.10.

A7.7 Proline Interactions with Various Additives

The ^{1}H-NMR spectra of proline in chloroform with methanol and acetic acid are presented in Figures A7.7 and A7.8.[1]

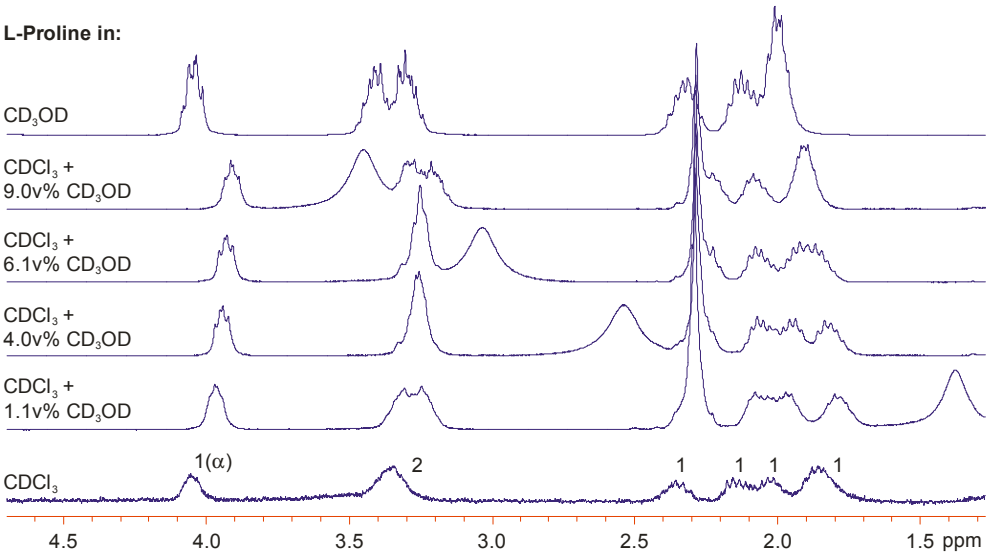

Figure A7.7 ^{1}H-NMR of L-proline in $CDCl_3/CD_3OD$ with standard toluene, shown is the gradual change in proline chemical shifts to resemble the spectrum in pure CD_3OD.

[1] Dr Mathew S.P. unpublished results

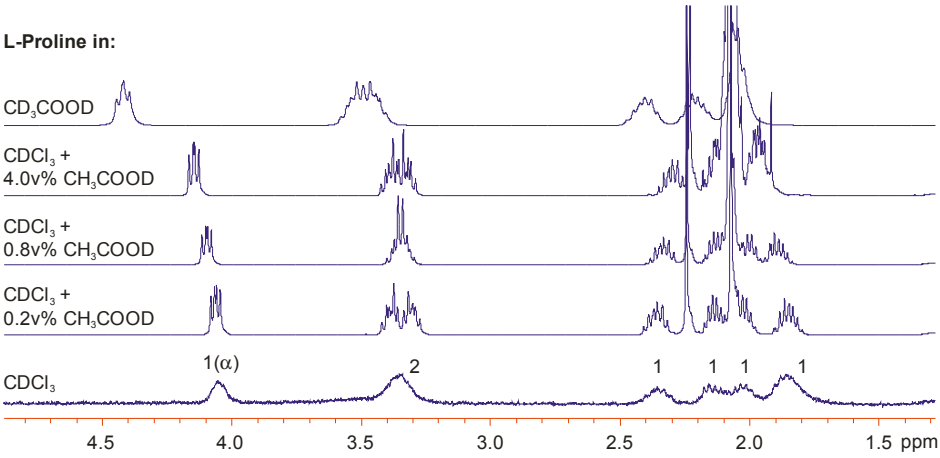

Figure A7.8 ^{1}H-NMR of L-proline in $CDCl_3/CH_3CO_2D$ with standard 2,5-dimethylfurane, shown is the gradual change in proline chemical shifts to resemble the spectrum in pure CD_3OD.